The Sky as a Laboratory

2008-2009

Project Director
Prof. Piero Rafanelli
Dept. of Astronomy, Padova University

Scientific Coordinators Dr. Stefano Ciroi Dr. Francesco Di Mille

Scientific Collaborators Dr. Valentina Cracco Dr. Rosaria Tantalo

Scientific Editorial Board Dr. Valentina Cracco Alessandra Frassati Rossella Spiga

Cover illustration Sergio Dalle Ave INAF- Padova Astronomical Observatory

Preface

This book collects the final scientific reports of the students, who took part in the observational training periods organized in February 2009 at the Asiago Astrophysical Observatory in the frame of the VIII Edition of The Sky as a Laboratory, the educational project of the Department of Astronomy of Padova University, addressed to the Secondary Schools of the Veneto Region (Italy). Created by Prof. Piero Rafanelli, currently Head of the Dept., and carried out by means of a close cooperation between the scientific and technical staff of the Dept., and the teachers of the participating schools, every year this project involves about 300-350 Secondary School students, 40-45 teachers and 35 institutes.

The main aim of The Sky as a Laboratory is to introduce a new approach in teaching and learning astronomy, through the interpretation of the observed celestial phenomena and the use of the physical and mathematical tools available to the students. This project allows the students to deepen the issues studied at school and makes a link among astronomy, physics, mathematics, and chemistry. In addition it guides the students to the university choice, since it allows them to be exposed to the university environment and scientific research.

The first part of the project consists of 7 lectures of fundamentals of astrophysics given by the teachers of the 10 reference schools and by the scientific staff of the Dept. Then, a competitive test allows to select the 50 most eligible and motivated students, who will attend a training period of 3 days and 3 nights at the 122 cm Galileo Telescope of the Asiago Astrophysical Observatory. These students will receive 1 or 2 ECTS from the Science Faculty of Padova University. On the basis of direct observations and data extracted from astronomical public archives, the students analyzed photometric and spectroscopic data of different astronomical targets to determine photometric and kinematic parameters of galaxies both isolated and in groups, colour-magnitude diagram, distance, age and metallicity of open and globular clusters, spectral classification, temperature, colour index and equivalent width of absorption and emission line stars, present star formation, star formation history and stellar populations of spiral galaxies, spectral properties of C/2007 N3 comet and finally optical spectroscopic classification of SWIFT X-ray sources (The Astronomer's Telegram, #1985, 2009) and of the supernova SN2009af (Central Bureau Electronic Telegrams, 1697, 2, 2009).

This training gave the students a chance to deepen the knowledge they acquired during astronomy classes both at school and during the project. The project ended on April 27th, 2009 with the official presentation of the scientific reports by the students at the Dept. of Astronomy.

ugriz photometry of candidate galaxy groups: 2MASXJ14391186+1415215 and 2MASXJ14530794+2554327

Giulia Boscolo "Papo" (1), Riccardo Ravagnan (2), Gloria Tiozzo "Lia" (2)

(2) Liceo "G. Veronese" sez. Classica, Chioggia Liceo "G. Veronese" sez. Scientifico Brocca, Chioggia

ABSTRACT

We studied the photometry of the two galaxy groups 2MASXJ14391186+1415215 and 2MASX J14530794+25554327 using 5 bands (u, g, r, i, z). This study allowed us to determine when a group is compact and isolated, using Hickson's criteria. Hickson established three criteria to define groups of galaxies. The first is the population: the group must be composed of at least four members. The second is the compactness: the galaxies have to be included in a limited field. The third is the isolation: the members of a galaxy group have to be distant from other galaxies.

I. INTRODUCTION

Groups of galaxies are the smallest aggregates of galaxies. They contain typically less than 50 galaxies in a diameter of 1 to 2 Mpc. For example the group that contains our galaxy, the *Milky Way*, is called the *Local Group* and contains more than 40 galaxies.

For this analysis we chose the galaxies with the same characteristics: size, brightness and relative distance.



Image 1: Group of galaxies 2MASX J14391186+1415215.

II. OBSERVATIONAL DATA

We used images extracted from the public archive of the Sloan Digital Sky Survey (SDSS). SDSS is a project that provides optical images covering more than a quarter of the sky and a three-dimensional map containing about one million galaxies and 120000 quasars. SDSS used a 2.5 m telescope, at Apache Point in New Mexico. For the photometric survey, five filters were used; every filter can select only a determined range of the electromagnetic spectrum of visible light. The five filters (u, g, r, i, z) and their average wavelengths are:

и	g	r	i	z
3551 Å	4686 Å	6165 Å	7481 Å	8931 Å

Our study was focused on the analysis of the photometric properties of galaxies around two X-ray sources: 2MASX J14391186+1415215 and 2MASX J14530794+2554327, in order to understand if they can be candidate galaxy groups. Since we do not have spectra for these galaxies, we cannot determine their redshift and therefore we are forced to use photometry.

2MASX J14391186+1415215			
Right Ascension	14h39m11.8s		
Declination	+14d15m22s		
Constellation	Bootes		

2MASXJ14530794+2554327			
Right Ascension	14h53m07.9s		
Declination	+25d54m33s		
Constellation	Bootes		

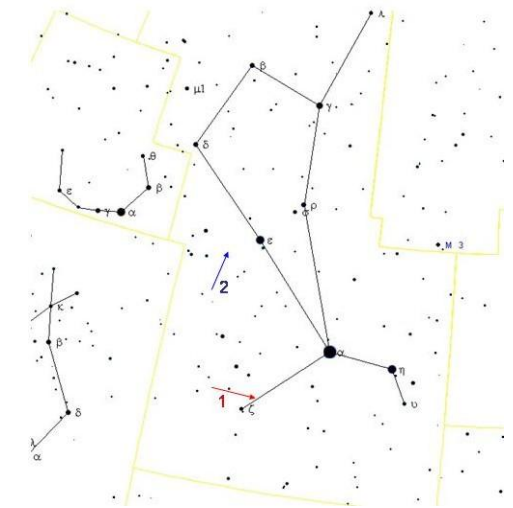


Image 2: Bootes constellation.

III. WORK DESCRIPTION

We used the program IRAF (Image Reduction and Analysis Facility) to analyze the images: each pixel in the image has a value in counts that is proportional to the flux of photons collected by the telescope. By using this program we can measure the light of the galaxies. We took five images. Every image was taken by the telescope using different filters (u, g, r, i, z).

To understand if a group of galaxies is isolated or not, we performed the following operations.

We started by displaying the images, then we selected the galaxies that appeared to belong to the same group for size, brightness and their reciprocal proximity. We numbered them and put a circle around each of them to easily identify them.

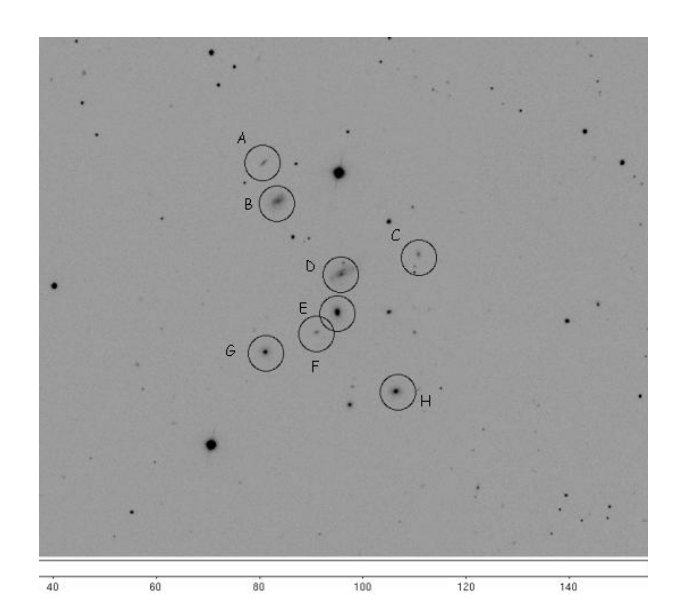


Image 3: The group 2MASX J14391186+1415215.

We searched for the centers of the galaxies and found their coordinates. We enclosed each galaxy in a circle with the smallest possible radius in which we calculated the photometry (the centre of the circle corresponds to that of the galaxy). Then we traced a larger concentric circle around the previous one, including each galaxy, in which we estimated the sky brightness to be subtracted.

With *IRAF* we calculated the magnitude of each galaxy, called "instrumental magnitude" (m_s). We converted instrumental into calibrated magnitudes using the photometric constants provided by SDSS (m_0 , k, X) and applying the following formula: $m = m_0 + m_s - k \cdot X$, where m_s is the instrumental magnitude, m_0 the photometric zero-point, k the atmospheric extinction coefficient and X the airmass.

For the second group of galaxies, we got 2 sets of constants, because the galaxies were distributed in two different frames:

Filter	и	g	r	i	z
m_0	23.78	24.44	24.04	23.69	21.09
k	0.554	0.213	0.136	0.069	0.062
X	1.116	1.119	1.112	1.114	1.117

Tab. 3: Group of galaxies 2MASX J14391186+1415215.

Filter	и	g	r	i	z
m_0	23.79	24.40	24.01	23.61	21.97
k	0.586	0.206	0.125	0.067	0.052
X	1.035	1.038	1.033	1.034	1.036

Tab 4: Group of galaxies 2MASXJ14530794+2554327; Frame 1.

Filter	и	g	r	i	z
m_0	23.754	24.36	23.96	23.57	21.90
k	0.603	0.209	0.128	0.087	0.077
X	1.012	1.013	1.011	1.012	1.013

Tab 5: Group of galaxies 2MASXJ14530794+2554327; Frame 2.

To analyse the properties of the candidate groups we used only the r filter.

In order to determine the compactness, we needed to calculate the surface brightness of all the galaxies together. First, we converted the calibrated magnitude of each galaxy into intensity:

$$m = -2.5 \log I \rightarrow I = 10^{-m/2.5}$$

Galaxy	r	I_r
а	13.591	0.3661 ·10-5
b	12.136	$1.398 \cdot 10^{-5}$
c	13.758	0.3139· 10 ⁻⁵
d	11.572	$2.350 \cdot 10^{-5}$
e	11.338	2.916 ·10 ⁻⁵
f	14.061	$0.2374 \cdot 10^{-5}$
g	12.063	$1.495 \cdot 10^{-5}$
h	11.665	$2.157 \cdot 10^{-5}$

Tab. 6: Group 2MASX J14391186+1415215.

Galaxy	r	I_r
\boldsymbol{A}	14.871	$0.1125 \cdot 10^{-5}$
В	12.253	$1.254 \cdot 10^{-5}$
С	12.772	$0.777 \cdot 10^{-5}$
D	11.760	1.975 ·10 ⁻⁵
E	13.908	$0.273 \cdot 10^{-5}$

Tab. 7: Group 2MASXJ14530794+2554327.

Then we measured the radius of the smallest possible circle containing the group of galaxies. This radius was originally in pixels, but we converted it into *arcsecs* knowing that each pixel of the image is a square covering an area of the sky corresponding to 0.4x0.4 arcsec.

For the first group we obtained 315 px = 126", and for the second group 153 px = 61".

We calculated the surface intensity of each group summing the intensities of each galaxy and dividing by the area of the circle:

$$I = \frac{\sum I_g}{\pi R^2}$$

where R represents the radius of the circle that contains the group of galaxies.

The sum of the intensities of the first group is 11.2334·10⁻⁵. The surface intensity of the first group is:

$$I = \frac{11.2334 \cdot 10^{-5}}{\pi \cdot 15876} = 2.25 \cdot 10^{-9}$$

The sum of the intensities of the second group is $4.3915 \cdot 10^{-5}$. The surface intensity of the second group is:

$$I = \frac{4.3915 \cdot 10^{-5}}{\pi \cdot 3721} = 3.76 \cdot 10^{-9}$$

Then we were able to calculate the surface brightness of each group of galaxies:

$$\mu_1 = -2.5 \cdot log_{10} (2.25 \cdot 10^{-9}) = 21.62 \text{ mag/arcsec}^2$$

The magnitude of the second group is:

$$\mu_2 = -2.5 \cdot log_{10} (3.76 \cdot 10^{-9}) = 21.06 \text{ mag/arcsec}^2$$

Since these two values are lower than 26 mag/arcsec², the Hickson's limit, we can assert that both galaxy groups are compact.

Finally, we had to define if the groups are isolated or not. To do this we drew a concentric circle to the smallest radius containing the galaxies, but with the radius three times larger. If we find other galaxies within this new circle having magnitudes similar or even brighter than those of the studied groups, they cannot be considered isolated.

In both cases our galaxy groups satisfy the isolation criterion proposed by Hickson.

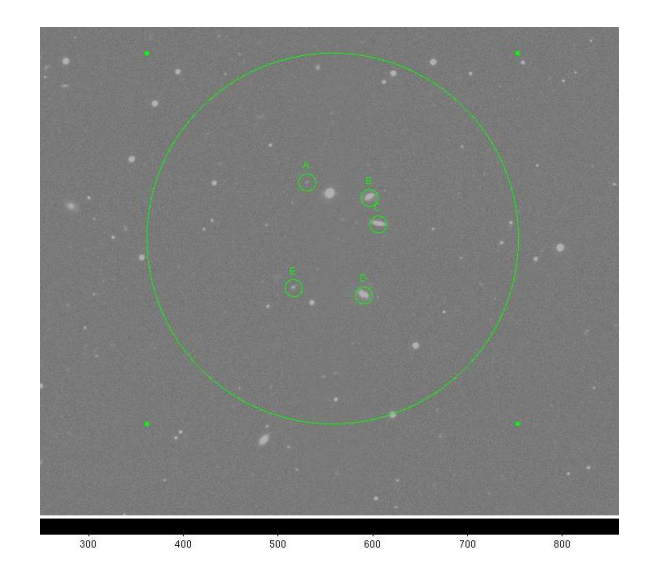


Image 4: The image represents the second group of galaxies and the circle with the radius three times larger than the circle that contains the group.

IV. RESULTS

According to the experimental data, we can say that we have identified candidate compact groups of galaxies. They satisfy the three criteria proposed by Paul Hickson in 1982. It is clear that only from their spectra and redshifts we can be sure that these groups of galaxies are physically connected.

Analysis of the luminosity of elliptical galaxies

Mattia Chillon, Nicola Chiodetto, Dario Di Gregorio, Nicolò Mazzucato

"ITIS F.Severi". Padova

ABSTRACT

Our work was focused on the study of elliptical galaxies by means of photometric and spectroscopic data. Using a specific software, we were able to define two apparent magnitude values for each galaxy referred to two different photometric filters. With some computations we obtained the absolute magnitude values that allowed us to compare the luminosity of galaxies with that of the Sun.

I. INTRODUCTION

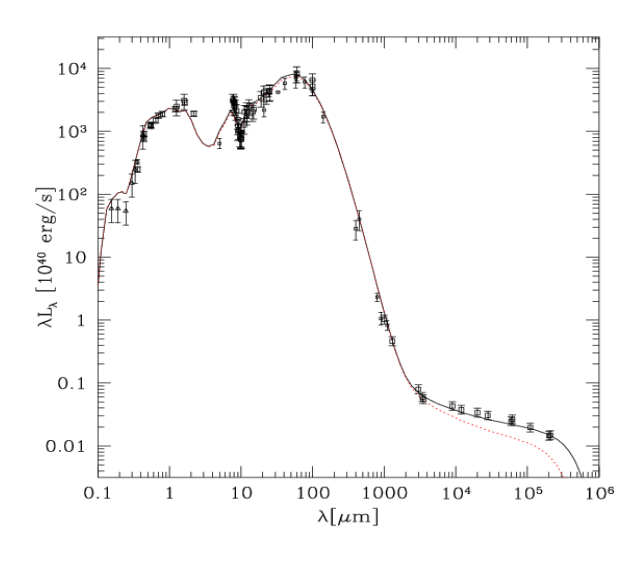
Magnitude is a scientific way to measure a celestial object brightness. There are two kinds of magnitudes: apparent and absolute magnitude. The first one depends on the distance between the celestial object and the observer and is related to the energy flux reaching the observer; the second one is independent of this distance set as default to 10 pc, and is related to the intrinsic energy emission called luminosity.

Dealing with galaxies, the magnitude is the sum of each star brightness value. To measure a galaxy total magnitude, we can apply the same technique used for stars, in spite of their large extension. Finally we must say that magnitude is always referred to a specific part of the electromagnetic spectrum selected by using filters, otherwise the value should be called bolometric magnitude and refer to the object whole output.

II. OBSERVATIONAL DATA

In this study, we considered only elliptical galaxies, which can be recognized according to their spectra. We selected our targets from the archive of the Sloan Digital Sky Survey (SDSS), which contains spectroscopic and photometric data of a large fraction of the sky.

After a first selection based on colour and distance (indirectly obtained from redshift), we were able to separate elliptical galaxies from the other ones looking at the presence of $H\alpha$ absorption line and checking their morphology by eye.



III. WORK DESCRIPTION

After classifying the galaxies, we selected particular parameters for every single galaxy. The parameters considered in our analysis, referred to both g and r filters, are the following:

- g and r instrumental magnitude (m_s): extracted by the analysis of the photon counts of the image obtained through the IRAF (Image Reduction and Analysis Facility) software. With this software we drew circles of increasing radius centred on the galactic centre and we determined the total flux within each circle thanks to the fact that every pixel corresponds to a well defined photon intensity. Then, taking into account the additive sky contribution and the exposure time of the analysed images, we could calculate the total instrumental magnitude of each galaxy:

Galaxy	ms(g)	ms(r)	m0(g)	m0(r)	k (g)	k(r)	x(g)	x(r)
SDSS J080550.31+372736.2	16.689	16.069	24.452	24.093	0.188	0.100	1.070	1.077
SDSS J162754.90+403621.8	18.307	17.341	24.601	24.070	0.196	0.108	1.036	1.040
SDSS J093118.81+444647.3	17.088	16.514	24.352	24.057	0.150	0.074	1.040	1.037
SDSS J105807.60+091634.0	15.650	15.113	24.442	24.063	0.155	0.106	1.256	1.271
SDSS J161845.79+392004.0	15.889	15.284	24.348	24.044	0.149	0.085	1.076	1.083
SDSS J153215.71+092755.9	16.127	15.564	24.388	23.992	0.196	0.111	1.251	1.237
SDSS J135039.09+350217.9	15.388	14.899	24.424	24.039	0.137	0.091	1.038	1.033
SDSS J133440.34+325704.0	15.827	15.284	24.416	24.016	0.218	0.132	1.007	1.005
SDSS J122541.68+124837.8	13.975	13.565	24.481	23.999	0.194	0.096	1.115	1.122
SDSS J075638.85+440741.0	23.992	15.745	24.510	24.128	0.187	0.112	1.091	1.084
SDSS J100910.06+541331.9	24.039	15.785	24.645	24.078	0.230	0.116	1.087	1.085
SDSS J030352.91+002454.9	24.016	15.225	24.442	24.012	0.148	0.076	1.233	1.226
SDSS J141532.92+501051.7	23.999	12.115	24.566	24.046	0.184	0.122	1.189	1.199
SDSS J124622.67+115235.7	15.806	15.237	24.440	24.027	0.194	0.096	1.123	1.130
SDSS J084051.14+315853.4	16.561	16.017	24.472	24.066	0.161	0.082	0.082	1.012

$$m_s = -2.5 \log \left(\frac{I - I_{sky} \cdot N_{pix}}{T_{exp}} \right) + 25$$

where N_{px} is the number of pixel in each circle and 25 is a constant added by us to have positive magnitudes. Finally we plotted a sort of growth curve having the apparent instrumental magnitude as a function of the circle radius, and we chose the radius where magnitude became constant:

- g_0 and r_0 magnitudes: photometric zero-points taken directly from our SDSS database, used to convert instrumental magnitudes into calibrated magnitudes, that is photon counts into physical units;
- g_k and r_k atmospheric extinction coefficients: a factor that shows how much of the electromagnetic radiation coming from astronomical sources is reduced by the presence of the Earth atmosphere (absorption and scattering);
- g_X and r_X airmasses: values related to the angular distance of each object from the zenith. The higher is this distance the higher is the effect of atmospheric extinction.

Parameters considered up to now are necessary to calibrate the magnitude. In fact a correction to the instrumental magnitude is needed, according to the galaxy position referring to the observer's celestial horizon. Effectively this physical measurement is influenced by the presence of large dense airmasses that block part of the radiation.

To compute calibrated apparent magnitudes we used the following formula:

$$m_c = m_0 + (m_s - 25) - k \cdot X$$

where m_c and m_0 are the calibrated magnitude and the zero-point for a generic photometric band.

From the values of the calibrated magnitude of both the filters, which belong to the photometric system *ugriz*, we obtained the value of the more commonly used V magnitude by applying the formula:

$$V = g - 0.52 (g - r) - 0.03$$

In order to obtain our final result, that is the luminosity of the galaxies, we had to calculate the absolute magnitude. This is possible by applying the Pogson's formula. As said before, apparent magnitude depends on distance, so the distance is needed and it is obtained using the redshift and the Hubble's law.

$$\begin{array}{ll} v=z\cdot c\\ \\ => & d=\left(\;z\cdot c\;\right)/\;H_0\\ \\ v=H_0\cdot d \end{array}$$

where v is the systemic velocity of the galaxy, z is its redshift, c the speed of light and H₀ the Hubble costant. After the distance was obtained and converted into parsec, we computed absolute magnitude:

$$M_V = V + 5 - 5 \log(d)$$

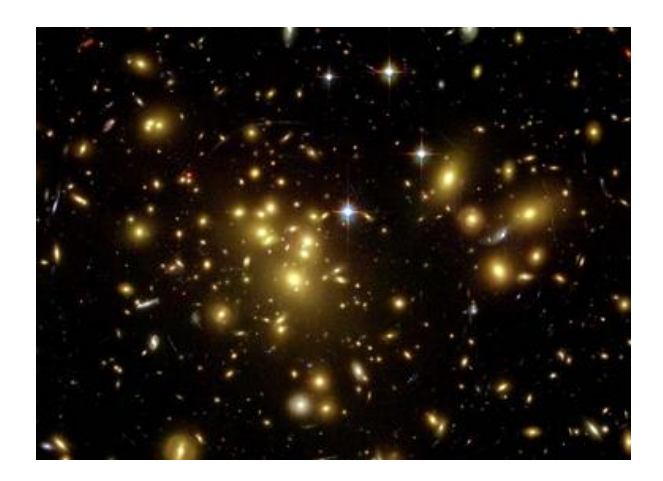
Since absolute magnitude is related to the luminosity, we used the absolute visual magnitude of the Sun $(M_V(\Theta) = +4.72)$ in order to measure the luminosity of our targets in solar units:

$$L_V\!/L_{\odot} = ~10^{~\text{-0.4 (Mv-M}\odot)}$$

Galaxy	g	r	V	Redshift (z)	D (Mpc)	M(V)	L/L0	σ*	log σ*
SDSS J080550.31+372736.2	15.940	15.055	15.450	0.034	141.67	-20.31	1.025E+10	215.48	2.33
SDSS J162754.90+403621.8	17.705	16.299	16.944	0.033	137.50	-18.75	2.438E+09	229.96	2.36
SDSS J093118.81+444647.3	16.284	15.494	15.843	0.035	145.83	-19.98	7.560E+09	137.05	2.14
SDSS J105807.60+091634.0	14.896	14.041	14.422	0.034	141.67	-21.33	2.641E+10	324.57	2.51
SDSS J161845.79+392004.0	15.077	14.235	14.609	0.032	133.33	-21.02	1.969E+10	234.43	2.37
SDSS J153215.71+092755.9	15.270	14.419	14.797	0.033	137.50	-20.89	1.761E+10	277.47	2.44
SDSS J135039.09+350217.9	14.671	13.844	14.211	0.021	87.50	-20.50	1.224E+10	169.88	2.23
SDSS J133440.34+325704.0	15.023	14.168	14.548	0.024	100.00	-20.45	1.172E+10	184.96	2.27
SDSS J122541.68+124837.8	13.240	12.457	12.803	0.002	8.33	-16.80	4.060E+08	118.92	2.08
SDSS J075638.85+440741.0	22.915	14.752	18.640	0.047	195.83	-17.82	1.037E+09	270.59	2.43
SDSS J100910.06+541331.9	22.867	14.737	18.609	0.048	200.00	-17.90	1.113E+09	172.21	2.24
SDSS J030352.91+002454.9	22.846	14.144	18.291	0.043	179.17	-17.98	1.197E+09	304.3	2.48
SDSS J141532.92+501051.7	22.826	11.015	16.654	0.044	183.33	-19.66	5.660E+09	264.41	2.42
SDSS J124622.67+115235.7	14.615	14.156	14.346	0.044	183.33	-21.97	4.743E+10	307.71	2.49
SDSS J084051.14+315853.4	15.613	14.999	15.264	0.048	200.00	-21.24	2.423E+10	280.18	2.45

IV. RESULTS

Comparing the values of the luminosities of our targets with respect to the solar value, we observe the compatibility of the data: values of about $10^{11}~L_{\odot}$ are justified by the fact that elliptical galaxies are often giant galaxies made by billions of stars.



To verify the reliability of our data, we put in a graph the logarithm of stellar velocity dispersion, measured by Guglielmo, Amoruso and Colombo (see their report), which is characteristic of each galaxy, as a function of absolute magnitude. In this way we aimed to reproduce the empirical relationship published by Faber & Jackson between the luminosity and the central velocity dispersion of stars typical of elliptical galaxies:

$$L \propto \sigma^{\gamma}$$

Where γ is the gradient of the line of our graph, and should be close to 4.

Expressing this formula in logarithmic terms and using the relation between luminosity and absolute magnitude we obtain a new relation between σ and M_v :

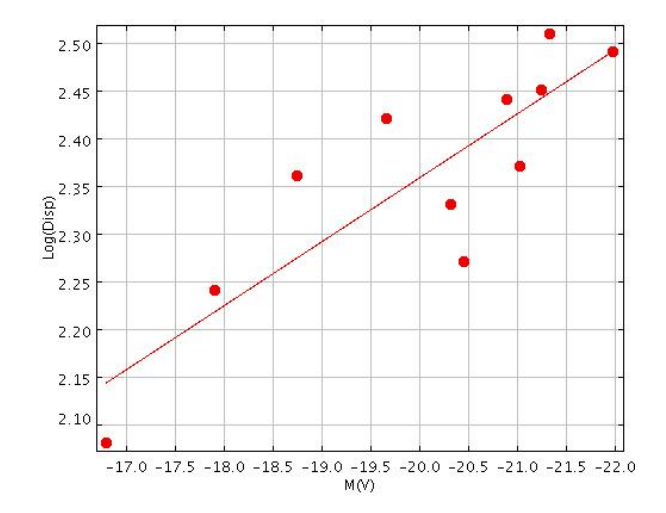
$$\log L = \gamma \cdot \log \sigma + \cos t$$

$$L = L_{sun} \cdot 10^{-0.4(M-M_{sun})}$$

$$\log L = \log L_{sun} - 0.4(M-M_{sun})$$

$$\begin{split} \log L_{sun} - 0.4 \big(M - M_{sun} \big) &= \gamma \cdot \log \sigma + cost \\ \log \sigma &= -\frac{0.4}{\gamma} M + cost \end{split}$$

This is the equation of a straight line having an expected slope of about -0.1. Plotting our data and calculating the linear regression, we obtained a good correlation (r = 0.85), but the slope is equal to -0.067 which corresponds to γ about 6. This is probably due to inaccurate measurements.



Morphological analysis of the galaxy NGC4686

Andrea Bavari, Gaetano Borgese, Francesco Cannarsa, Carlo Damiano Maria Spedicato

Scuola Navale Militare "F. Morosini", Venezia

ABSTRACT

In this work we determined the morphology of the galaxy NGC 4686 by means of the photometric analysis of images extracted from the Sloan Digital Sky Survey public archive.

I. INTRODUCTION

Hubble's morphologic classification, introduced by the american astrophysicist Edwin Powell Hubble in 1925, divides galaxies in four main groups: elliptical galaxies (E), normal (S0) and barred (SB0) lenticular galaxies, normal (S) and barred (SB) spiral galaxies, and irregular galaxies (Irr). The projection of a galaxy onto the sky plane produces a bi-dimensional image, the study of which let us recognize the morphological type of the galaxy considered. To succeed in this process the geometric components of the galaxy are fundamental: bulge, disk, and possible bars or spiral arms. In this report we analyze the images of the galaxy NGC 4686. A method to study the morphology of a galaxy is to analyze its isophotes. The isophotes are ideal lines linking points of a source with the same intensity. Each ellipse is defined by the following parameters: mean intensity (concerning photon counts), centre (x_0,y_0) , semi-major axis (SMA), ellipticity and position angle (the angle between the North direction and the semimajor axis, calculated from North to East). By putting this information in a graph, considering these parameters as a function of the distance from the galactic centre, we can infer the galaxy morphological type. The photon counts collected by the CCD (Charge Coupled Device) have to be converted in apparent magnitudes by subtracting the average sky intensity multiplied by the area of the galaxy in pixels and dividing the result by the exposure time.

II. OBSERVATIONAL DATA

In our morphological study of the galaxy NGC 4686 we used images taken from the Sloan Digital Sky Survey public archive in the u, g, r, i, z bands, covering the visible spectral range.

Here are listed some properties of NGC 4686:

Right Ascension	12h 46m 39.7sec
Declination	+54° 32' 03"
Major Diameter	2.3 arcmin
Apparent Magnitude	13
Constellation	UMa

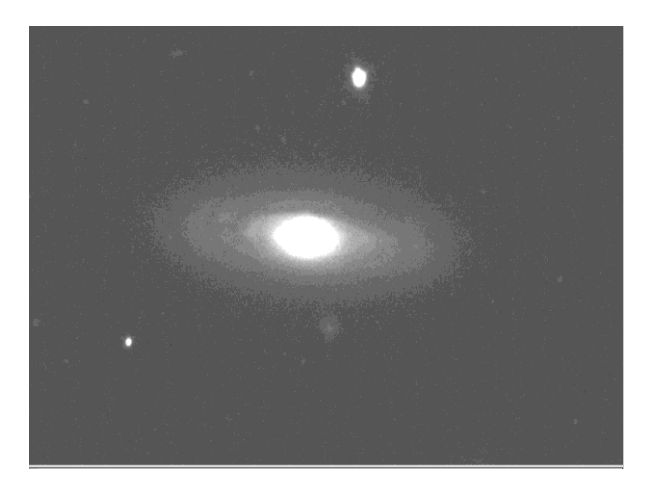


Fig 1: Image of NGC 4686.

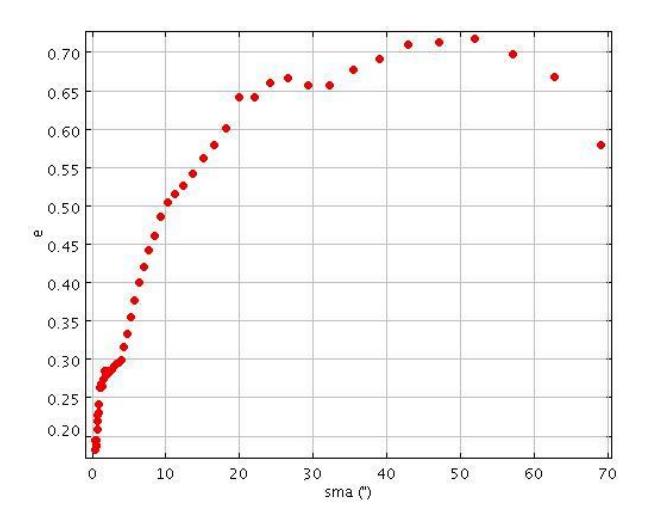
III. WORK DESCRIPTION

The images were analyzed with the IRAF and DS9 softwares. DS9 is the displayer we used to view our images. The IRAF task ELLIPSE was used to reproduce the galaxy's isophotes fitting them with ellipses. In this way, we obtained the morphological parameters of the galaxy, like the ellipticity and the position angle, and also their trend with the distance from the galaxy centre.

The image below shows the trend for the ellipticity defined as:

$$e = 1 - \frac{b}{a}$$

where a is the semi-major axis and b is the semi-minor axis.



In this graph, the SMA is given in arcseconds and it is shown how the ellipticity grows continuously from the centre to the end of the galaxy.

Since for each ellipse we had the mean intensity of the correspondent isophote of the galaxy, this analysis gave us the light intensity as a function of the distance from the centre. With the ellipses we were able to build a model of the galaxy light distribution and subtract it from the original image. The result was an image containing the residuals, which are the deviations from the model (such as bars, spiral arms, etc).

In the two following images are shown the outputs of this procedure.

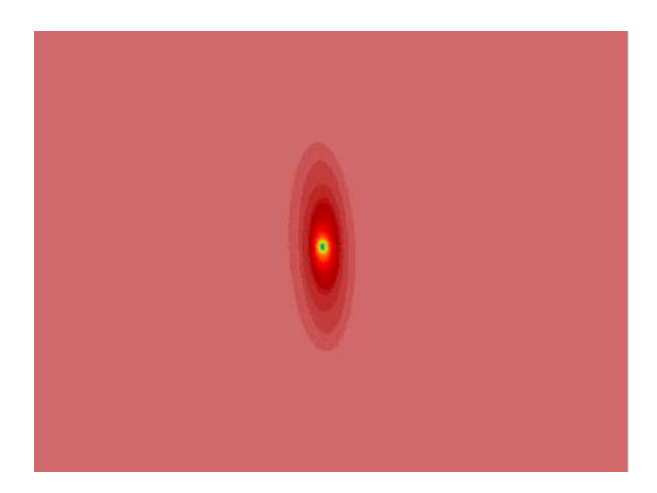


Fig 3: Model given by the interpolation of the ellipses.

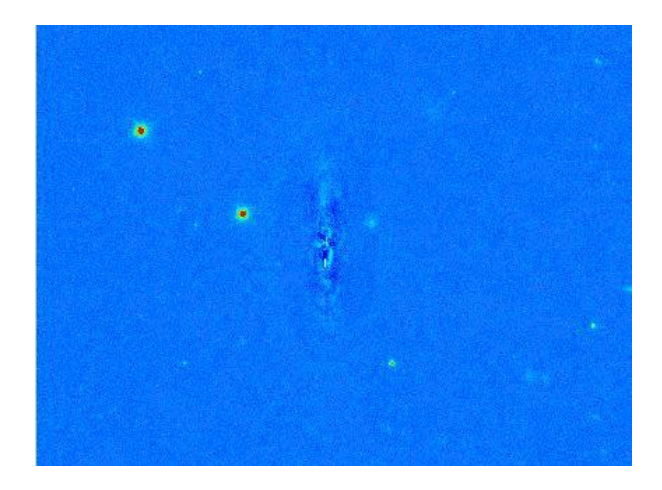


Fig 4: Residuals of the galaxy after the subtraction of the model.

Running again the task ELLIPSE, this time keeping fixed the centre of the ellipses, we recreated the galaxy's brightness profile, which is the surface brightness as a function of the SMA. To do this, we calculated the intensity of the galaxy light contained in every ring between two consecutive ellipses. Then we subtracted the sky intensity multiplied by the number of pixels contained in each ring and divide everything by the exposure time multiplied by the angular area of a pixel, which is in this case 0.4"x 0.4". The surface brightness μ is then given in (mag/arcsec²) by:

$$\mu = -2.5 \log \left(\frac{I_{gal} - I_{sky} \cdot N_{px}}{T_{exp} \cdot Area_{px}} \right)$$

After plotting on a graph the brightness profile, we applied experimental laws and determined their best fit parameters.

In order to find the bulge intensity, we used the effective radius and intensity we had found fitting the previous graph with an exponential law:

$$\Sigma_b = 5.36 \, \Sigma_e \, \mathrm{e}^{-1.68 \, {}^\mathrm{t}/\mathrm{r_e}}$$
 With:
$$r_e = 3.3$$

$$\Sigma_e = 165$$

Therefore the bulge intensity is:

$$I_b = 11.93 \cdot I_e \cdot r_e^2 = 21436$$

In order to find the disk intensity, we used the scale length and the central intensity we had found fitting the previous graph with the Freeman's law:

$$\Sigma_d = \Sigma_0 e^{-r/h}$$

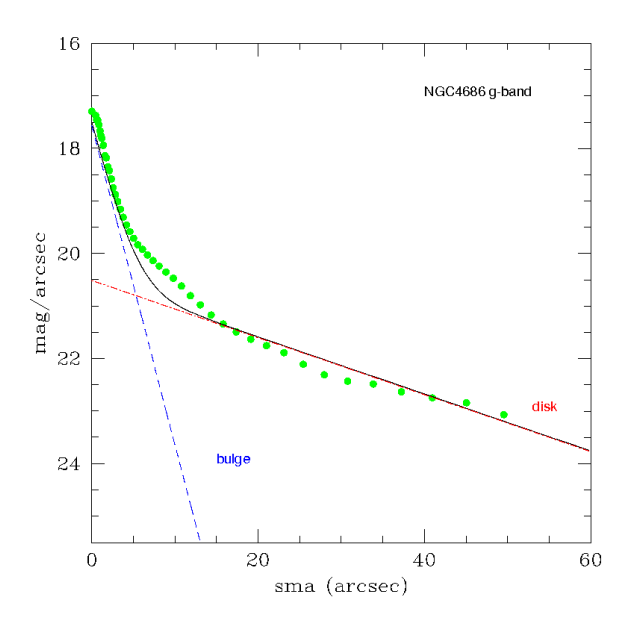
$$h = 20$$

$$\Sigma_0 = 45$$

Therefore the disk intensity is:

$$I_d = 2\pi \cdot I_0 \cdot h^2 = 113097$$

The following graph shows the brightness profile reproduced with an exponential law for the bulge and the Freeman's law for the disk.



We then calculated the intensity of the bulge related to the total intensity. This ratio shows the importance of the bulge component, therefore it gives an idea of the shape and classification of the examined galaxy:

$$\frac{I_{bulge}}{I_{bulge} + I_{disk}} = \frac{21436}{134533} = 0.16$$

Another method to see the importance of each component is to make a colour map by applying the following formula to the r and g fluxes:

$$g - r = 2.5 \log \frac{I_r}{I_g}$$

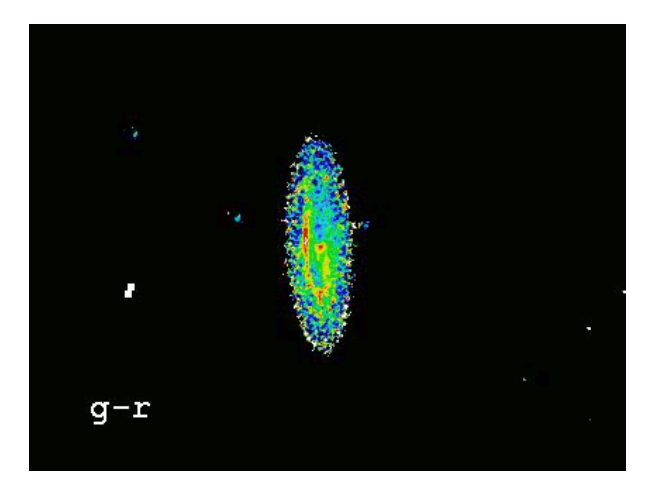


Fig 6: NGC 4686 colour map (g-r).

In order to have a more precise classification, we transformed the previous intensities into instrumental magnitudes through the formula:

$$m = -2.5\log(I)$$

Therefore:

$$m_b = -10.83$$

 $m_d = -12.63$

$$m_{tot} = -12.82$$

We then passed from instrumental (in photon counts) to calibrated (in physical units) magnitudes by correcting for atmospheric extinction, photometric zero point and airmass:

$$m_{cal} = m_0 + m_{inst} - K \cdot X$$

where:

K is the atmospheric extinction coefficient that depends on λ and therefore changes for every photometric band; X is the airmass given by:

$$X = \frac{1}{\cos(\frac{\pi}{2} - h)}$$

where h is the height of the object on the horizon. The calculations gave us:

$$m_{b,cal} = 13.37$$

 $m_{d,cal} = 11.57$
 $m_{tot,cal} = 11.38$
 $\Delta m = m_{b,cal} - m_{tot,cal} = 1.99$

From the difference between the bulge and the total magnitudes and the figure in Simien & DeVaucouleurs (1986) we got a morphological T-type 4 corresponding to a Sbc galaxy.

IV. RESULTS

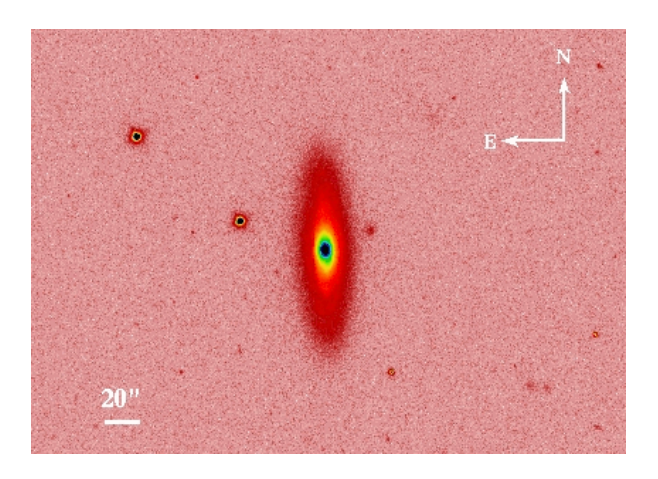
We studied the morphology of NGC 4686 analyzing the radial trend of ellipticity and position angle. This analysis showed that this object does not have a bar.

By fitting the brightness profile with various laws, we can infer that the galaxy has two components: a bulge and a disk.

The small ratio between the bulge intensity and the total intensity is typical of a non prominent bulge.

Based on these results we can classify NGC 4686 as a Sbc galaxy.

Our results do not agree with those in literature, being the galaxy is classified as Sa.



Morphological study of elliptical galaxies

Silvia Guerra⁽¹⁾, Matteo Mannino⁽²⁾, Enrico Paccagnella⁽³⁾

(1) ITIS "F. Severi", Padova (2) Liceo "I. Nievo", Padova (3) Liceo "Tito Livio", Padova

E tenebris tantis tam clarum extollere lumen (Lucrezio, "De rerum natura", III)

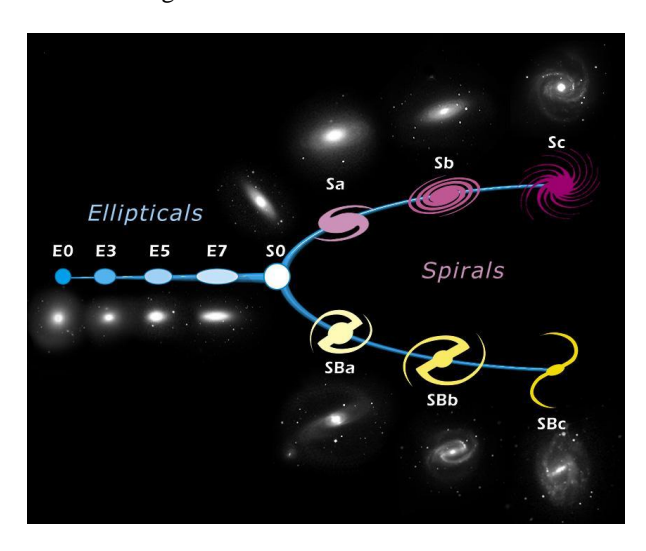
ABSTRACT

The analysis of the brightness profile is a method that allows to study the morphology of galaxies. The aim of our work was to identify elliptical galaxies using this method. We chose galaxies with redshifts between 0.01 and 0.05, in order to work with relatively nearby objects.

I. INTRODUCTION

Galaxy morphological classification is a widely used system in astronomy; following this method galaxies are divided into four groups, based on their shape:

- Ellipticals
- Spirals
- Lenticulars
- Irregulars



Edwin Hubble classification scheme (also known as Hubble tuningfork diagram).

We decided to work on elliptical galaxies, so called because of their ellipsoidal shape, which range from circular (E0) to elongated, narrow, and cigar-shaped (E7). This type of galaxies is mainly composed of old stellar populations, distributed homogeneously, which

give them red colors; their brightness decreases from center to boundaries.

Visual classification of elliptical galaxies might not be so easy, especially in case of low resolution images. To be sure of a correct morphological classification, we had to compare our data with an experimental law, discovered by the French astronomer De Vaucouleurs.

II. OBSERVATIONAL DATA

Because of bad sky conditions we could not make any direct observation at the telescope. Instead, we based our research on archival data we extracted from the website of the Sloan Digital Sky Survey (http://www.sdss.org/dr7/). We made the first selection looking for galaxies that seemed to be elliptical, without bars or any spiral structure. We chose galaxies with redshift between 0.01 and 0.05 to study nearby objects.

Galaxy name	Redshift
SDSS J135039.09+350217.9	0.021
SDSS J133440.34+325704.0	0.024
SDSS J161845.79+392004.0	0.032
SDSS J153215.71+092755.9	0.033
SDSS J162754.90+403621.9	0.033
SDSS J105807.60+091634.0	0.034
SDSS J080550.30+372736.1	0.034
SDSS J093118.81+444647.3*	0.035

SDSS J030352.91+002454.9	0.043
SDSS J124622.67+115235.7	0.044
SDSS J141532.92+501051.7	0.044
SDSS J084051.14+315853.4	0.047
SDSS J075638.85+440741.0	0.047
SDSS J100910.07+541331.9	0.048

III. WORK DESCRIPTION

First of all, we made a visual selection of the galaxy images on the basis of their shape.

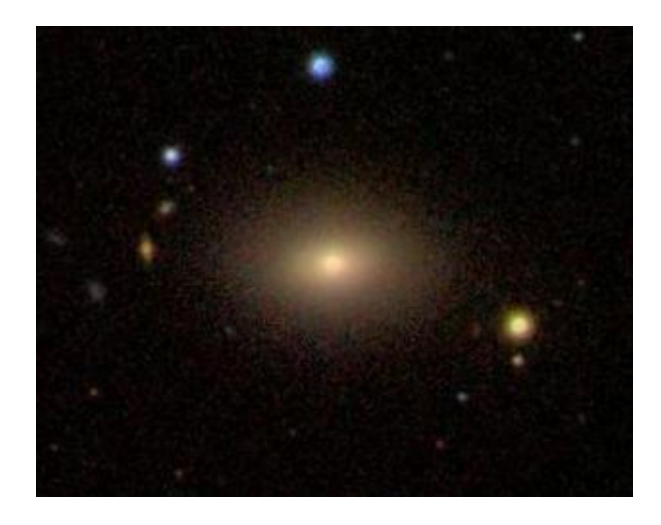
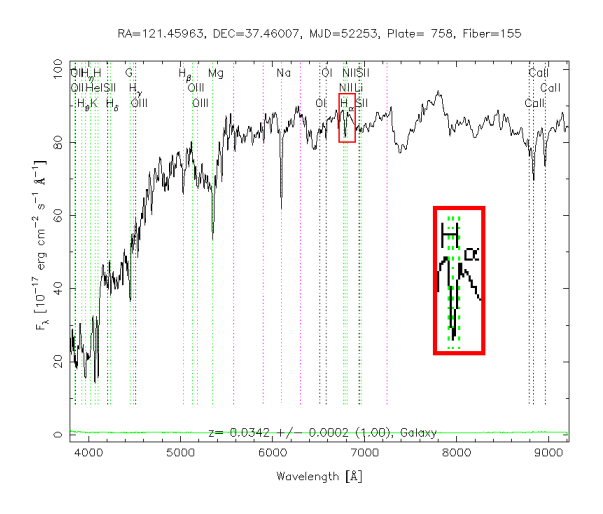


Image of the galaxy SDSS J161845.79+392004.0.

Then we analysed the spectrum of these galaxies, to check if it had an absorption line at the wavelength of the $H\alpha$ line, because the temperature of population II stars is not high enough to cause emission lines.

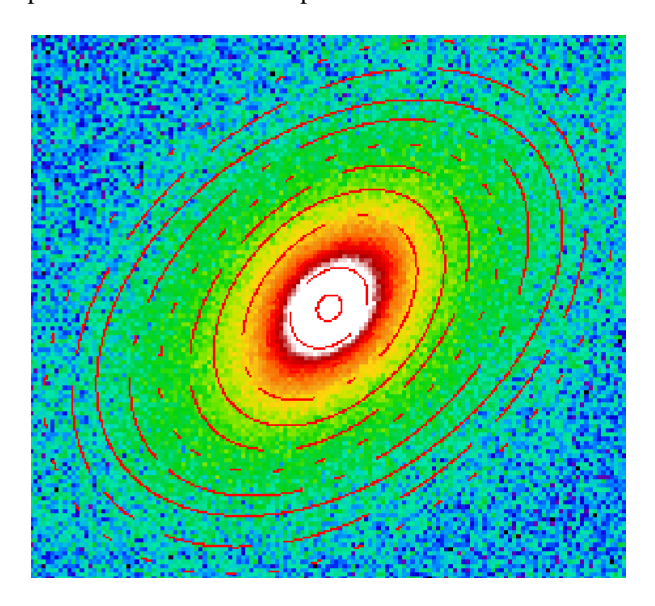


Spectrum of the galaxy SDSS J080550.30+372736.1.

Before describing the technique used to study the galaxies, a definition of "isophote" is necessary.

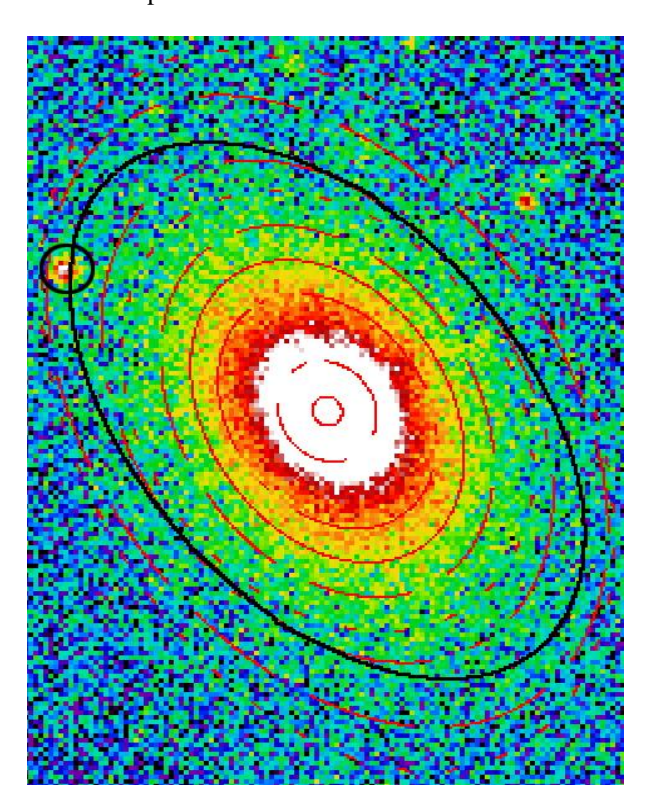
An isophote is an ideal curve joining points of equal light intensity from a given source. These lines rarely define regular shapes, but the real light distribution; we approximated the isophotes with ellipses to simplify our analysis.

The first step was to fit the isophotes of the galaxies we studied, using IRAF software, giving the coordinates of the centre of the galaxy and the values of the geometric parameters of the first isophote.



Isophotes for the galaxy SDSS J161845.79+392004.0.

It was necessary to pay attention to bright sources close to each galaxy, which could modify the fit of the external isophotes.



Isophotes for the galaxy SDSS J075638.85+440741.0.

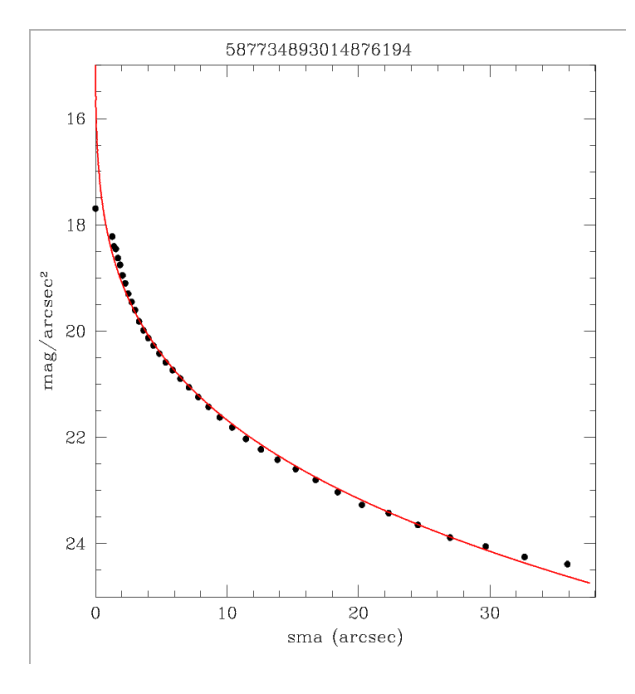
Then we calculated the magnitude of each galaxy, considering the total intensity within the most external isophote. We also removed the brightness of the sky and we took into account the exposure time of the image, using this formula:

$$m = -2.5 \log \left(\frac{I - I_{sky} \cdot N_{px}}{T_{exp}} \right) + cost$$

where I is the intensity within the isophote that contains all the galaxy, I_{sky} is the average intensity of the sky, N_{px} is the number of pixels contained in the isophote and T_{exp} is the exposure time.

Then, we obtained the graph of the surface brightness profile $(mag/arcsec^2)$ as a function of the radius, by calculating the intensity of the galaxy in each ring between an isophote and the following one, and taking into account the area of the sky covered by each pixel (in our case 0.4×0.4 arcsec):

$$\mu = -2.5 \log \left(\frac{I - I_{sky} \cdot N_{px}}{T_{exp} \cdot Area_{px}} \right) + cost$$



Graph of the De Vaucouleurs' equation for the galaxy SDSS J105807.60+091634.0.

On the graph derived from the data of the isophotes (black dots) we fitted the De Vaucouleurs' equation (red line):

$$I = I_e \cdot e^{-7.67 \left[\left(\frac{R}{R_e} \right)^{\frac{1}{4}} - 1 \right]}$$

$$\mu = -2.5 \log I + \cos t = \mu_e + 8.32 \left[\left(\frac{R}{R_e} \right)^{\frac{1}{4}} - 1 \right] + \cos t$$

where R_e is the effective radius, within which half of the total light of the system is contained, I_e is the surface intensity at R_e and μ_e is the surface brightness at R_e .

We had to find experimentally the value of these two parameters, in order to find the De Vaucouleurs' equation which better approximates the brightness profile of elliptical galaxies.

IV. RESULTS

Experimental results confirmed our first selection. Only one out of the 14 studied galaxies was not an elliptical.

We managed to find effective radius and surface intensity with great accuracy.

Galaxy name	I _e (cts/arcsec ²)	r _e (arcsec)
SDSS J135039.09+350217.9	7.5	11.7
SDSS J133440.34+325704.0	5.5	10.5
SDSS J161845.79+392004.0	8.5	9
SDSS J153215.71+092755.9	8.5	7.7
SDSS J162754.90+403621.9	40	2
SDSS J105807.60+091634.0	5.2	12.5
SDSS J080550.30+372736.1	6.4	6.6
SDSS J093118.81+444647.3*	2	15
SDSS J030352.91+002454.9	4	15
SDSS J124622.67+115235.7	5.8	11.4
SDSS J141532.92+501051.7	8	7
SDSS J084051.14+315853.4	6	8
SDSS J075638.85+440741.0	1.5	20.5
SDSS J100910.07+541331.9	4	11.3

Inaccuracies were sometimes due to close bright sources that might be the cause of the presence of deviations from the De Vaucouleurs' profile.

Studying the galaxy 587732054858137697* we were not able to reproduce the brightness profile with the De Vaucouleurs' law, as clearly visible from the graph reported below.

Our conclusion is that this galaxy is not an elliptical, despite the initial hypothesis we made by analysing its image and spectrum.

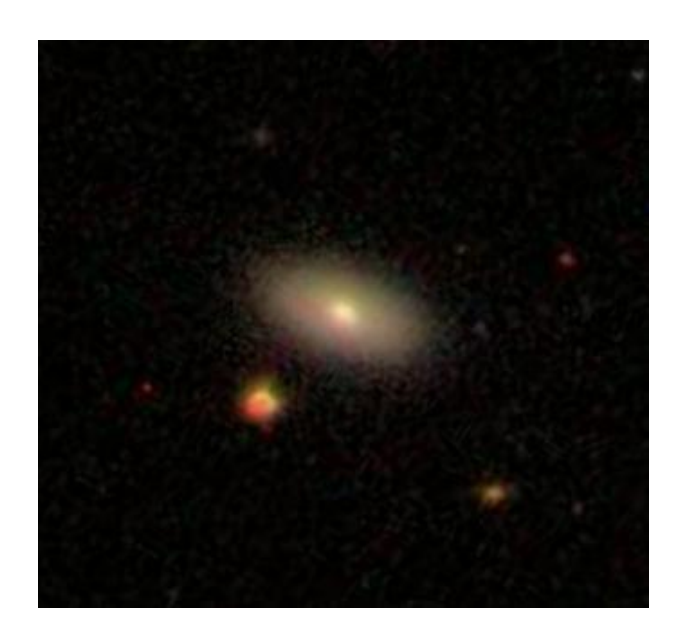
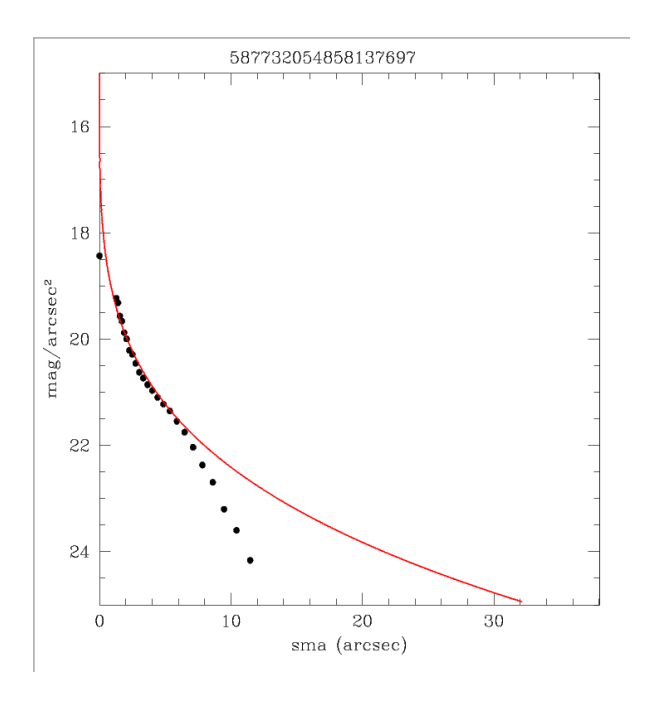
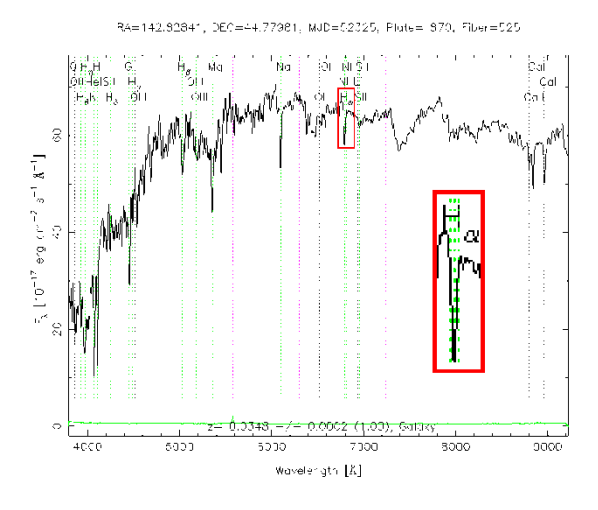


Image of the galaxy SDSS J093118.81+444647.3*.



Graph of the De Vaucouleurs' equation for the galaxy SDSS J093118.81+444647.3*.



Spectrum of the galaxy SDSS J093118.81+444647.3*.

Morphology of the galaxies around the X-ray source 2MASXJ14391186+1415215 through GIM2D

Alessandro Baccarin, Laura Gavagna, Carlo Alberto Soncin

Liceo "G. Veronese", Chioggia

ABSTRACT

We considered a group of galaxies in the constellation of Bootes and we studied the r-band photometry of these objects, in order to obtain their morphological classification. We developed a model using GIM2D and, by means of the information provided by this program, we determined the morphological type of each galaxy, the brightness values of their bulge and disk, if any.

I. INTRODUCTION

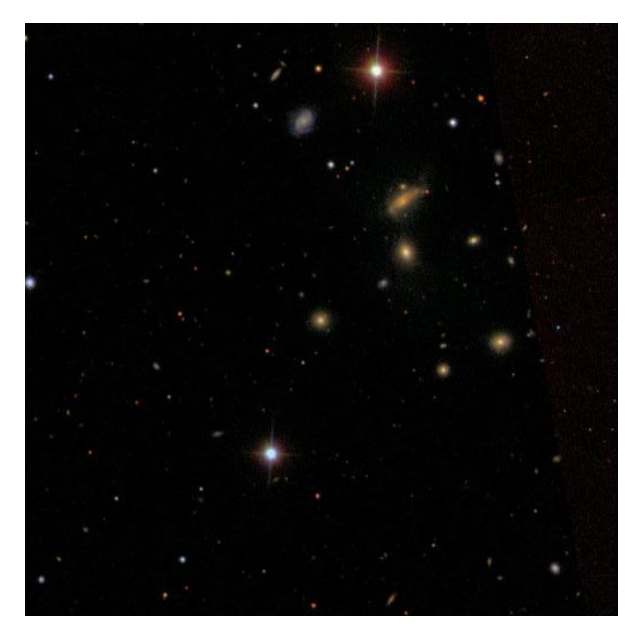


Fig 1: The Sloan Digital Sky Survey image of the studied galaxies.

Studying the morphology of a group of galaxies means to classify these objects according to their shape. The morphological classification is the first step to understand the physics of galaxies. In order to do this, we considered the Hubble sequence, the classification scheme which divides the galaxies in four different families: elliptical, lenticular, spiral and irregular. The spiral galaxies are composed of a bulge and a disk with at least two spiral arms or structures extending from the

bulge. They are indicated with the letter S followed by the letters a, b, c, that depend on the prominence of the bulge with respect to the disk, the wrapping of spiral arms, and the resolution of the disk. The elliptical galaxies are classified with letter E and with a number that can have values from 0 to 7 depending on the eccentricity. These galaxies have a diffused structure and do not have any disk. The lenticular galaxies S0 are intermediate between elliptical and spiral, and different from the latter because their disk contains few interstellar matter, and do not show any spiral structure. Finally there are also peculiar galaxies, known as irregular galaxies, that just have an irregular shape, sometimes due to interaction with other galaxies.

The programs we used to do this work were: IRAF: used to view and analyze the images; GIM2D: used to perform the decomposition of a galaxy into bulge and disk by using mathematic models.

II. OBSERVATIONAL DATA

We used r-band images of a group of galaxies around the X-ray source 2MASX J14391186+1415215 extracted from the archive of the Sloan Digital Sky Survey. The group under examination had never been studied before, for this reason these galaxies have no name. We only knew that they all are in the constellation of Bootes. Here we report the celestial coordinates of each object studied:

	RA	DEC
A	14 39 17.5	+14 16 18.3
В	14 39 21.3	+14 15 10.7
С	14 39 15.1	+14 16 29.0
D	14 39 11.9	+14 15 22.1
Е	14 39 10.9	+14 17 24.9

Tab 1: Coordinates of the galaxies belonging to the group we studied.

III. WORK DESCRIPTION

To analyze our galaxies we used GIM2D (Galaxy Image Two Dimensional), a program that uses the images of galaxies and builds detailed models of these celestial objects by using information such as the brightness of the bulge and of the galactic disk.

First, the atmospheric turbulence (seeing effect) on the images must be taken into account, because it causes a deterioration on the quality of the images of the observed astronomical objects. In particular, we have to create a model of the point spread function (PSF), that is a model of the stellar shape: in fact, stars should be point-like sources, but they appear as extended circular spots because of the seeing effect. Since seeing affects also galaxy images, modeling mathematically some stars, we have the information to apply in order to obtain the right models of the galaxies.

Each pixel is represented by a number that indicates the quantity of photons received by the detector. The instrumental magnitude let us know the exact number of photons emitted by the galaxy collected by the CCD. Its value m_s is given by the formula:

$$m_s = -2.5 \cdot \log \left(\frac{I - N_{px} \cdot I_{sky}}{T_{exp}} \right)$$

where I = intensity of the galaxy, N_{px} = number of pixels occupied by the galaxy, I_{sky} = intensity of the sky and T_{exp} = exposure time.

The so obtained magnitude must be further corrected with the following relationship: $m = m_s + m_0 - k \cdot X$, where m_0 = photometric zero point. It is a constant depending on the used filter. In our case, for the r filter m_0 = 24.037 mag; k is the atmospheric extinction coefficient and it is inversely proportional to the wavelength: k = 0.136. X = 1/cosec z is the airmass, where z is the distance of the target from zenith: X = 1.112. Subtracting $k \cdot X$ from the magnitude, we obtain a value corrected for atmospheric extinction.

We worked mainly with two functions: the Sersic's Law and the Freeman's Law. Both of them represent the brightness of galaxies, namely the surface brightness measured along the major axis of the galaxy: the first one is used for the bulge, the central component of the galaxy, and the other one for the galactic disk.

Sersic's Law:
$$S = S_e \exp \{-b[(R/R_e)^{1/n} - 1]\}$$

R is the distance from the center of the galaxy, and it is a variable. $R_{\rm e}$ is the effective radius, the radius within which half of the light of the bulge is contained. n is called Sersic index. $b_{\rm n}$ is a constant which depends on the value of n. Finally, $S_{\rm e}$ is the surface intensity at the distance $R=R_{\rm e}$

For n = 4 we obtain the De Vaucouleurs' law, which reproduce the surface brightness profile of elliptical galaxies:

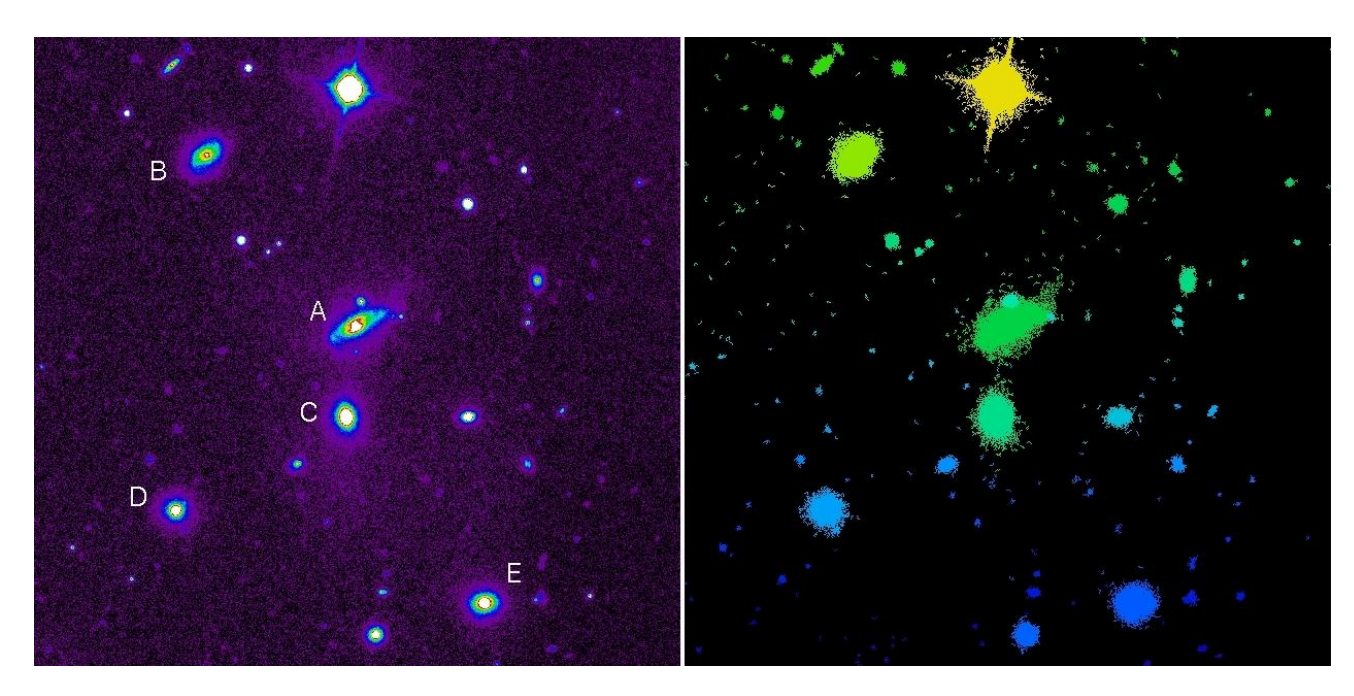


Fig 2: Legenda and Mask of our galaxies.

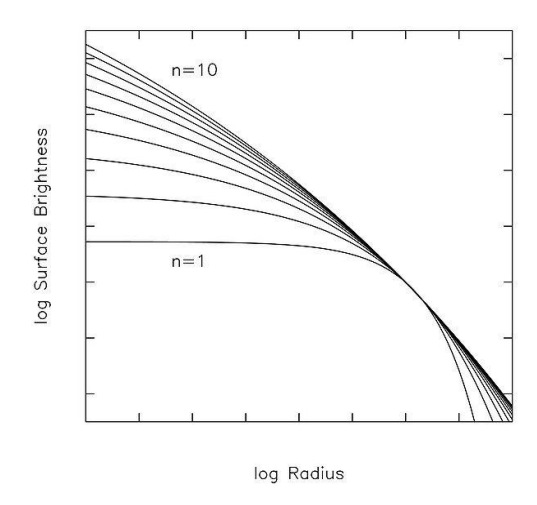


Fig 3: Sérsic models with different indices n.

De Vaucouleurs' Law: $I = I_e \exp \{-7.67[(R/R_e)^{1/4} - 1]\}$

where I_e = surface brightness at R_e .

For n=1 we obtain the exponential profile often used for the bulge of spiral galaxies:

$$I = 5.36 I_e \exp \{-1.68 (R/R_e) \}$$

Freeman's Law:

$$S = S_0 \exp(-R/h)$$

where R is the distance from the centre, and it is a variable. h is the scale length of the disk $(R = h \Rightarrow S = S_0/e)$

The model developed by GIM2D gave us information about the total brightness (L_{tot}) and the relationship between the bulge brightness and the total brightness of the galaxy (B / T).

Then we calculated $\Delta m = -2.5 \log (B/T)$ and thanks to the following graph, we could determine the morphological type of each galaxy.

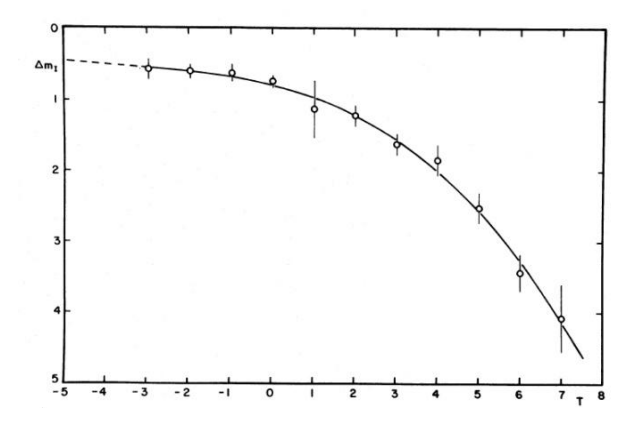


Fig. 4: Plot taken from Simien & De Vaucouleurs (1986).

T	-5	-3	-2	0
Type	Е	E-S0	S0	S0/Sa

T	1	2	3	4	5
Type	Sa	Sab	Sb	Sbc	Sc

Tab. 2: T-type and morphological classification.

Gal.	Ltot	B/T	Morph.	L bulge	L disk
			type		
A	149329	0.49	S0/Sa	74266	75063
В	66950	0.12	Sc	8283	58667
С	130512	0.92	Е	119985	10527
D	63303	0.44	S0/Sa	28177	32126
Е	89512	0.32	Sa	28724	60788

Tab. 3: Results of the fitting.

We determined the value of the brightness for bulge and disk of individual galaxies using the following formulae:

$$\begin{split} L_{bulge} &= L_{TOT} \cdot (B/T) \\ L_{disk} &= L_{TOT} - I_{bulge} \end{split}$$

Finally, we used GIM2D again, changing a bit the input parameters in order to check for possible influence on the results. We confirmed the results previously obtained for all galaxies except A, that was found to be an Sc rather than an Sa.

Gal.	Ltot	B/T	Comparison with fit	Morphological type
A	126666	0.09	Different	Sc
В	663645	0.01	Ok	Sc
С	131026	0.93	Ok	Е
D	63315	0.46	Ok	S0/Sa
Е	89457	0.32	Ok	Sa

Tab. 4: Additional test obtained changing input parameters.

IV. RESULTS

Galaxies A and B resulted to be two spirals of type c, galaxy C is an elliptical, D is an intermediate between a S0 and a Sa and finally E is a Sa.

Fig 5 shows the results provided by GIM2D: in the first line are drawn the images of our five galaxies. The second line reports the model of the galaxies, elaborated by the program. Finally, the last line contains the residuals, the differences between image and model.

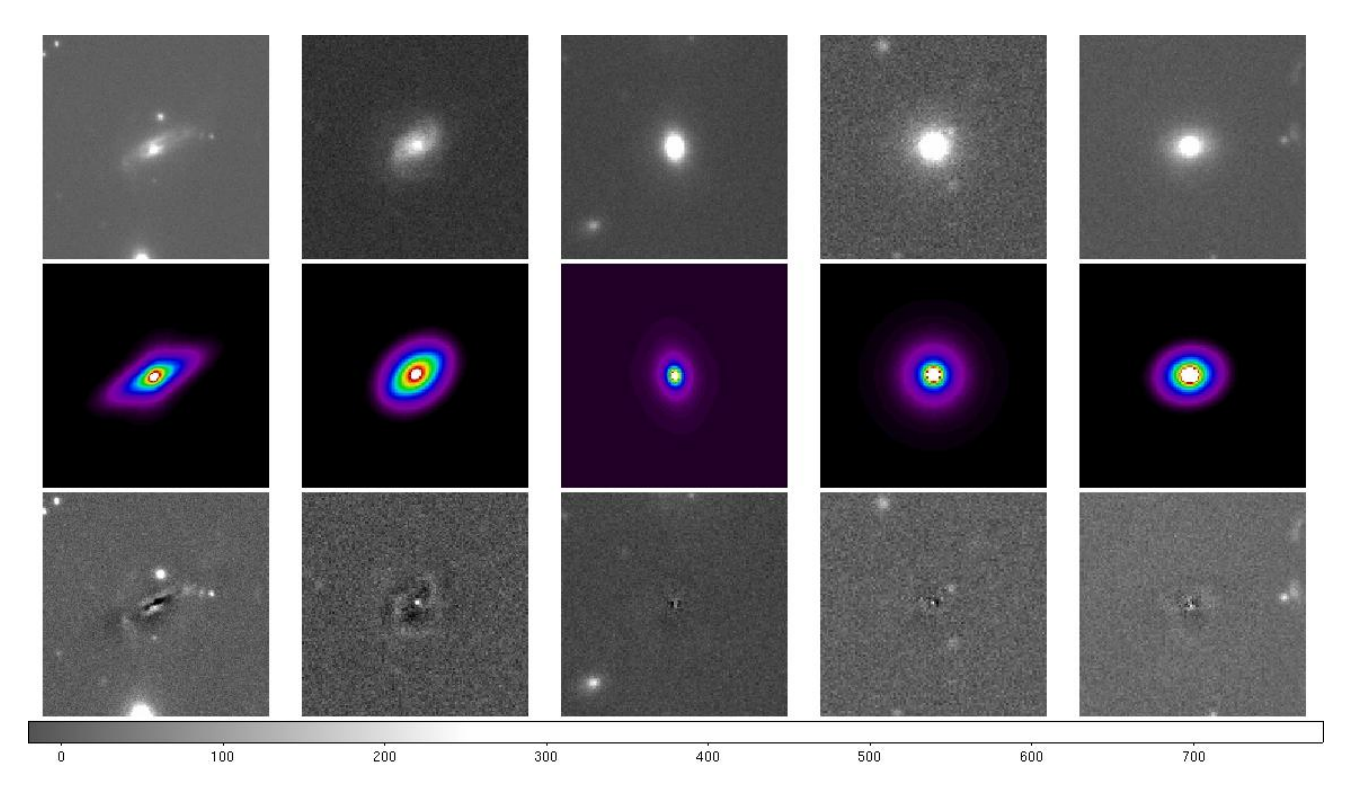


Fig. 5: on the three lines are placed the images of galaxies, the models developed by GIM2D, and the residuals.

V. BIBLIOGRAPHY

"Geosfera, La Terra e lo spazio", Rita Cavallone Peretti, editore Bulgarini Firenze, 2007

Simien & De Vaucouleurs, Astrophysical Journal v.302, p564, 1986

Sloan Digital Sky Survey: http://www.sdss.org/www.wikipedia.org

National Radio Astronomy Observatory: www.nrao.edu

Astronomy Department, University of Padova: http://dipastro.pd.astro.it/

Velocity dispersion in elliptical galaxies

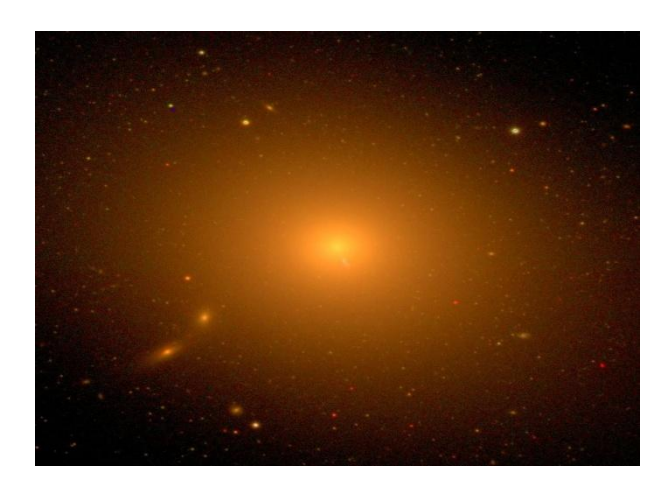
Valentina Guglielmo, Nicola Amoruso, Angelo Colombo

Liceo scientifico "E. Curiel", Padova

ABSTRACT

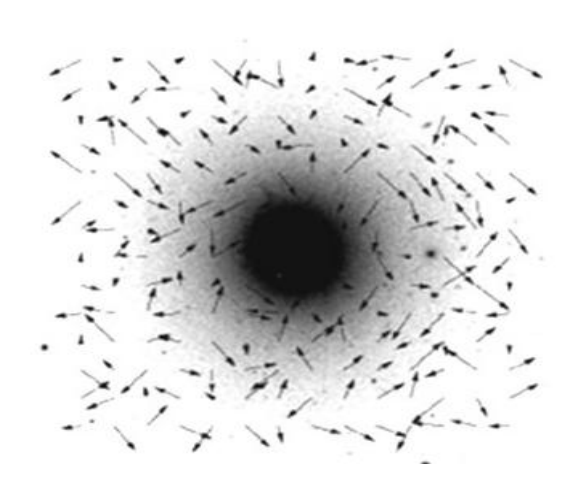
The aim of our experience is to calculate the velocity dispersion of the stars in elliptical galaxies through the cross-correlation technique, undertaken by Tonry and Davis (1979). Relating this parameter to the effective radius, obtained by morphological analysis, it is also possible to calculate the mass of the galaxy, and verify how mass and velocity dispersion are related.

I. INTRODUCTION



An elliptical galaxy has an approximately elliptical shape and is composed mostly of old stellar populations (classes GKM). Its spectrum is the sum of the spectra of the stars which is made of. The stars of elliptical galaxies have a chaotic motion and the radial components of their velocity vectors generate shifts in their spectra. The result is the sum of similar but differently shifted spectra, which produce a broadening of the absorption lines. This information allows us to apply the cross-correlation technique, which consists of making a comparison between a galaxy spectrum and an old star spectrum, used as a template to determine the velocity dispersion which gives an indication about the chaotic orbits of stars around the centre of mass of the galaxy.

Velocity dispersion grows with mass: the more massive the galaxy is, the more gravity makes the motion chaotic.



II. OBSERVATIONAL DATA

The data were taken from the database of the Sloan Digital Sky Survey (www.sdss.org) because bad weather conditions did not allow us to observe the sky directly. This archive contains data of about 230 million astronomical objects like stars, galaxies and quasar, contained in a quarter of the sky and taken by a 2.5m telescope situated in the Apache Point Observatory, New Mexico.

Searching among the red galaxies with redshift between 0 and 0.1, to guarantee a sufficient spatial resolution, we selected 13 elliptical galaxies. The selection was made observing both images and spectra (which contain data of the central zone of the galaxy, about 3"), in which the H α line had to be in absorption. This happens because the photosphere of the stars is colder than the inner layers, so it absorbs part of the radiation which goes through it. Then, the radiation is re-emitted, but in a different direction, causing lack of light at some wavelength, so the stellar spectrum has a Planck curve shape with many absorptions.

Elliptical galaxies are dominated by old stars light, therefore their spectra are similar to a mix of a G and K star spectrum. In spiral galaxies, where often hot stars are present, there are large zones of ionized gas which produce spectra with emission lines.

We downloaded spectra and redshift values of the following galaxies.

nr	Galaxy name	Redshift
1	SDSS J135039.09+350217.9	0.021
2	SDSS J133440.34+325704.0	0.024
3	SDSS J161845.79+392004.0	0.032
4	SDSS J153215.71+092755.9	0.033
5	SDSS J162754.90+403621.9	0.033
6	SDSS J105807.60+091634.0	0.034
7	SDSS J080550.30+372736.1	0.034
8	SDSS J030352.91+002454.9	0.043
9	SDSS J124622.67+115235.7	0.044
10	SDSS J141532.92+501051.7	0.044
11	SDSS J084051.14+315853.4	0.047
12	SDSS J075638.85+440741.0	0.047
13	SDSS J100910.07+541331.9	0.048

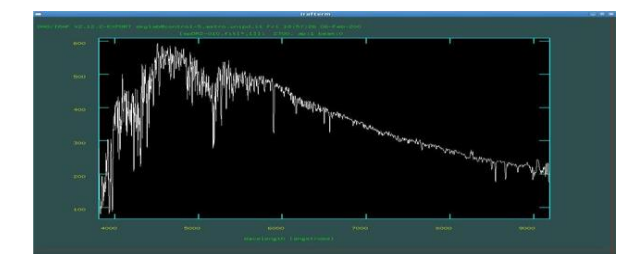


Fig. 3: Spectrum of the template star.

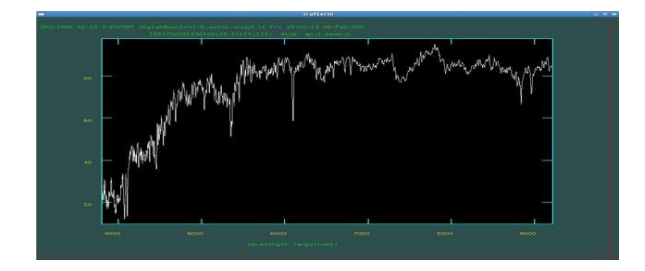
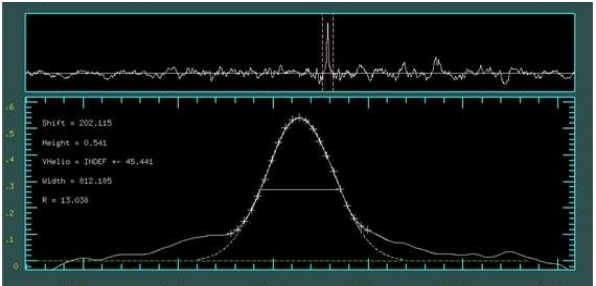


Fig. 4: Example of spectrum of an elliptical galaxy.

III. WORK DESCRIPTION

Once we selected the galaxies spectra to study, we compared them with the template star, subtracting from both spectra their continua and removing their different shapes.

The comparison was made with the program FXCOR of IRAF package, which decomposes every signal in a sum of sinusoidal functions through the Fourier transformation⁽¹⁾. The product of the transformed signals generates the correlation function, which is similar to a Gaussian function. The stronger the



correlation is, the higher the peak of the curve is, to a maximum of 1 for the perfect correlation, i.e. autocorrelation.

More in detail, the peak height is index of the superposing grade of the two spectra: it depends on the presence of the same absorption or emission lines.

The program also measures the width of the peak at the middle height (FWHM), which is useful to calculate the velocity dispersion.

First of all we need to calculate the intrinsic FWHMi:

$$FWHMi = \sqrt{FWHM^2 - FWHMa^2}$$

where FWHM is obtained correlating galaxy and template, while FWHMa is the autocorrelation of the template spectrum.

Once the intrinsic FWHMi is calculated, the velocity dispersion can be found with the following formula:

$$\sigma = \frac{\text{FWHMi}}{2.35}$$

Once every galaxy dispersion is measured, we calculated the average and standard deviation, which gives an indication about how much the average is representative of the measurements:

$$\overline{\sigma} = \frac{\sum \sigma_i}{N} \qquad \sigma = \sqrt{\frac{\sum (\sigma_i - \overline{\sigma})^2}{(N-1)}}$$

To calculate the mass we used the formula⁽²⁾:

$$M = \frac{r_{\rm e} \cdot \sigma^2}{0.33 \cdot G}$$

Where r_e is the effective radius, i.e. the radius within which half of the galaxy light is contained and it gives an estimate of the luminosity distribution of the stars (the shorter the radius is, the more stars are concentrated in the centre of the galaxy); its value had been calculated in arcsec by Guerra, Mannino, Paccagnella (see their report *Morphological study of elliptical galaxies*) and then converted into km by means of the distance D:

$$D = \frac{c \cdot z}{H_0}$$

where z is the redshift and $H_0 = 72 \text{ km s}^{-1} \text{ Mpc}^{-1}$ is the Hubble constant, and the scale in Mpc/arcsec:

$$scale = \frac{D}{206265}$$

Every value obtained was put in the following table:

nr	D(Mpc)	D(Km)	Ref(")	Scale	Ref(Km)
1	87.5	2.7E+21	11.7	1.31E+16	1.53E+17
2	100.	3.09E+21	10.5	1.5E+16	1.57E+17
3	133.33	4.12E+21	9.0	2.0E+16	1.8E+17
4	137.5	4.25E+21	7.7	2.06E+16	1.59E+17
5	137.6	4.25E+21	2.0	2.06E+16	4.12E+17
6	141.7	4.38E+21	12.5	2.12E+16	2.65E+17
7	141.7	4.38E+21	6.6	2.12E+16	1.4E+17
8	179.2	5.54E+21	15.0	2.68E+16	4.03E+17
9	183.3	5.67E+21	11.4	2.75E+16	3.13E+17
10	183.3	5.67E+21	7.0	2.75E+16	1.92E+17
11	195.8	6.05E+21	8.0	2.93E+16	2.35E+17
12	195.8	6.05E+21	20.5	2.93E+16	6.01E+17
13	200.	6.18E+21	11.3	3.0E+16	3.39E+17

In order to have a comparison term with our sample, we analyzed other galaxies. We found a clear spiral galaxy showing a very low correlation peak, likely due the fact that its spectrum, mainly formed by young stars (OB spectral class), is very different from that of the template star. Other galaxies had uncertain morphology and were discarded. In other cases the correlation gave values similar to those of the ellipticals, but this does not mean that they actually are elliptical. The stellar velocity dispersion, the effective radius and the mass were calculated only for the elliptical galaxies.

IV. RESULTS

We selected 13 elliptical galaxies to measure the stellar velocity dispersion and calculate their mass.

We compared the nuclear spectra of these galaxies with template star spectra by means of the cross-correlation method to determine the stellar velocity dispersion.

The average σ value is 250 \pm 50 km/s. The effective radius of the same galaxies were measured by our colleagues who studied their morphology.

Finally we applied the Virial theorem to estimate the total mass.

The average M value (in solar masses) is $4 \pm 3 \cdot 10^{11}$. The values are listed in the following table.

nr	M (Mo)	R (")	σ (Km/s)
1	4.95E+10	2.00	229.96
2	1.01E+11	11.70	169.88
3	1.22E+11	10.50	184.96
4	1.48E+11	6.60	215.48
5	2.24E+11	9.00	234.43
6	2.28E+11	11.30	172.21
7	2.77E+11	7.70	277.47
8	3.05E+11	7.00	264.41
9	4.19E+11	8.00	280.18
10	6.35E+11	12.50	324.57
11	6.73E+11	11.40	307.71
12	8.47E+11	15.00	304.30
13	1.00E+12	20.50	270.59

V. BIBLIOGRAPHY:

All data were found in:

- -Sloan Sky Digital Survey archives;
- -Theoretical issues given during the course:
- -The article "A Survey of Galaxy Redshifts. Data Reduction Techniques" by Tonry and Davis, The Astronomical Journal, vol. 84, num. 10, october 1979.

VI. NOTES

$$F(a) = \frac{1}{\sqrt{2\pi}} \int_{-\infty}^{\infty} f(u) e^{iau} du$$

2. The formula used to calculate the mass comes from the Virial theorem, following the relation:

$$2E_k + U = 0$$

$$Mv^2 - \frac{GM^2}{r} = 0$$

$$M = v^2 \frac{r}{G}$$

$$v = const \cdot \sigma$$

$$M = \sigma^2 \frac{r}{G} \cdot \frac{1}{0.33}$$

Photometric redshifts of the galaxies near the X-ray source 2MASX J14391186+1415215

Alvise Bastianello⁽¹⁾, Francesca Carnesecchi⁽¹⁾, Paolo Corposanto⁽¹⁾, Anna Vera Milner⁽²⁾

(1) Liceo Scientifico "Benedetti", Venezia (2) Liceo Classico "Polo", Venezia

ABSTRACT

The aim of this work is to measure the distance of some galaxies belonging to what appears to be a small group, and so to determine which ones are only prospectively aligned. The distance was obtained by Hubble's law and the recession velocity of the galaxies, by comparing their broadband ugriz photometric data to rest-frame template spectra of galaxies with different morphology.

I. INTRODUCTION

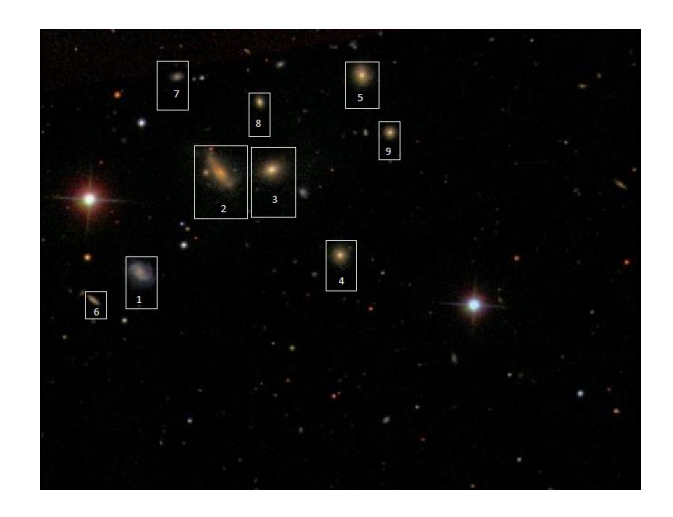
The recession of the galaxies is a common phenomenon of every zone of the sky. It is a motion that, keeping the same characteristics, could be seen from any part of the Universe.

An empirical observation leads to fix a directly proportional dependence between the recession velocity of the galaxy and its own distance. This experimental law is called Hubble's law. In order to determine the recession velocity, the spectral shift expected by Doppler's effect is exploited: the apparent frequency of an electromagnetic wave, emitted by a source moving relatively to the observer, changes from the measured frequency of the source at rest, depending on the velocity. In particular, if the source and the observer are approaching to one another an apparent increase of the frequency is noticed, vice versa a decrease is noticed. Being the galaxies all receding the spectrum appears shifted towards lower frequencies. This phenomenon is called *redshift*.

II. OBSERVATIONAL DATA

The data were extracted from the public archive of the Sloan Digital Sky Survey (SDSS). They consist of images of the same field around the X-ray source 2MASX J14391186+1415215 obtained with broadband filters u, g, r, i, z, which cover the spectral regions from near-ultraviolet to near-infrared. Nine objects were selected having been certainly identified as galaxies.

The considered galaxies are highlighted in the following figure. A number is associated to each of them in order to easily identify them.



III. WORK DESCRIPTION

First of all we need to reconstruct the spectrum of the observed galaxies. This is done by means of a photometric analysis, which allows us to determine a flux value for each galaxy in each broadband filter (ugriz). We applied the software SExtractor (Source-Extractor) to our images, which is a program that builds a catalogue of objects for each analyzed frame. This program identified the galaxies, by using the parameters we had previously set, and calculated the

counts detected for each source, subtracting the sky contribution.

Galaxy	u (3551 Å)	g (4686 Å)	r (6165 Å)	i (7841 Å)	z (8931 Å)
1	1456.0	47308.0	57841.9	63956.2	11590.4
2	1222.3	50396.1	108338.0	144327.0	33052.2
3	2746.2	61701.9	112801.0	142925.0	30159.0
4	1042.5	28606.7	54781.3	72735.7	15901.1
5	1985.0	45274.4	81062.4	102823.0	23172.9
6	251.3	6288.8	11020.5	14164.5	3420.9
7	140.4	6775.1	9873.0	10791.6	1771.0
8	661.7	15086.9	27824.3	33527.8	7641.5
9	689.2	17178.1	31206.1	39987.8	9175.9

The so-obtained flux is still in photon counts and has to be converted in magnitudes. Therefore, if the instrumental magnitude of the target per time unit is given by the formula:

$$m_{t} = -2.5 \log \left(\frac{E}{t_{\rm exp}} \right)$$

being E the collected energy and t_{exp} the exposure time, then, the real apparent magnitude of the target, called m, is:

$$m = m_0 + m_t - kx$$

where m_0 is a constant named *photometric zero point* which depends on the filter used, while the kx product is the correction term for atmospheric extinction, which depends on the *extinction coefficient* k, and on the *airmass* x, that is a function of the target altitude above the horizon (h), precisely:

$$x = \frac{1}{\sin h}$$

Considering together the two equations containing magnitudes we have:

$$m = m_0 - 2.5 \log \left(\frac{E}{t_{\rm exp}}\right) - kx$$

From Pogson's formula, we know that:

$$m = -2.5 \log \left(\frac{f}{f_0} \right)$$

being f the flux and f_0 the referring flux of the photometric system. Therefore, by rearranging the last two equations, we obtain:

$$\frac{f}{f_0} = \frac{E}{t_{\text{exp}}} 10^{0.4(kx - m_0)}$$

From the SDSS website we know that the flux, in Jansky units, is given by the following formula:

Magnitudes

Galaxy	u (3551 Å)	g (4686 Å)	r (6165 Å)	i (7841 Å)	z (8931 Å)
1	19.59	16.85	16.31	15.93	15.92
2	19.78	14.28	15.63	15.05	14.78
3	18.90	16.56	15.59	15.06	14.88
4	21.06	18.87	17.79	17.18	16.76
5	19.25	16.90	15.94	15.42	15.17
6	21.49	19.04	18.11	17.57	17.24
7	22.13	18.96	18.23	17.86	17.96
8	20.44	18.09	17.11	16.63	16.37
9	20.40	17.95	16.98	16.44	16.17

$$s = 3631 \frac{f}{f_0} \qquad Jy$$

As a consequence:

$$s = 3631 \frac{E}{t_{\text{exp}}} 10^{0.4(kx - m_0)} \qquad Jy$$

But Jansky are expressed in frequency units (1 Jansky = 10^{-23} erg cm⁻² s⁻¹ Hz⁻¹) instead of wavelength units (erg cm⁻² s⁻¹ Å⁻¹), so we had to multiply by c/ λ^2 and we obtained:

$$s = 3631 \frac{c}{\lambda^2} \frac{E}{t_{\text{exp}}} 10^{0.4(kx - m_0)}$$

Using this formula we calculated the flux values for each galaxy in each filter (characterized by a central wavelength) and we were able to trace a spectrum profile based on 5 points.

Computed flux (in 10⁻¹⁶ erg cm⁻² s⁻¹)

Galaxy	u (3551 Å)	g (4686 Å)	r (6165 Å)	i (7841 Å)	z (8931 Å)
1	1.26	9.04	8.57	8.24	5.85
2	1.06	516.60	257.85	648.13	1180.80
3	2.41	64.72	273.93	663.01	1139.50
4	0.32	1.41	2.18	2.62	2.71
5	1.72	8.65	12.00	13.25	11.70
6	0.22	1.20	1.63	1.83	1.73
7	0.12	1.29	1.46	1.39	0.89
8	0.57	2.88	4.12	4.32	3.86
9	0.60	3.28	4.62	5.15	4.63

Comparing our spectra with the ones of galaxies at a redshift z=0 we determined the galaxy's redshift, the receding velocity, and then the distance using Hubble's law. The redshift is expressed by the formula:

$$z = \frac{\lambda - \lambda_0}{\lambda_0}$$

where λ is the observed wavelength of a spectral line, λ_0 is the same at rest.

The Doppler effect is expressed by:

$$\lambda = \lambda_0 \sqrt{\frac{1 + \frac{v}{c}}{1 - \frac{v}{c}}}$$

where v is the receding velocity. We have therefore:

$$v = c \frac{(1+z)^2 + 1}{(1+z)^2 - 1}$$

Finally, being by Hubble's law v = H d

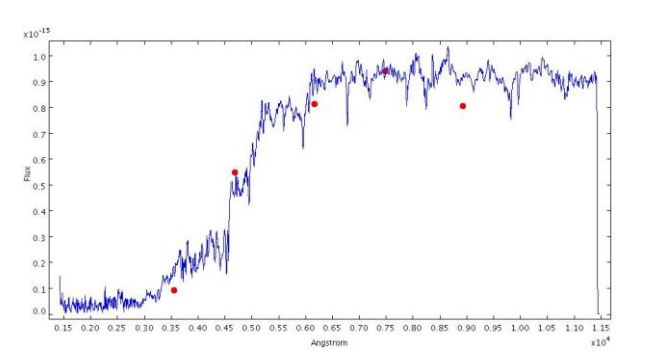
$$d = \frac{c}{H} \frac{(1+z)^2 + 1}{(1+z)^2 - 1}$$

IV. RESULTS

First of all, by analyzing the results, we found an unexpected problem: due to the small number of photometric data, the spectrum shape was uncertain, and as a consequence the galaxy's morphology was also uncertain. This is also caused by the photometric redshift method being not very precise, especially when not used with an adequate software. For these reasons some spectra were attributed, in some cases, to two different types of galaxies which correspond to highly discordant redshifts. For example, the spectrum of the galaxy n. 4 was fitted with that of a Seyfert 2, confirmed after a comparison with literature, at redshift 0.5 and distance of about 1600 Mpc. But for galaxy number 9, we obtained two different redshifts and distances, 2250 Mpc and 470 Mpc. We chose the first one taking into account that this galaxy appeared much smaller than galaxy 4, and therefore we hypothesized that it was more distant. In other cases we were unable to decide between the two options, both being reliable. For example, the galaxy number 1 in both cases resulted to have a Sc morphology, with redshift 0,5 and therefore distance of 1600 Mpc, or redshift 0,8 and consequently distance 2200 Mpc.

To summarize, we can say that the distances found let suggest that these galaxies form a group. Nevertheless, we are not able to confirm it, because of the uncertainties of the applied method.

Galaxy	Type	z	V (km/s)	D (Mpc)
1	Sc	0.5	115305	1600
2	Sc	0.79	157173	2180
3	E	0.72	148321	2060
4	Sy2	0.5	115305	1600
5	Sa	0.22	58840	820
6	Sc	0.8	158381	2200
7	Sc	0.78	155952	2165
8	Sc	0.8	158381	2200
9	Sc	0.83	161922	2250



Optical counterparts of Swift X-ray sources

Luca Vicariotto⁽¹⁾, Marta Zaccaria⁽¹⁾, Matteo Zorzan⁽²⁾

(1) Liceo Sperimentale "Don G. Fogazzaro", Vicenza (2) Liceo Scientifico "G. B. Quadri". Vicenza

ABSTRACT

We studied optical spectra of four x-ray sources in an object list from ATEL 1794, in which 16 new AGN have been detected in the 14-195 KeV band by the Swift/BAT All-Sky Hard X-ray Survey. The selected objects are: SWIFT J1246.9+5433, SWIFT J0544.3+5910, SWIFT J1439.2+1417, SWIFT J1453.1+2556, according to the BAT name. All these objects were classified, and redshift and bolometric luminosity were estimated.

I. INTRODUCTION

Active Galactic Nuclei (AGNs) were discovered in the mid-1950s, as powerful radio sources. Up to now, several types of AGNs have been recognised, and astronomers believe that we are simply observing the same source viewed with different orientations, according to the widely accepted Unified Model. Despite the half a century of successful works, AGNs have not yet been completely understood both in their structure and inner physics. Hence, the detection and study of new AGNs is very important, and will help astronomers to obtain a better physical model of these objects. AGNs are intensively studied in the whole wavelength range. In this paper we studied optical spectra of four unclassified X-ray sources selected from an object list appeared in ATel #1794 (http://www.astronomerstelegram.org/?read=1794). In this telegram, 16 new AGNs had been detected by the Swift/BAT telescope; six of them had been classified, while the remaining ones did not have optical spectra.

II. OBSERVATIONAL DATA

The observations were obtained on February 19th 2009, with the 122 cm "Galileo" telescope of the Asiago Astrophysical Observatory equipped with the Boller & Chivens spectrograph at Cassegrain focus (f/16). A 300 grooves/mm grating was employed. The spectral range was from 330 to 790 nm. HD19445 and HD74721 were the spectrophotometric standard stars employed to perform flux calibration, while wavelength calibration came from Ne and Hg-Ar comparison lamps.

The table below contains the observed objects list:

Object Swift/BAT	R.A.	Dec.	Exp. time (sec)
J0544.3+5910	05h44m23s	+59°07'36"	3600
J1246.0+5433	12h46m40s	+54°32'03"	1200
J1439.2+1417	14h39m12s	+14°15'22"	2400
J1453.1+2556	14h53m08s	+25°54'33"	2400

The objects have the following counterpart (ATel #1794)

Object name (Swift/BAT)	Counterpart
J0544.3+5910	2MASX J05442257+5907361
J1246.9+5433	NGC 4686
J1439.2+1417	2MASX J14391186+1415215
J1453.1+2556	2MASX J14530794+2554327

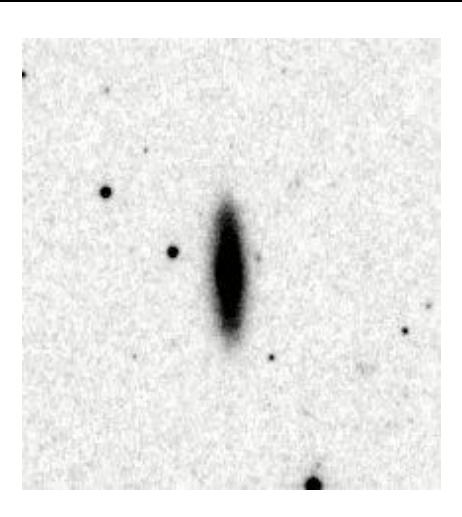


Fig. 1: NGC 4686.

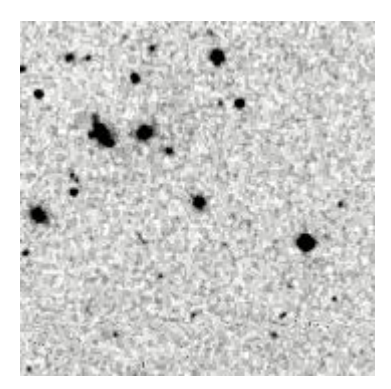


Fig. 2: J1439.2+1417.

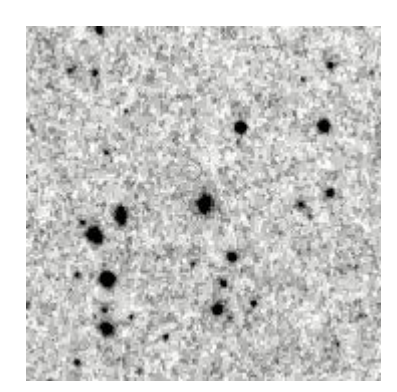


Fig. 3: Swift J1453.1+2556.

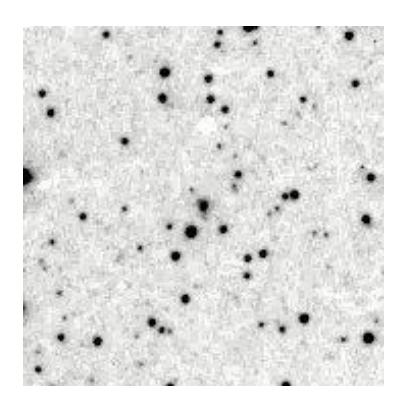


Fig. 4: Swift J0544.3+5910.

III. WORK DESCRIPTION

After the reduction and calibration of the spectra in the standard way, using IRAF software (http://iraf.noao.edu), we obtained monodimensional spectra. We began by comparing typical AGN spectra with ours. After the spectra comparison, we can propose the following classification:

NGC 4686: at first sight it shows the typical spectrum of a normal galaxy, with no clear evidence of emission lines in our spectral range. However, since the BAT telescope detected an X-ray event from this object, a more detailed analysis should be undertaken. Indeed, weak [N II]6583 and [O III]5007, besides absorbed H α 6563, are visible. Therefore NGC 4686 could be a LINER.

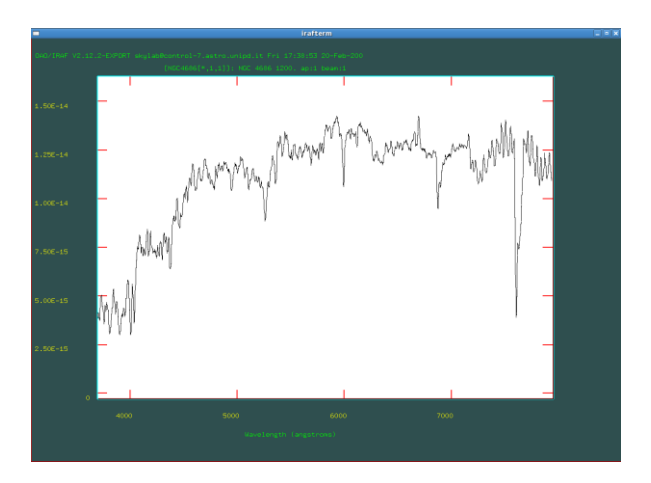


Fig. 5: NGC 4686.

Swift J0544.3+5910: we stress the strong similarities with a typical Seyfert 2 spectrum (see for example NGC 4941 spectrum for comparison). Note the narrow $H\alpha$ and [N II] lines (in blend), as well as the strong [O III].

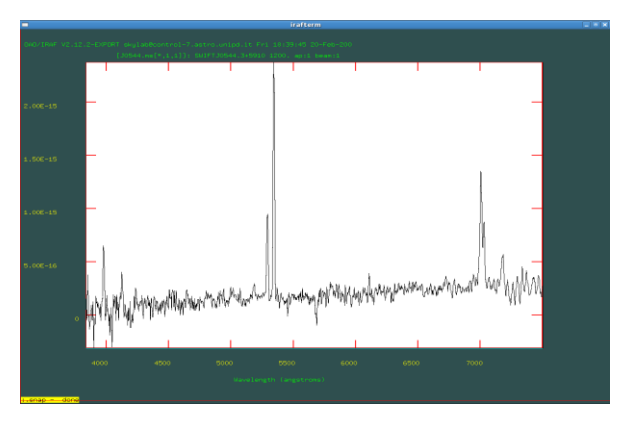


Fig. 6: Swift J0544.3+5910.

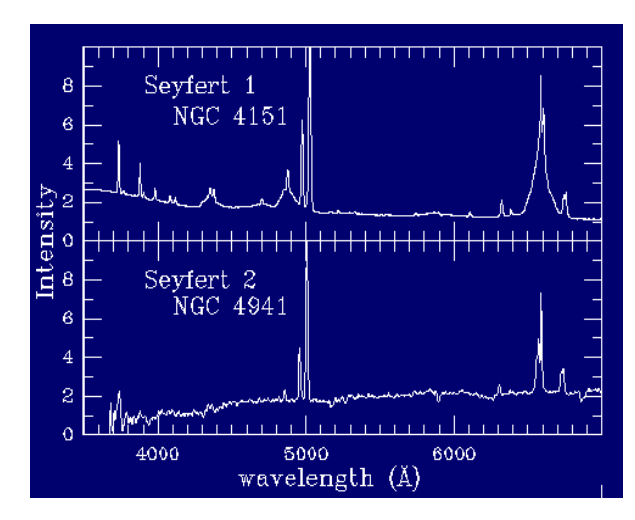


Fig. 7: Typical Seyfert galaxies spectra.

Swift J1453.1+2556: the broad H α emission line shows that this is a QSO. Note also the broad H β 4861 line and the narrow [O III].

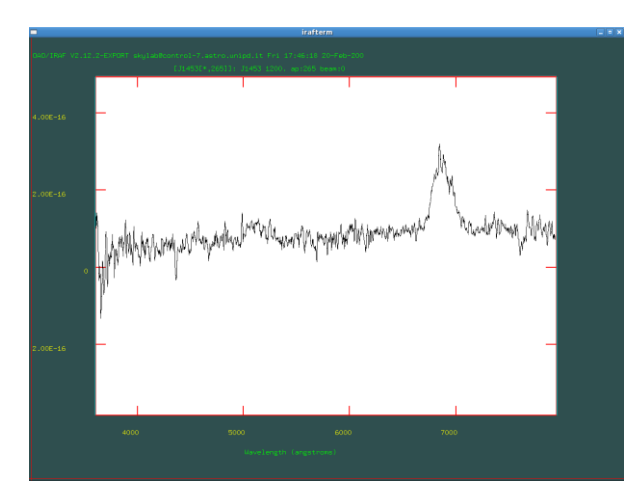


Fig. 8: Swift J1453.1+2556.

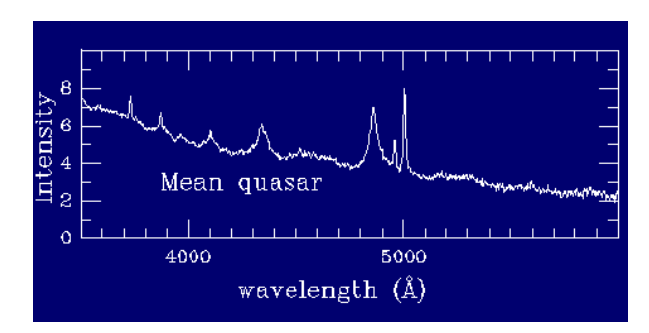


Fig. 9: generic QSO spectrum.

Swift J1439.2+1417: the optical spectrum of this object does not show emission nor absorption lines. The classification of such object is not clear. We propose it could be a BL Lac object.

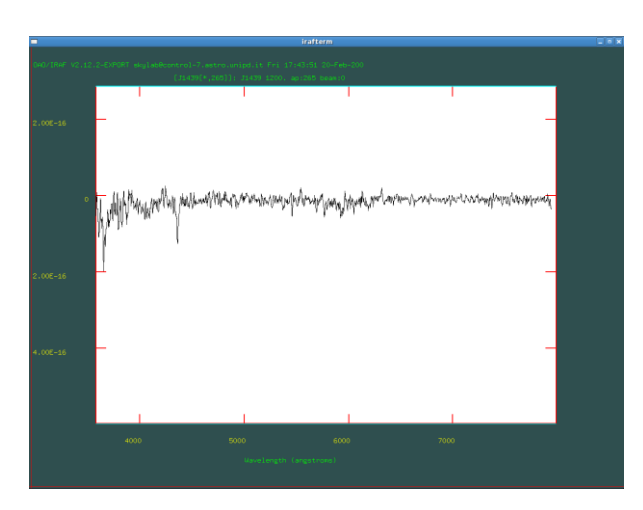


Fig. 10: Swift J1439.2+1417.

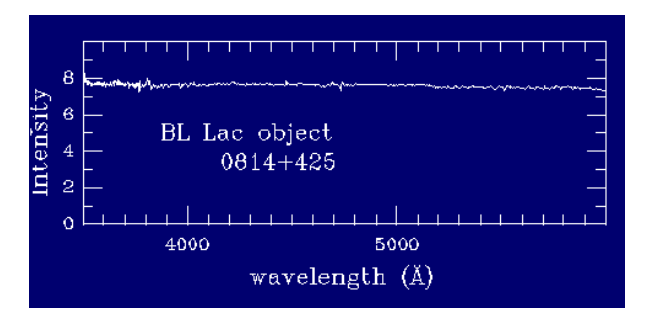


Fig. 11: BL Lac typical spectrum

Next step was to measure the redshift. After emission lines identification and peak measurement, the redshift was determined by the well known formula:

$$z = \frac{\lambda - \lambda_0}{\lambda_0}$$

We calculated for every spectrum the mean value and considered as an error estimate the root mean square. We evaluated the correction for the motions of the observer in relation to the Sun by the following formula:

$$V_{\oplus} = -V_K \cos \beta [\sin(\lambda - \lambda_{\ominus}) + e \sin(\lambda_{\Box} - \lambda)]$$

where λ and β are the ecliptic coordinates of the object, λ_{\odot} is the sun longitude at the observation date, λ_{π} is the perielium longitude, V_K is the Earth tangential velocity around the Sun and e is the Earth orbit's eccentricity. Then we calculated the velocity correction in relation to the 3 K background using the formula:

$$v_{con} = v + v_{apex} \left(\sin b \sin b_{apex} + \cos b \cos b_{apex} \cos(l - l_{apex}) \right)$$

where I and b are Galactic coordinates of our objects, V is the uncorrected velocity and l_{apex} and b_{apex} are the Galactic coordinates of the Sun motion's apex with respect to the 3 K background.

Object Swift/BAT	Heliocentric correction (km/s)	3K background correction (km/s)
J1246.0+5433	3.24	159.53
J0544.3+5910	-20.90	-8.56
J1439.2+1417	23.25	207.10
J1453.1+2556	19.88	166.86

The velocity (in km/s) was computed according to the formula

$$V = z \cdot c$$

The Hubble law allowed to estimate the distance of our objects:

$$d = \frac{z \cdot c}{H_0}$$

assuming that $H_0 = 75$ km/s/Mpc.

Object Swift/BAT	Redshift (10 ⁻³)	Corrected velocity (10 ³ km/s)	Distance (Mpc)
J1246.9+5433	15 ± 3	4.7 ±0.9	64 ± 10
J0544.3+5910	67 ± 1	20.2 ±0.3	268 ± 11
J1439.2+1417	-	-	-
J1453.1+2556	48 ± 1	14.5 ± 0.3	192 ± 10

Because no spectral lines were found in its spectrum, the object Swift J1439.2+1417 has not a redshift nor a distance estimate.

Finally, we estimated the bolometric luminosity of Swift J0544.3+5910 and Swift J1453.1+2556 following Collin and Huré (2001):

$$L = I_{5100} \cdot 5100 \cdot 4\pi d^2$$

$$L_{bol} \approx 9 \cdot L$$

Object	$L_{bol~({ m erg/s})}$
J1246.9+5433	-
J0544.3+5910	$6.15 \cdot 10^{43}$
J1439.2+1417	-
J1453.1+2556	$2.65 \cdot 10^{44}$

IV. RESULTS

To summarize: we obtained the optical spectra of four X-ray sources. From a preliminary analysis of the data we can suggest that strong nuclear activity justifying the X-ray emission is found in three targets, a Seyfert 1, a Seyfert 2 and a LINER. The last one resemble a featureless continuum, like that observed in BL Lacs. A more detailed and quantitative analysis is published in Atel #1985 (Ciroi et al. 2009).

V. BIBLIOGRAPHY

Collin, S. Huré J. M. 2001, A&A, 372,50;

Tueller et al., 2009;

Barbieri, C: dispense di Astronomia Università di Padova, AA 2008/09;

W. H. Baumgartner et al. ATEL #1794;

S. Ciroi, F. Di Mille et al. ATEL #1985;

http://nedwww.ipac.caltech.edu/;

http://heasarc.nasa.gov/docs/swift/swiftsc.html;

Optical spectroscopy of comet C/2007 N3Lulin

Noemi Furlani⁽¹⁾, Davide Santato⁽²⁾

(1) "Liceo Classico Celio", Rovigo (2) "Liceo Scientifico P. Paleocapa", Rovigo

ABSTRACT

We report the results of optical CCD spectroscopy of the comet C/2007 N3 Lulin on February 19^{th} 2009, when it was at a geocentric distance of Δ =0.45 AU. Lulin passed its perihelion on January 10^{th} 2009. The wavelength range from 3700 to 8000 Å showed a prominent emission band of the CN(0-0) detected at 3880 Å. Also, the forbidden oxygen [O I] emission line at 6300 Å is clearly visible. From a comparison of these and other reported observations, such as for example comet C/1995 O1 Hale-Bopp made by A. Fitzsimmons and I. M. Cartwright and others made by U. Fink and M. D. Hicks, C/Lulin appears to be a normal comet, albeit highly active.

I. INTRODUCTION

Comet C/2007 N3 Lulin (Fig. 1) was discovered on July 11^{th} 2007, at Lulin Astronomic Observatory on Taiwan island, by a team of astronomers under the supervision of professor Quanzhi Ye (Sun Yat-sen University), when the comet was at a visual magnitude of ≈ 18.9 . On February 19^{th} 2009 Lulin was located in the Virgo constellation, near Spica (Fig. 2), at a visual magnitude of 6.1. The results of the optical spectroscopic observations of C/Lulin show the chemical composition of the comet.



Fig. 1: Picture of C/2007 N3 comet.

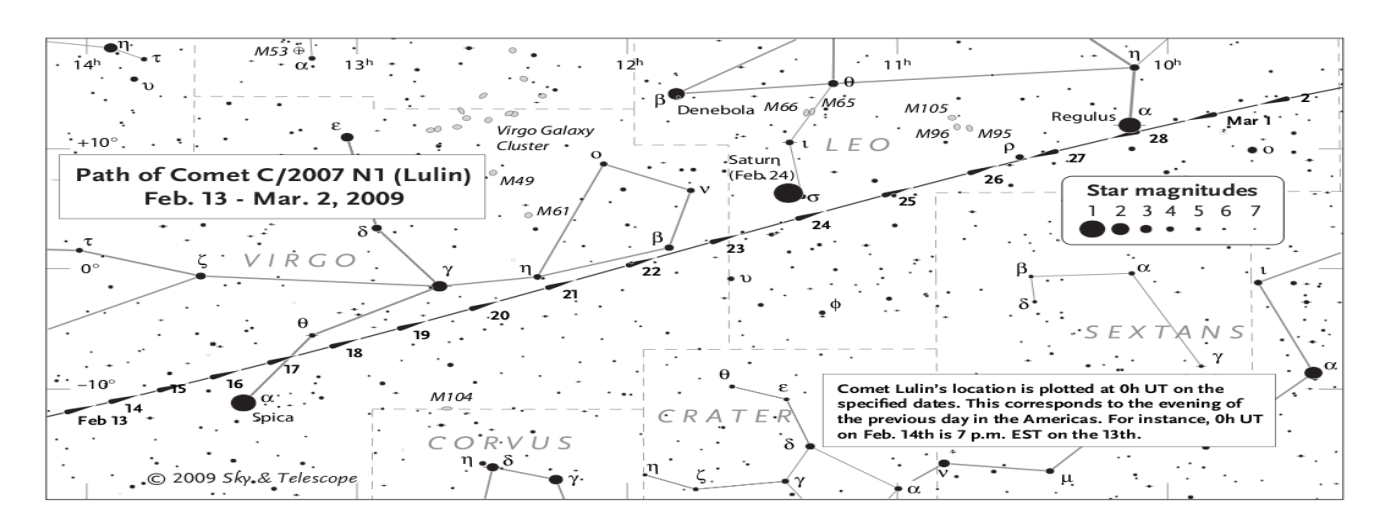


Fig. 2 Sky chart reporting the position of the comet.

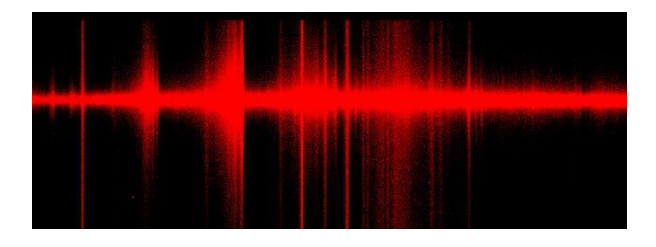
II. OBSERVATIONAL DATA

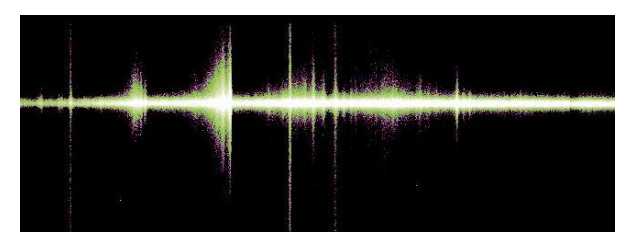
We studied the C/2007 N3 Lulin comet with a Boller & Chivens spectrograph, mounted at the 122 cm telescope (F=1950 cm, Cassegrain) of the Asiago Astrophysical Observatory. A slit width of 2.5 arcsec resulted in an instrumental resolution of ≈ 10 Å.

The exposures were obtained when the position of the comet was $RA = 12^h 49^m 35^s$ and $DEC = -04^\circ 51'13''$. We had to wait until 01:00 UT to let the comet rise and observe it. The sky spectrum, which had to be subtracted from the comet one, was taken pointing the telescope at a distance that allowed us to observe it outside the coma.

III. WORK DESCRIPTION

For our observations, three 180s exposures of the comet's nucleus (Fig. 3) were obtained from 01:22 UT to 01:34 UT. During the three exposures we had to maintain the nucleus centred on the slit manually. We had to do this because, like all other comets, Lulin has got its own motion. For the spectroscopy of the coma we applied an exposure time of 300 seconds.





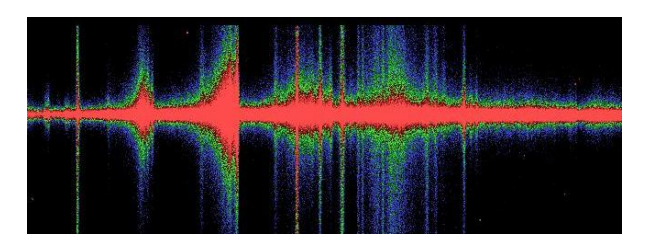


Fig. 3: The three spectra of the comet obtained at the 122 cm telescope of the Asiago Astrophysical Observatory.

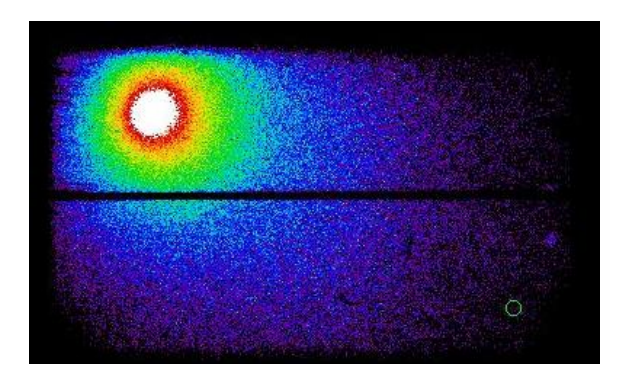


Fig. 4: Image of the Comet C/2007 N3 Lulin obtained through the guiding camera of the spectrograph.

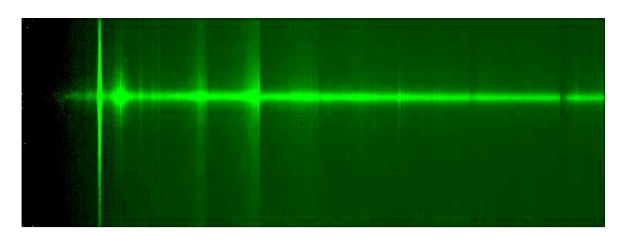


Fig. 5: Spectrum resulting from the sum of the three exposures.

We used the IRAF astronomical package to reduce the observed spectra with a standard reduction procedure. First of all, the raw spectra were bias subtracted and flat-field corrected. In order to convert pixel values along the dispersion axis into Angstrom units, we used spectra of comparison lamps, emitting lines at known wavelength. Spectrophotometric standard stars, whose energy distribution as a function of wavelength is known, were observed and measured to convert photon counts into energy, measured in erg/cm²/s/Å.

Once completed this procedure, we obtained the spectrum of the comet expressed in physical units, then we subtracted the night-sky spectrum in order to eliminate light and spectral features produced by our atmosphere. Finally, we summed together the three spectra to increase the signal and the quality of the data of the nucleus.

IV. RESULTS

We compared the resulting spectrum with those of other comets, as comet C/2001 A2 LINEAR, to identify the emission features (lines and bands). We found the following elements: CN, C_3 , CH, C_2 , NH_2 and [O I], and absorption lines $H\beta$ and $H\alpha$.

The production rate of H_2O (Q[H_2O]) could be determined from [O I]6300 luminosity (L(6300)) by:

$$Q(H_2O) = L(6300) \cdot \frac{\sum A_{ki}}{A_{ki}} \cdot \frac{k(H_2O)}{k(OI)}$$
$$Q(H_2O) = L(6300) \cdot 1.330 \cdot \frac{12.0 \cdot 10^{-6}}{1.0 \cdot 10^{-6}}$$

$$Q(H_2O) = L(6300) \cdot 16$$

where $Q(H_2O)$ is the water production rate per second, L(6300) is the luminosity of [O I] emission at 6300\AA ,

the branching ratio $\frac{A_{ki}}{\sum A_{ki}}$ is the transition probability

of the 6300Å line from the [O I] ¹D level divided by the sum of all transitions from that level (essentially the 6364Å line). Although values for the mean life of this level range from 101s to 148s, (Wiese *et al.* 1966; Mendoza 1983; Froese-Fischer and Saha 1983), the branching ratio to the 6300Å line is consistent within a few parts per thousand, so there should be little uncertainty in that number.

The second branching ratio $\frac{k(OI)}{k(H_2O)}$ represents the

production of [O I] atoms in the ¹D state divided by the total photon destruction rate of water. There is a reasonable agreement for a value of $12\pm0.5\cdot10^{-6}$ for the total water destruction rate (e.g., Huebner and Carpenter 1979; Festou 1981; Crovisier 1989; Fink and DiSanti, 1989).

In our case:

$$Q(H_2O) = L(6300) \cdot 16$$

$$Q(H_2O) = 4\pi d^2 \cdot \varphi_{photons} \cdot 16$$

$$Q(H_2O) = (5.73 \cdot 10^{22} \cdot 2850) \cdot 16$$

$$Q(H_2O) = 2.61 \cdot 10^{27}$$
 molecules of H₂O per second.

Comparing our data with the ones from other observations, we found out that we should use 0.07, instead of 16, to multiply the luminosity of CN and find out the production rate of CN:

$$Q(CN) = L(6300) \cdot 0.07$$

In this case:

$$Q(CN) = 1.59 \cdot 10^{27} \cdot 0.07 = 1.11 \cdot 10^{26} \,\text{mol} \cdot \text{s}^{-1}$$

The branching ratio
$$\frac{Q(CN)}{O(H_2O)} = 0.042$$

If we apply the same procedure to the spectrum of the coma we find out that the branching ratio $\frac{Q(CN)}{Q(H_2O)}$ is almost six time larger than the nucleus' one.

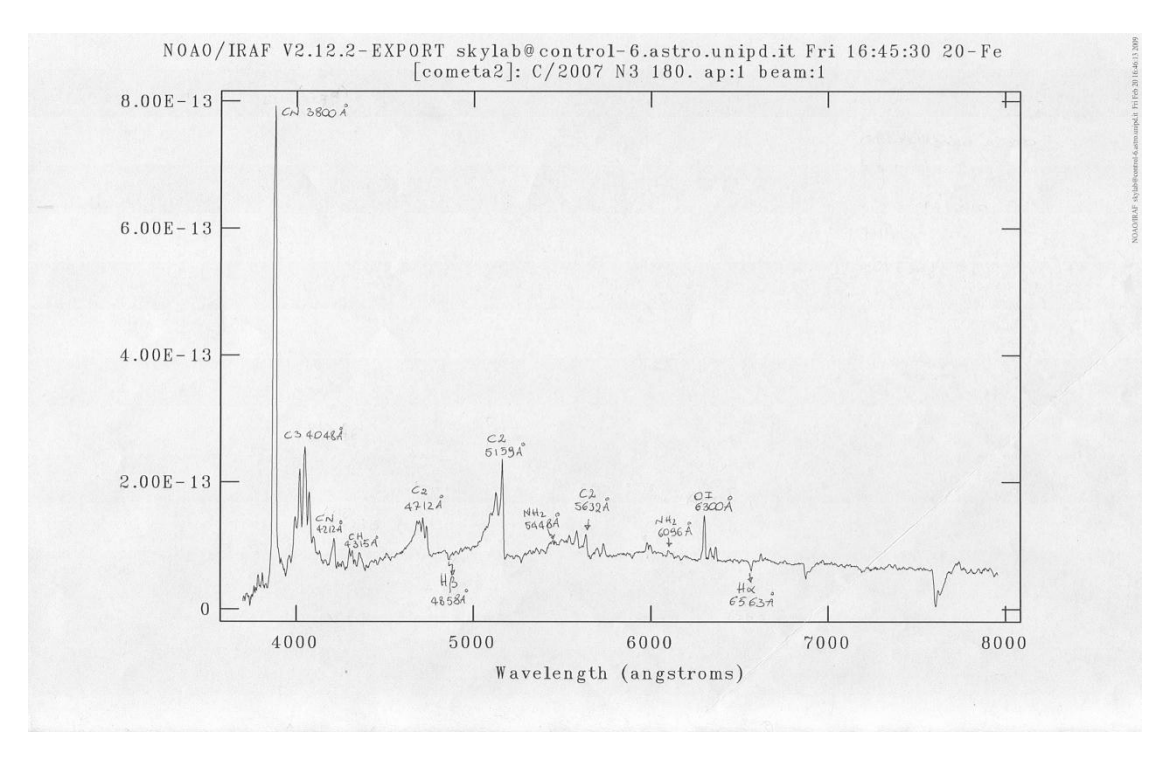


Fig. 6: Spectrum of the comet with identified spectral features.

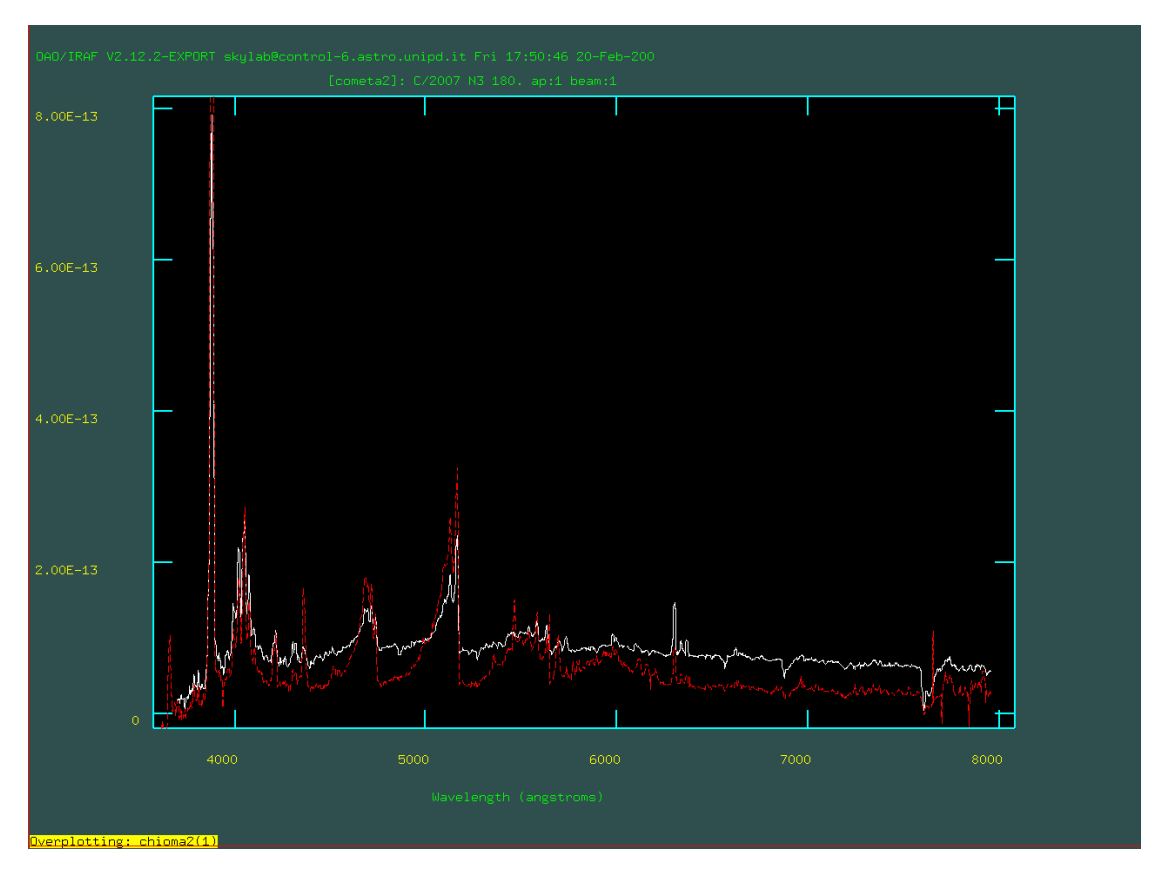


Fig. 7: Coma's spectrum (red) over nucleus's spectrum (white).

Spectral classification of the supernova SN2009af

Marco Rossi, Paolo Rosson

Liceo Scientifico "U. Follador", Agordo (BL)

ABSTRACT

The aim of this work is the classification of the supernova SN2009af in UGC1551 observed at the Asiago Astrophysical Observatory with the 122 cm "Galileo" telescope. By analysing the spectra and the well evident P-Cygni profile of the $H\alpha$ line we were able to classify our object as a type II SN. We also calculated other parameters such as ejecta velocity, absolute magnitude and luminosity.

I. INTRODUCTION

A supernova is a star that undergoes a tremendous explosion and a sudden brightening: during this time its luminosity becomes comparable to that of an entire galaxy.

An important feature for the classification of the SNe is the light curve, which is a plot of magnitude as a function of time. In the graph below (Fig. 1) we can see a maximum peak followed by a decline.

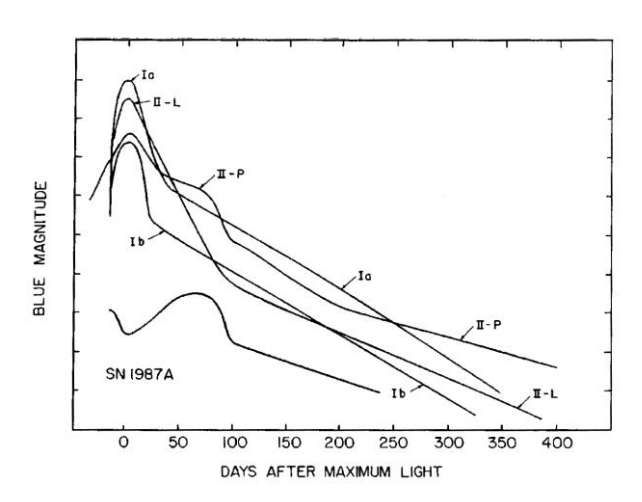


Fig. 1. Light curves of different SN types.

SNe can be divided in two main classes that are classified on the basis of the presence or absence of hydrogen lines in their spectra as type I SNe (SNI) or type II SNe (SNII), respectively.

If a type I SN shows the SiII line it is called SN Ia. The type Ib is characterized by the presence of HeI. If the SN shows neither SiII nor HeI it is called Ic.

The categories of the type II are based on the light curves. The type IIP shows a slower decline (plateau) followed by a normal decay, while the type IIL shows a linear decline of the light curve. Moreover we can find type IIb SNe which look like type II SNe at the beginning but then their spectrum becomes more similar to a SN Ib/c.

Some peculiar type Ib/c and IIn SNe with explosion energies $E > 10^{52}$ erg are often called hypernovae.

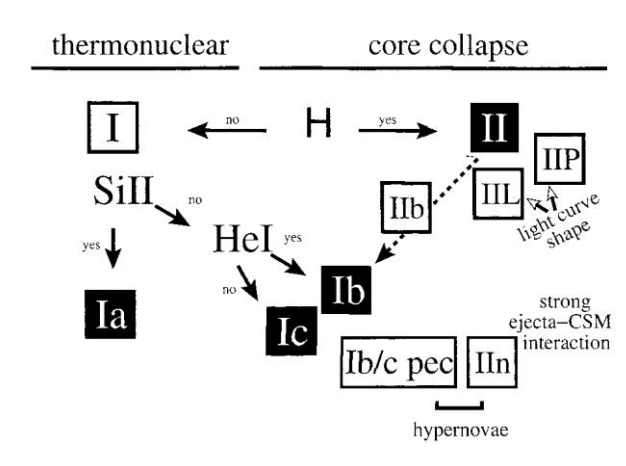


Fig. 2. The current classification scheme of supernovae.

SNIa are discovered in all type of galaxies, elliptical ones as well, and are not associated with the arms of spirals as strongly as other SN types.

The overall homogeneous spectroscopic and photometric behaviour of SNIa has led to a general consensus that they are associated with the thermonuclear explosion of a white dwarf.

The uniformity of their light curves, their high luminosity and relatively small luminosity dispersion at maximum (<M_B> = -18.6) allow us to use them as standard candles in order to determine distances.

The spectra of SN Ia are characterized by lines of intermediate mass elements such as calcium, oxygen, silicon and sulphur during the peak phase and by the absence of H at any time. Then the contribution of the Fe lines increases and several months after the maximum the SN Ia spectra are dominate by [Fe II] and [Fe III] lines.

Type II are observed in arms of spiral galaxies which are rich in gas and dust and where star formation is ongoing and young stars are abundant. Type II SNe are associated with the death of massive stars due to the collapse of the Fe core at the end of evolution. These stars have large H-rich envelopes evident also in their spectra. Stellar evolutionary calculations suggest that stars with $M > 8\text{-}10~\text{M}_\odot$ undergo all major burning stages ending with a growing Fe core.

Supernovae are very important because they are the main source of the heavy elements found in the universe.

II. OBSERVATIONAL DATA

The Supernova we studied is SN2009af belonging to the galaxy UGC1551 in the constellation of Aries.



Fig. 3. SN 2009af in UGC1551.

Right Ascension	02h03m37.5s
Declination	+24d04m32s
Classification	SB IV-V
Velocity	1671 km/s
Redshift	0.008909
Magnitude	13.50
Major Diameter	2.8 arcmin
Minor Diameter	2.3 arcmin
Distance	37.09 Mpc

Fig. 4. Astronomical data of UGC1551

We observed the SN using the 122 cm telescope "Galileo" at the Asiago Astrophysical Observatory on February 18^{th} 2009. We took 5 x 20 min exposures in order to collect a stronger signal.

III. WORK DESCRIPTION

The raw spectra give us information about how photons are dispersed by the spectrograph. However, we cannot make any measure of energy, wavelength or any other feature. Therefore, raw data have to be transformed into scientific data. Moreover, any other light source that reaches the spectrograph disturbs our spectrum, and so we must apply some corrections in order to isolate the light from the object we are interested in.

For the spectroscopic analysis of SN 2009af we used the program IRAF through which we were able to correct the errors in the image and to extract the spectrum. The program uses four types of files:

BIAS, which is obtained through an almost null duration exposure (with the shutter closed) and must be subtracted from the data we took;

FLAT-FIELD, i.e. the data based on the continuum spectrum of a lamp, which allow us to correct the errors deriving from the lack of homogeneity in the CCD:

WAVELENGTH CALIBRATION FRAMES, i.e. a Hg-Ar-Ne spectral lamp used to compare the pixel position on the CCD of the emission lines produced by this lamp with their known wavelengths (in angstrom);

FLUX CALIBRATION FRAMES, i.e. one or more standard stars, whose flux as a function of wavelength is known; its observed intensity on the CCD in photon counts units is compared with physical units.

In addition, we have to subtract the spectral lines and the diffuse emission produced by the sky. Finally, we have to add the 5 exposures to increase the quality of the spectrum, that is to increase the signal-to-noise ratio of the spectrum.

As a result the obtained information can be represented into a wavelength-flux graph.

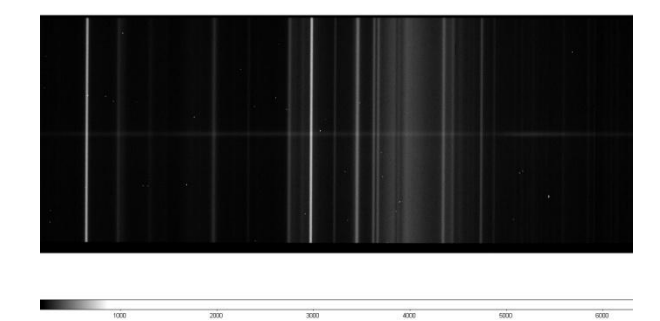


Fig. 5. Spectrum of SN2009af, February 18th.

In the spectrum we can notice the typical P-Cygni profile.

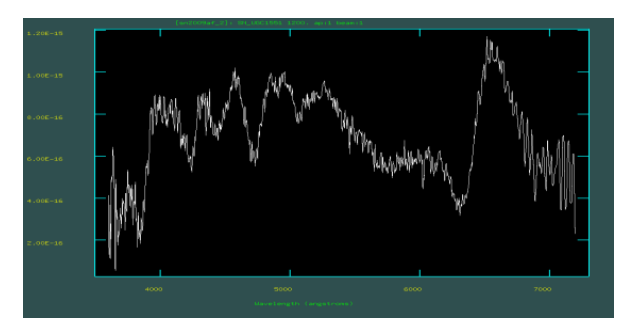


Fig. 6. Spectrum of SN2009af λ - \mathbf{F}_{λ} .

The P-Cygni profile is visible in stars with a powerful stellar wind or an expanding shell of gas. In particular, we can observe some blueshifted absorption lines and some redshifted emission lines.

The absorption lines derive from the part of the expanding photosphere that is coming towards the observer. Their radial velocity corresponds mainly to the expansion velocity of the ejected material and the Doppler shift is obviously negative. On the contrary, the emission lines come from the lateral regions of the shell which move on average perpendicularly to the line of sight. This singular profile was first observed in the celestial body called P-Cygni (34 Cygni).

For each element in the ejected atmosphere of our SN, we can see a P-Cygni profile, which can be well evident as in the Ha line, or not very defined, as in the case of the HB line. By overlaying a gaussian function on the absorption profile, we are able to calculate the wavelength of the Hα line of the ejecta and therefore their velocity, using the following equation:

$$z = \frac{(\lambda - \lambda_0)}{\lambda_0} = \frac{v}{c}$$

$$z = \frac{(6301 - 6563)}{6563} = -0.0399207$$

 $v = -0.0399207 \cdot c = -11967945.15 \text{ m/s} \approx -12000 \text{km/s}$

This is the expansion velocity of the gas that composes the photosphere of the supernova derived from the blueshift. Although, we must subtract the velocity of the host galaxy UGC 1551, V= 2670 km/s, the real expansion velocity of the ejecta is the following:

$$v = -12000 - 2670 = -14670 \text{ km/s}$$

We calculated the distance of the SN from the redshift of the galaxy UGC 1551 (z = 0.00891) using Hubble's law:

$$v = H_0 D$$

finding a distance of 37 Mpc.

We compared the SN with other 3 stars in the same field in order to estimate the apparent magnitude.

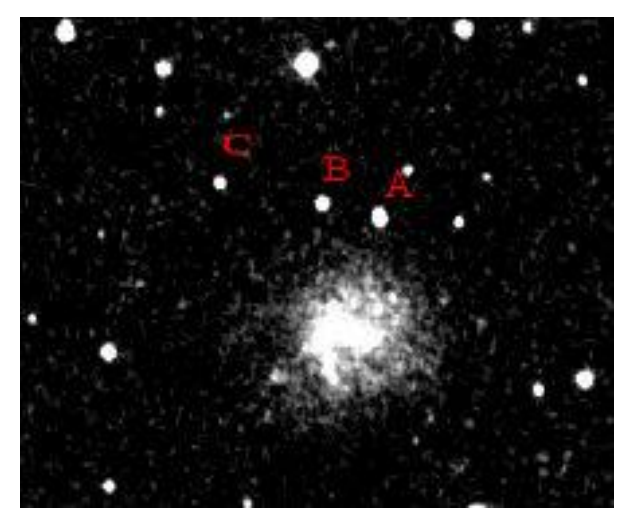


Fig. 7. Image of the stars A, B and C near the galaxy UGC1551.

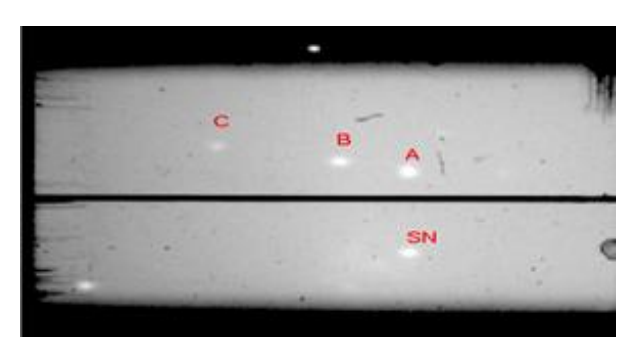


Fig. 8. Image of the SN and the stars A, B and C we took from the spectrograph.

At first, we took the apparent magnitude of the stars A, B and C from the USNO-B1.0 catalogue.

A) mag: 15.25 B2

14.37 R2 Instrum: 12.64

13.59 IMag

B) mag: 16.15 B2

15.21 R2 Instrum: 12.82

14.63 IMag

C) mag: 18.01 B2

16.28 R2 **Instrum: 13.47**

15.04 IMag

Instrumental magnitude of the SN: 12.79mag.

Then, we calculated the difference between the instrumental magnitudes of the stars we had chosen and that of the SN:

$$x = A - SN = -0.15$$

 $y = B - SN = 0.03$

$$z = C - SN = 0.68$$

After that, we subtracted the differences we found from the values of the magnitude of the stars in the catalogue in R2 bands.

$$A_{R2} - x = 14.52$$

$$B_{P2} - v = 15.18$$

$$\begin{split} B_{R2} - y &= 15.18 \\ C_{R2} - z &= 15.60 \end{split}$$

We calculated the average which is 15.10.

Then we calculated the absolute magnitude from the apparent magnitude:

$$M = m + 5 - 5\log_{10} d$$

Where M = absolute magnitude, m = apparent magnitude and d = distance in pc.

The absolute magnitude is -17.75.

Finally we used Pogson's law to calculate the luminosity of the SN:

$$M - M_{sun} = -2.5 \times \log \frac{L}{L_{sun}}$$

The luminosity is $4.14 \times 10^{35} \text{ W} = 4.14 \times 10^{42} \text{ erg/s}$ $(1.08 \times 10^9 \text{ L}_{\odot})$.

IV. RESULTS

To classify a supernova we should have both the spectrum and the light curve. Since we did not have the latter, we tried to make some hypotheses by studying only the spectrum. Certainly, it is not a type I SN for the presence of hydrogen lines. On the contrary, we are able to classify it as a type II Supernova, because of the strong $H\alpha$ emission. Moreover, by comparing the spectrum of SN 2009af to that of type II SN 1992H, taken 20 days after maximum published by Filippenko (1997), we noticed an evident similarity between the two spectra.

We compared SN 2009af with one of the most studied type IIb SNe, 1993J in M81. We overlaid the spectrum of SN2009af with the one of SN 1993J on April 21st.

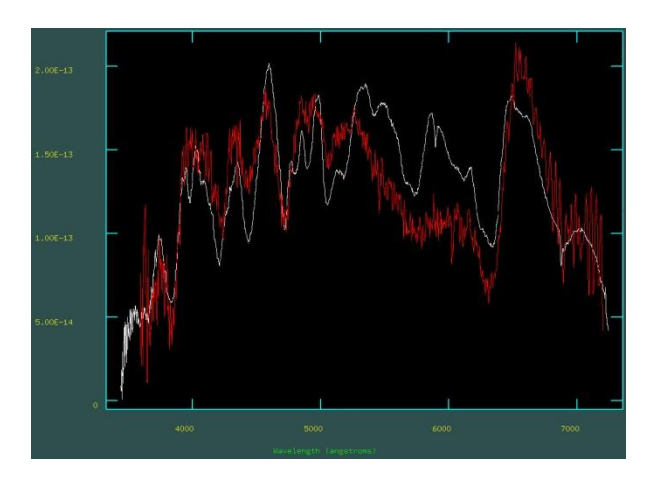


Fig. 9. Comparison between the spectra of the SN2009af (red) and the SN1993J (white) in the $21^{\rm st}$ day after the explosion.

We noticed an evident similarity in particular in the regions 3700 - 5000 Å and 6200 - 6900 Å. In these ranges we can see that the P-Cygni profiles are almost analogous. However, the spectra are not very similar between 5000 Å and 6200 Å. This means that we cannot exclude the possibility of a type IIb classification for SN 2009af. To do this we should

analyse the supernova for a long period, taking some spectra at different dates in order to create a chronological evolution of the star.

At present, we are unable to define if SN 2009af is a SN II-P, SN II-L or another subclass. We should have the light curve and more detailed studies of the supernova.

V. BIBLIOGRAPHY

Classification of Supernovae, Massimo Turatto, 2003.

Optical spectra of supernovae, Alexei V. Filippenko, 1997.

Optical Observations of Supernova 1993J from La Palma - Part One - Days 2 TO 125, *Lewis J.R. et al.*, 1994.

Exploring the optical transient sky with the Palomar transient factory, *Arne Rau et al.*, 2008.

http://www.daviddarling.info/encyclopedia/P/P_Cygni _profile.html.

http://www.astrosurf.com/prosperi/ccd/calibra.html.

Nasa/Ipac extragalactic database.

Photometric analysis of the open cluster NGC2420 and the globular cluster NGC6229

Elena Boldrin⁽¹⁾, Davide Bombieri⁽¹⁾, Luca Ercole⁽²⁾

(1) Liceo "Giuseppe Berto", sez. Scientifico, Mogliano Veneto (2) Liceo "Giordano Bruno", sez. Scientifico, Mestre

ABSTRACT

We studied the photometry of the globular cluster NGC6229, and the open cluster NGC2420, by using g, r and i bands. By transforming g,r, i into BVR Johnson-Cousins photometric bands, we built a color-magnitude diagram (CMD) in this photometric system, and we determined the distance modulus (DM) of NGC2420, through the ZAMS (Zero Age Main Sequence) fitting, and of NGC6229, by comparing $M_V(RR \text{ Lyrae})$ with V(RR Lyrae) in the Horizontal Branch (HB). Finally, we estimated the age of both NGC2420 and NGC6229 by fitting different sets of isochrones, for different metallicities Z, onto CMD. The age of NGC6229 has also been estimated by determining the difference $M_V(TO)$ - $M_V(HB)$.

I. INTRODUCTION

A star cluster is a group of stars born at the same epoch from the same molecular cloud with the same chemical composition, kept together by the gravitational force. We can distinguish between globular and open clusters. The first ones are generally bigger and composed of a high number of old population II stars, and are distributed in the whole galactic halo. They have a visible spherical shape due to the strong gravity, which keeps a high stellar density in their centre. They do not have any gas or dust.

Open clusters have a lower number of stars, so their gravitational bound is weaker. They are generally very bright, because they contain young stars at a high temperature. By analyzing the light coming from an open cluster we can estimate its age. An abundance of blue stars implies that the cluster is young. The stellar density can be extremely variable, sometimes similar to that of the field stars, making the cluster hard to be recognized; anyway it is always lower than the density of the central areas of a globular cluster. Open clusters can be found only in the galactic disk of spiral galaxies and in irregular ones.

Generally, since all the stars in a cluster have about the same age, chemical composition and distance, every difference in the stellar parameters is caused just by the initial mass of each star, that determines a different evolution.

When we create a color-magnitude diagram (CMD) or a H-R diagram of the stars in a cluster, its shape depends on the age of the cluster, showing an almost complete main sequence (MS) when younger than 500 Myr. Obviously, when the age of the cluster grows, all the typical features of the diagram become evident. The point in the diagram where the stars leave the MS is called turn-off (TO), and can be used to calculate the age of the cluster.

Since every star of the cluster is close to the others, the difference between apparent and absolute magnitudes, called distance modulus (DM), is constant. Therefore a CMD becomes a H-R diagram and it allows to estimate the distance if we have the DM.

II. OBSERVATIONAL DATA

We carried out the photometry of the globular cluster NGC 6229 (fig.1) and of the open cluster NGC 2420 (fig. 2).



Fig. 1: NGC6229.



Fig. 2: NGC2420

The globular cluster NGC6229, situated in the Hercules constellation, at RA = $16^{\rm h}$ $46^{\rm m}$ $58^{\rm s}$.9 DEC = +47° 31' 40" (J2000), has an angular size of about 4,5' and it is of class 4, while the open cluster NGC2420, in the Gemini constellation, at RA = $07^{\rm h}$ $38^{\rm m}$ 23.9° DEC= +21° 34' 27" (J2000), has angular size of about 10' and it is of class I 1 r.

We used the images extracted from the Sloan Digital Sky Survey (SDSS) Data Release 6, a survey conducted with the 120 Mpx CCD (*Charge Coupled Device*) of the 2.5-meters telescope in Apache Point (New Mexico, USA).

We did the photometry in the three photometric bands g, r and i, then we transformed them into the more common B, V and R bands of the photometric system by Johnson-Cousins.

The characteristic wavelengths of the photometric bands *ugriz* are:

u	3551 Å
g	4686 Å
r	6165 Å
i	7481 Å
Z	8931 Å

III. WORK DESCRIPTION

To carry out the photometric analysis of the images we used IRAF (*Image Reduction and Analysis Facility*) program, in particular DAOPHOT and IMAGES packages and their *daofind*, *phot*, *psf*, *allstar*, *tvmark* and *imexamine* tasks.

The techniques we can use for the photometric analysis are the aperture photometry and the Point Spread Function (PSF) fitting. The first one consists in adding up the pixel counts within circles centered on each object and subtracting off an average sky count, determined in a circle ring around the object, to obtain the effective flux of electromagnetic radiation. In this case this technique was not suitable because of the high stellar density, that made inaccurate, or even impossible for the globular cluster, the average sky count determination.

Therefore, we applied the PSF photometry. This is a mathematical model of stellar profile which describes the average distribution on the CCD surface of the photons coming from a single star. This distribution, because of the Earth atmosphere effect (seeing), has the trend of a Gaussian curve, whose typical width (FWHM) determines what we considered the edge of the star. To build the PSF model we chose stars that showed a regular distribution of light. These stars ought to be quite isolated, in order to avoid overlapping of the tail end of the light profiles. Besides, they had to be regularly distributed throughout the whole image. By using the *psf* command, we obtained an average profile model which, once applied to every star of the image, allows to define the exact position of the star and the flux.

From the flux values we subtracted the light intensity of the sky background and, dividing it by the exposure time, we obtained the star instrumental magnitude. We applied this procedure to the images in g, r and i band of both clusters.

Since the instrumental magnitude is only an indication of the photon flux collected by the detector, we had to obtain a standard magnitude, which can be determined with the following equation:

$$m = m_0 + (m_s - 25) - kx$$

where m_0 = constant depending on the considered filter, m_s = instrumental magnitude, k = atmospheric extinction coefficient, x = air mass and 25 = constant applied by the program to the instrumental magnitude values, to make them positive.

The parameters values, acquired by the SDSS catalogue for our *fields*, are:

NGC 2420	g	r	i
m_0	24.45	24.07	23.74
k	0.14	0.09	0.03
X	1.06	1.06	1.06

NGC 6229	g	r	i	
m_0	24.58	24.12	23.75	
k	0.20	0.11	0.06	
X	1.18	1.18	1.18	

Once we obtained the photometric values for all the stars, which were 915 in g, r and i band in case of the open cluster NGC2420 and 1970 in the same bands in case of the globular cluster NGC6229, we converted them in B, V and R magnitudes by using the transformation equations elaborated by Jordi et al. $(2006)^{[1]}$.

Then we used them to elaborate the CMD (B-V vs V), from which we determined the distance, the HR (colorabsolute magnitude) diagram (B-V vs M_{ν}), and the age of the two clusters. For NGC2420 we corrected the B-V color index with color excess $\langle E(B-V) \rangle = 0.05$ taken from literature for this cluster $^{[2][3][4]}$, according to the usual relation:

$$(B-V) = (B-V)_0 + \langle E(B-V) \rangle$$

deducing (B-V)₀, and the V band data for the interstellar absorption according to the relation

$$V = V_0 + R < E(B-V) >$$

where we put R=3.1.

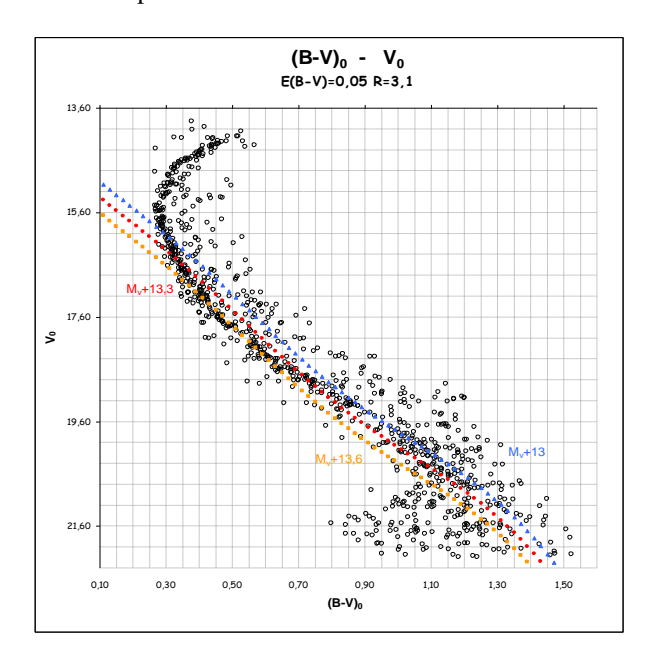


Fig. 3: ZAMS fitting.

To find the cluster distance we shifted the ZAMS, obtained with Johnson's data [5] until we fitted the

correct diagram, determining the distance modulus DM and obtaining (fig. 3):

$$DM(NGC2420) = 13.3 \pm 0.2$$

To determine the age of NGC2420 we fitted isochrones with different metallicities Z obtained from *CMD 2.1 input form* at http://stev.oapd.inaf.it/cgi-bin/cmd_2.1 getting the best result with ages between 1,26 Gyr and 1.59 Gyr and metallicity Z=0.01, as fig. 4 shows.

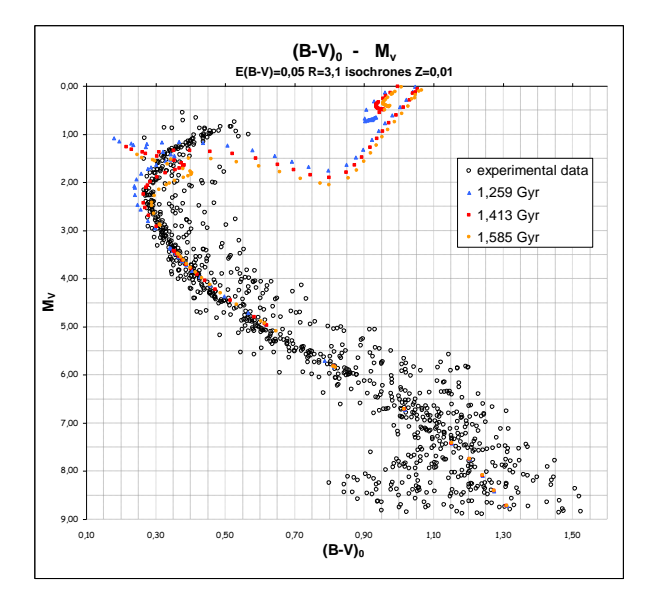


Fig. 4: CMD of NGC 2420 and Isochrones.

The correction of B-V and V values has not been done for the globular cluster NGC6229 since its E(B-V) proves to be equal to 0 or at most 0.01 from literature. We built up the $(B-V)_0$ vs. V diagram (fig. 5),

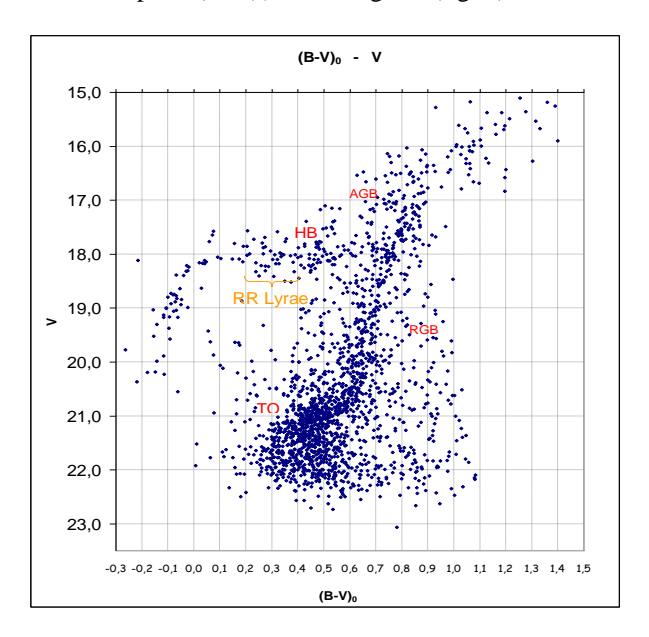


Fig.5: (B-V)₀ vs. V diagram.

and we deduced the DM by using the HB experimental visual magnitude and in particular the region where the pulsating variable stars RR Lyrae fall. These stars have a typical B-V color index between 0.2 and 0.4, and

their absolute magnitude is known, since it depends on [Fe/H]. It has been estimated in various ways for the globular clusters at M_v =0.60±0.12 at [Fe/H]= -1.5 in particular after the studies carried out through HIPPARCOS satellite ^[6].

The HB, and therefore the RR Lyrae, have a visual magnitude of +18.1, therefore by comparing the observed visual magnitude with the absolute one we can obtain a DM = M_v – V = 0.60 – 18.10 = -17.50.

Afterwards we deduced also for this cluster the HR diagram (B-V vs M_{ν}) and we fitted different-metallicity isochrones to establish its age. We obtained the best fit with isochrones with metallicity of Z=0.001, and ages between 10.00Gyr e 14.13Gyr.

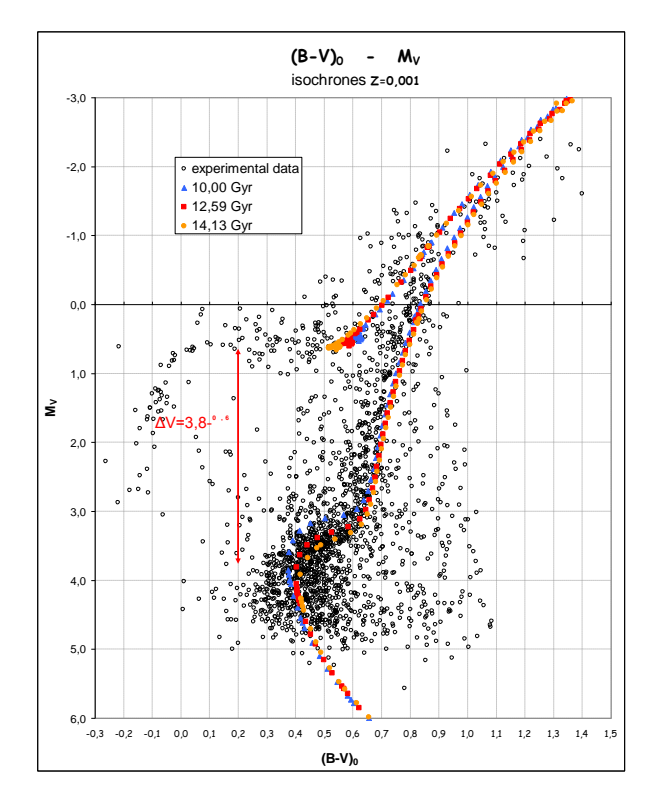


Fig. 6: CMD of NGC 6229, Isochrones and ΔV .

An other method we applied to calculate the age is based on the difference between the stars which are on the HB and those on the TO according to the following equation:

$$Log t_9 = 0.37 \Delta V - 0.03$$

where $\Delta V = M_V(TO) - M_V(HB) = 3.2$.

IV. RESULTS

The distance of the two clusters is calculated starting from the DM given by the equation:

$$M - m = 5 - 5 \text{ Logd}$$

which gives, for the open cluster, a distance of 4.6 kpc, a measure which remarkably differs from the officially accepted values. Likewise, the age determination of

1.4Gyr does not agree with the one reported in literature, although the sources report meaningfully different data, and this is due to the peculiar characteristics of the cluster. In this study, there is, probably, a systematic error in the acquisition of the photometric data, which causes the translation of B-V values of about -0.2, so that ZAMS are fitted to a higher DM, consequently increasing the estimated distance and the isochrones fitting, therefore the valued distance.

For the globular cluster our results totally agree with those in literature; in fact, with the isochrones-fitting method, the distance is proven to be 31.6kpc and the age 12.6Gyr. This is substantially confirmed by the age determination of 14.2Gyr, obtained with the HB-TO distance method.

V. BIBLIOGRAPHY

- [1] Empirical color transformations between sdss photometry and other photometric systems, K. Jordi, E.K. Grebel, and K. Ammon, Astronomy & Astrophysics manuscript no. 6082 February 5, 2008.
- [2] The gap in the color-magnitudine diagram of NGC2420: a test of convective overshoot and cluster age, Pierre Damarque, Ata Sarajedini and X.-J. Guo, The Astrophysical Journal, 426:165-169, 1994 May 1.
- [3] *UBVI* ccd photometry of the open cluster NGC2420, Sang Hyun Lee, Yong-Woo Kang and Hong Bae Ann, Korean Astronomical Society 14:61-67, 1999.
- [4] Galactic globular and open clusters in the sloan digital sky survey. I. Crowded field photometry and cluster fiducial sequences in *ugriz*, *AAVV*, APJS.
- [5] Basic Astronomical Data, Chicago U.P., page 216 chapter 11 "Photometric System", Johnson Iriarte.
- [6] An astrometric calibration of RR-Lyrae periodluminosity-metallicity relations, George Fritz Benedict, Hubble Space Telescope.

Properties of stars: temperature, colour index and equivalent width of spectral lines

(1) Elena Monai, (2) Ilaria Pagotto, (3) Elisabetta Artusi, (4) Leonardo De Luca

(1) Liceo Scientifico "Enrico Fermi, Padova (2) Liceo Scientifico "G.Galilei" Caselle di Selvazzano (Pd) (3) Liceo Scientifico "G Barbarigo" Padova

(3) Liceo Scientifico "G.Barbarigo", Padova (4) Liceo Scientifico "Enrico Fermi, Padova

ABSTRACT

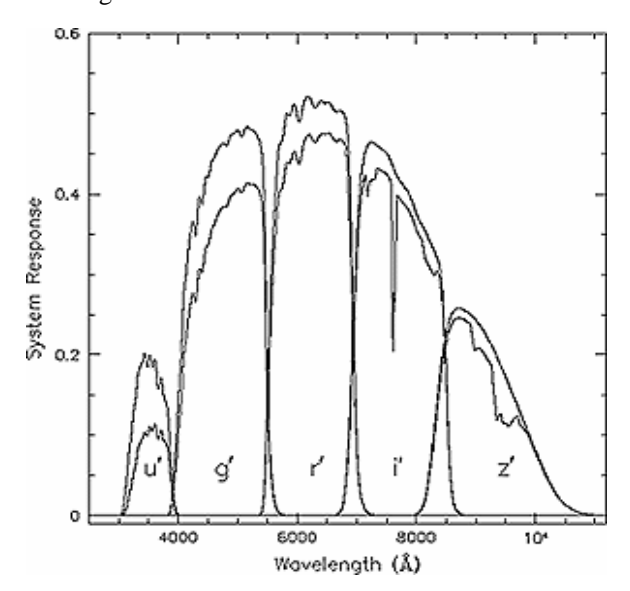
Stars can be distinguished by their colour, temperature and mass. These three features are closely linked to each other: the hotter the star is, the more the colour is towards blue, because it emits most of its energy at shorter wavelengths. We were able to build some diagrams which linked the colour and the temperature of some stars, in order to deduce the temperature of a larger amount of stars.

I. INTRODUCTION

With our research we wanted to achieve two goals:

- 1. Starting from a limited number of stars, we verified and analyzed the linear trend of the function in the color-temperature diagram and we have applied this relation to a large amount of stars to get easily their temperature.
- 2. Through the study of the spectrum of 10 stars at different temperatures we analyzed the trend of the equivalent width of the absorption lines $H\alpha$ and CaII K, as a function of temperature.

A color index is the difference between two magnitudes of the same star obtained with two different photometric filters. We used the *ugriz* filters that have characteristic wavelengths in the range of the visible light.

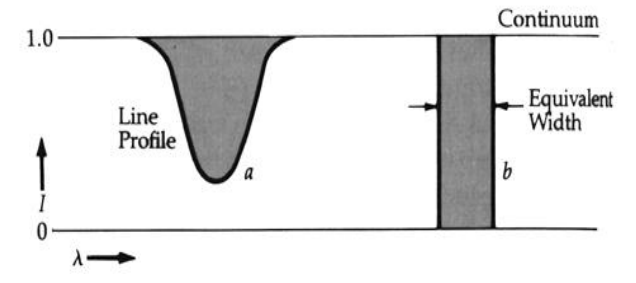


The equation of the colour - temperature diagram we are going to verify is:

$$y = Bx + A$$

where y is the color index and x is the reciprocal of the temperature (1/T).

The equivalent width (EW) is defined as the width of the rectangle whose height corresponds to the absorption of 100% of the radiation and whose area, namely the absorbed energy, is the same of the real spectral line.



Despite the name, the equivalent width does not give information about the width of the lines. A wide and shallow line or a narrow and deep line can represent the absorption of the same number of photons and therefore have the same equivalent width.

From the mathematical point of view:

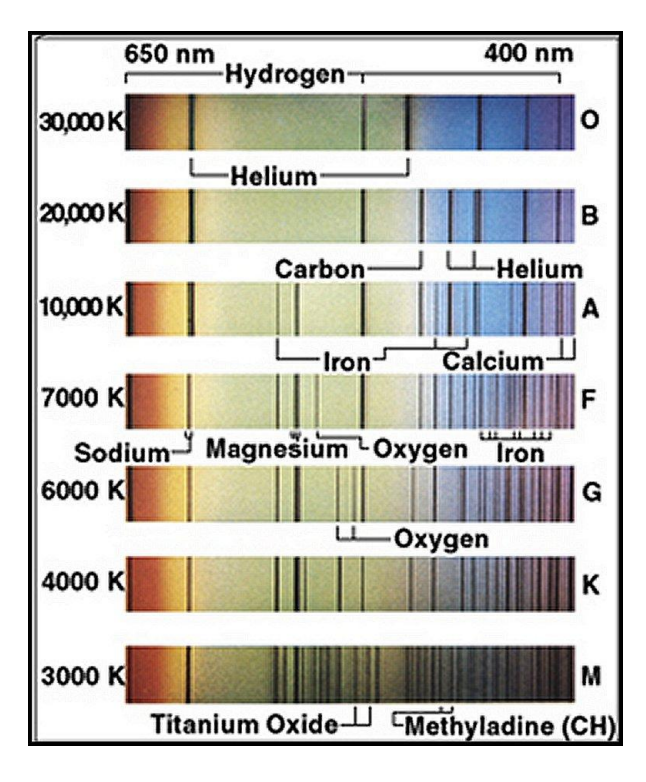
$$EW = f / I_{cont}$$

where:

f is the absorption line flux (erg/cm² s); I_{cont} is the intensity of the continuum (erg/cm² s Å); from this we get:

$$[EW] = [\mathring{A}]$$

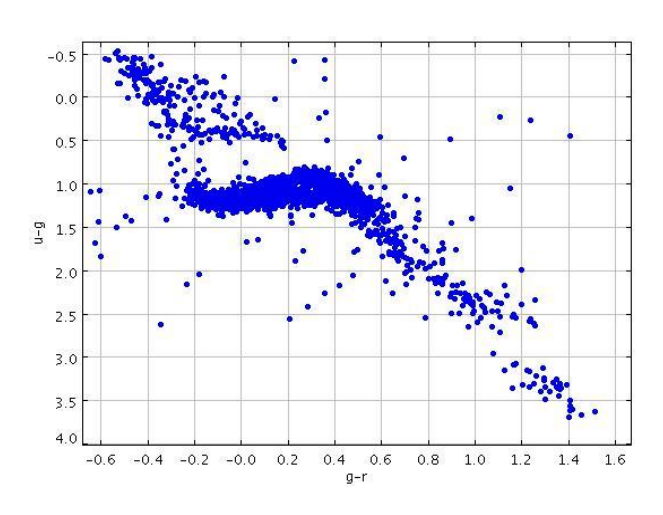
Experimentally we see how the absorption lines are different from one another depending on the temperature. Their behavior therefore is the following:



II. OBSERVATIONAL DATA

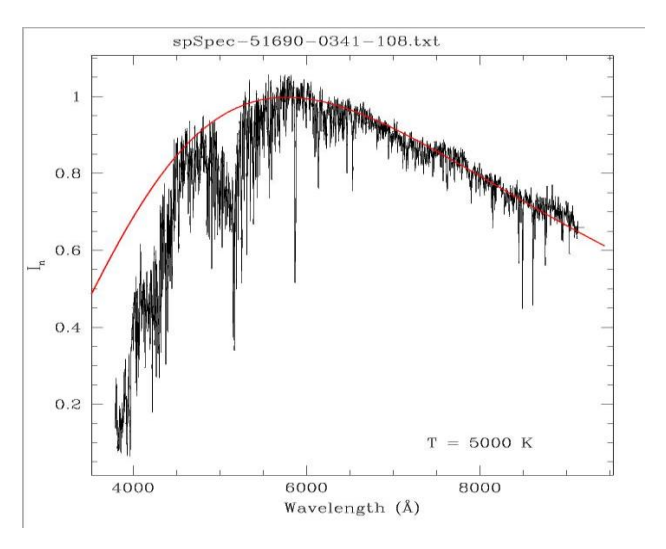
A sample of 5000 stars was taken from the archive of the Sloan Digital Sky Survey (<u>www.sdss.org</u>) with the respective information, including the magnitudes taken with the *ugriz* filters.

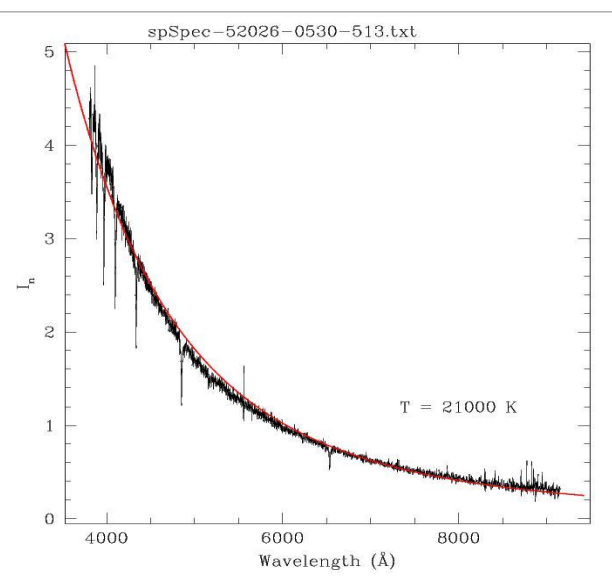
III. WORK DESCRIPTION



We obtained the g-r and u-g color indices by calculating the difference between the magnitudes of g and r (g-r) filters and between the magnitudes of the u and g (u-g) filters of all the 5000 stars. Then, we put these values in a plot to obtain a color-color diagram. We selected 26 stars out of the 5000, taken from different parts of the color-color diagram, so that the stars had different temperatures, and we extracted their spectra.

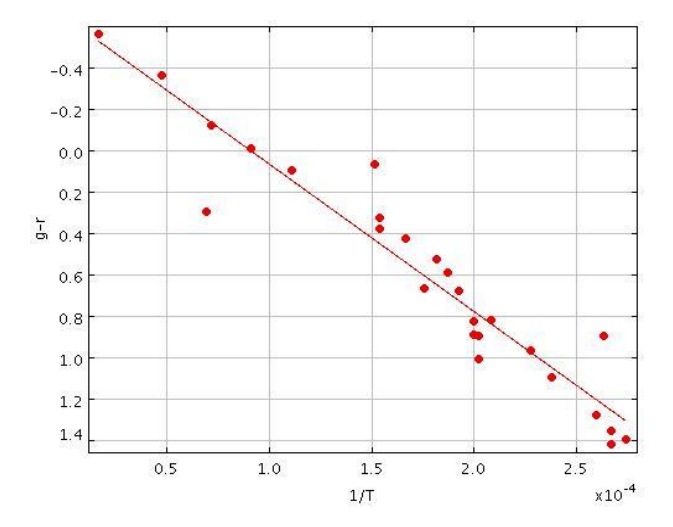
We normalized the spectra so that in every spectrum the intensity is 1 at wavelength λ =6000Å. By applying to every spectrum Planck's law and changing every time the temperature value until we found the best fitting to the observed spectrum, we estimated the approximate surface temperature of the stars.





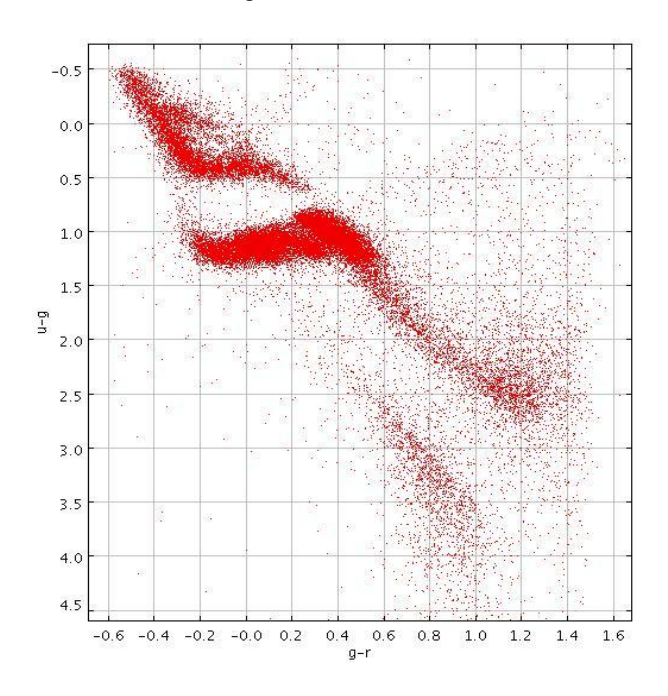
In these plot the black curve is the actual spectrum of the star, while the red one is Planck's law. After finding the temperature of these 26 stars, we built 4 plots putting on the x-axis the reciprocal of the stellar temperature (1/T) and on the y-axis a different color index for every plot (g-r; u-g; r-i; g-i). In this way we verified that the color index is inversely proportional to the temperature.

In these plots the trend of the data can be easily fitted with a straight line.



The straight line which best fits the above data, is given by the following equation:

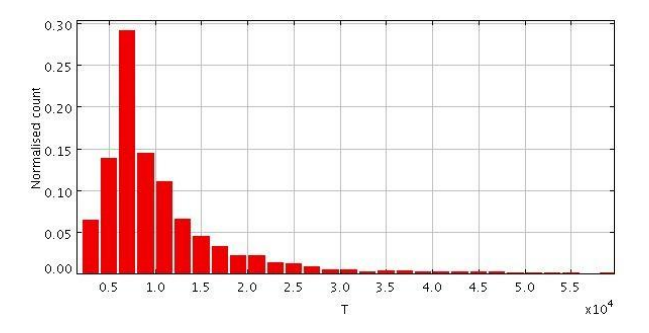
$$g - r = -0.647 + (7151/T)$$



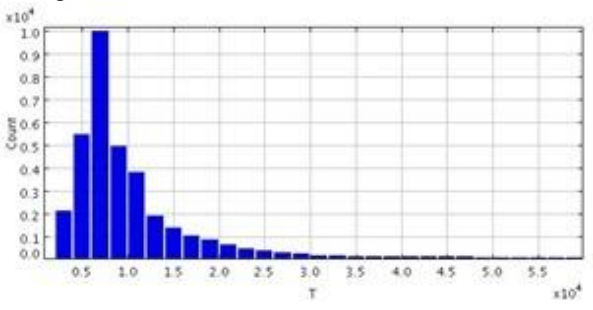
Then, we extracted from the same archive, a list of 100000 stars and we built a new color-color plot (u-g vs. g-r).

We applied the color index-temperature relation first to the 5000 and after to the 100000 stars. By means of the known color indices, we obtained the temperature of the stars and we created histograms plotting on the x-axis the temperature just found for the 5000 and 100000 stars, and in the y-axis the number of stars calculated in fixed intervals of temperature.

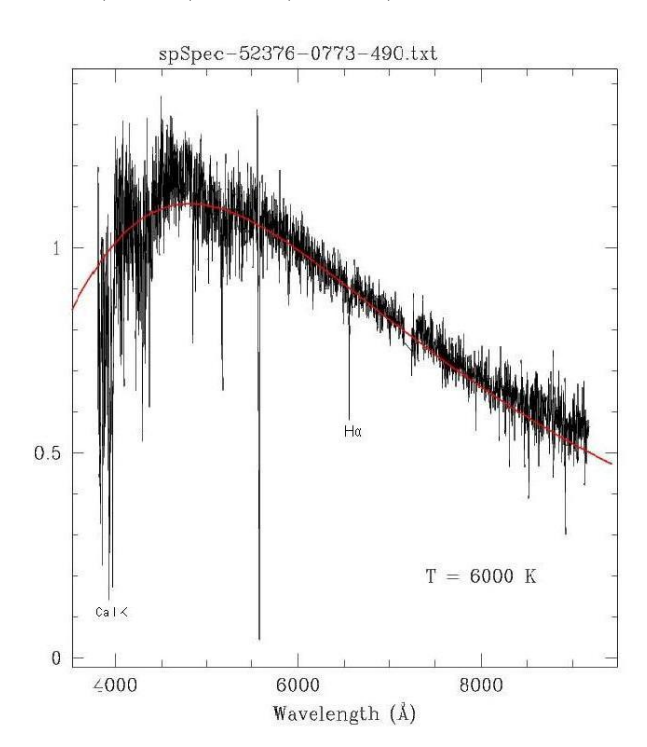
We can see that in the interval between 5000 K and 15000 K there is the highest amount of stars. Histogram of the 5000 stars:

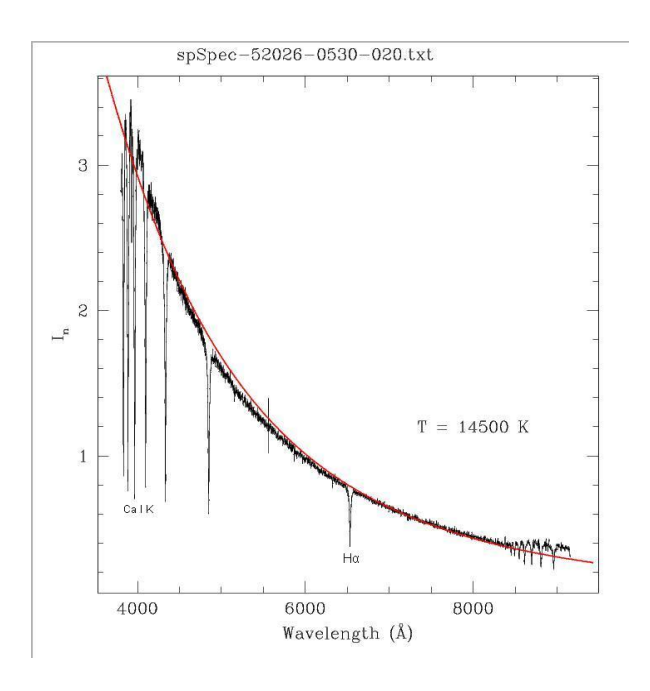


Histogram of the 100000 stars:

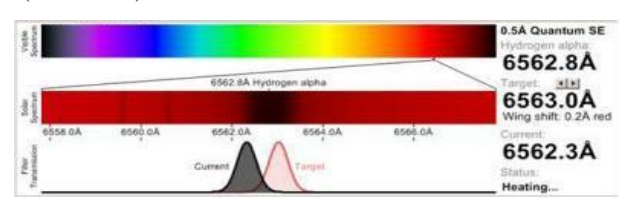


In order to study the equivalent width of the spectral lines in connection with the temperature, we considered the spectra of 10 stars at different temperatures: 3650K, 3850K, 4400K 5200K, 6000K, 6500K, 9000K, 14500K, 21000K, 60000K.

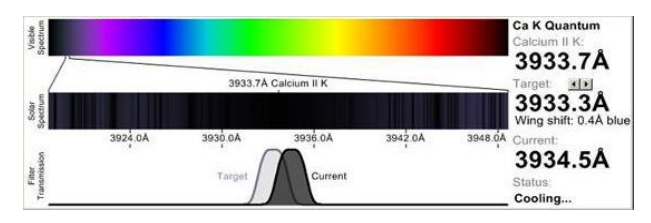




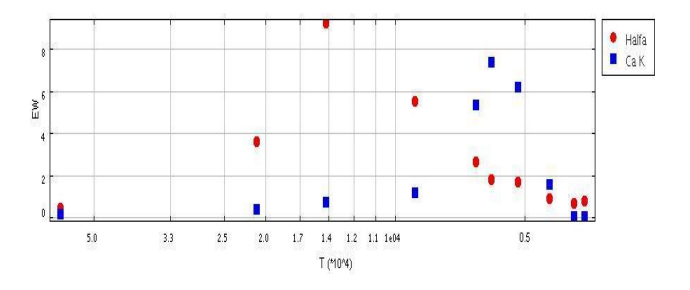
We measured the absorption lines corresponding to $H\alpha$ (at 6563 Å):



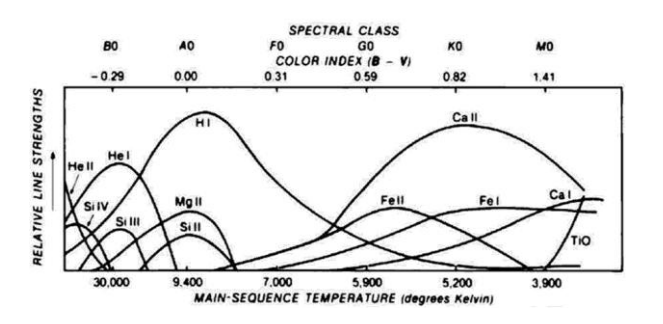
and Ca II K (at 3934 Å):



We calculated the equivalent width using the program IRAF. Furthermore we compared EW with T, in a logarithmic scale, so we found the following graph:



A peak of Ca K is well visible around 5000 K, while a peak of H is approximately at 11000 K, so we verified the expected behavior of spectral lines typical of these elements as shown in the following figure:



IV. RESULTS

In the first part of the work, we verified that there is a linear relation between the color of the stars and the reciprocal of their temperature.

In the second part, we verified the expected behavior of spectral lines typical of H and Ca II K.

Spectroscopic analysis of NGC2346 following hypothesis concerning its central object

Emanuele Brentegani⁽¹⁾, Tobia Dambruoso⁽²⁾, Nicola Giacobbo⁽²⁾, Gaetano Moronese⁽¹⁾, Francesco Piubello ⁽²⁾, Valentina Quintarelli ⁽¹⁾

(1) Liceo Scientifico "E. Medi" Villafranca VR (2) Liceo Scientifico "G. Fracastoro" Verona

ABSTRACT

The analysis of the planetary nebula is linked to the increasing knowledge of the final phases of stellar evolution. The physical and chemical characteristics of the gas outcoming from the star can be detected from the spectroscopic analysis of the nebular part. These measures can be used to build theoretical models about the main characteristics of the star which has originated the planetary nebula itself. From the outcomes we can understand how to figure out the development phases of pre-white dwarf and whether the centre of the nebula is occupied by one or more objects.

I. INTRODUCTION



Fig. 1: The "butterfly" nebula NGC 2346.

During the rising on the asymptotic branch a star loses mass. When the inner parts get below $0.3~M_{\odot}$, the most external parts get into resonance and go beyond the escape velocity.

Progressively the star gets rid of the whole envelope, expelled as subsequent layers expanding at high velocity.

This is the planetary nebula phase, during which we can observe the star surrounded by the expelled layers. At the end of this phase, after the total expulsion of the gas, we have an object with a relatively high density

and temperature; the degenerate gas cannot contract anymore: a white dwarf is formed. NGC2346 (Butterfly Nebula) is an astronomic object belonging to this category.

The purpose of our work is to analyse spectroscopically the chemical abundances of the nebular part, aiming at a future use of the obtained information in order to apply it to a model which might indicate temperature and luminosity of the central object.

The resulting chemical abundances proved to be coherent with their values in literature (Walsh 1983). Once their values were applied to the building model CLOUDY program, the output was contrasting with the spectral class of the central object found in literature and therefore we formulated different hypothesis regarding its nature and structure.

II. OBSERVATIONAL DATA

Name	NGC 2346
Object category	Planetary Nebula
Constellation	Monoceros
Coordinates (2003)	RA:07 ^h 09 ^m 41 ^s
Coordinates (2003)	Dec: -00° 48' 56"
Apparent Magnitude	11.7
Redshift	0.000073
Radial Velocity	21.8 km/s
Distance H _o =75 km s ⁻¹ Mpc ⁻¹	≈ 2000 ly (610 pc)

Angular Size	≈ 0.9'
Linear Diameter	0.3 ly
Spectral Class of the central star	A5-V

Tab.1: Data regarding the analysed nebula.

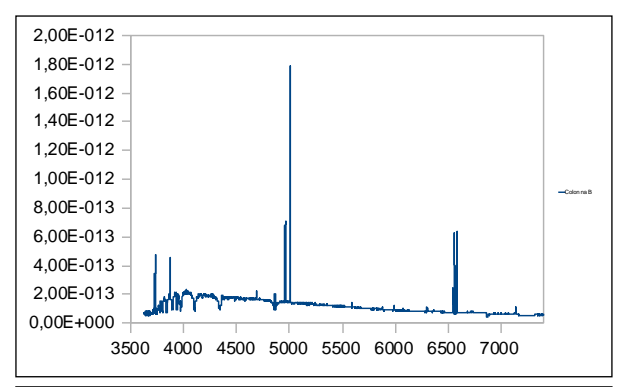
Grating	600 lines/mm
Slit Aperture	3 arcsec
Telescope 122 cm	Cassegrain
Equivalent Focal	19 m

Tab.2: Data regarding the configuration of the spectrograph.

III. WORK DESCRIPTION

The spectra we used were taken from three different parts of the nebula, with three distinct angles. First, we corrected them for bias and flat field. For wavelength calibration we used the emission spectra of a HgAr lamp and of a Ne lamp, while for the conversion from counts into flux we used a comparison spectrum of a spectroscopic standard star with known flux as a function of wavelength.

Finally, we subtracted from the data the contribution given by the sky. We used the IRAF software both for data reduction and analysis.



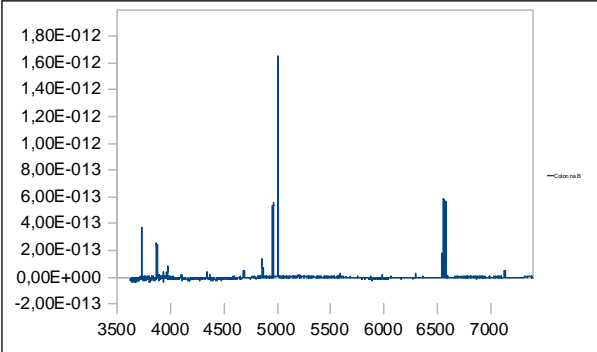


Fig.2: One-dimensional spectra of NGC2346. In the first spectrum there is the contribution of the central star, in the second spectrum the star contribution is subtracted. In abscissa we have Å in ordinate erg/cm²/s/Å.

In Fig. 2 the two spectra represent the nebula emission respectively with and without the contribution of the central star. For the graphic representation of the above mentioned spectra we used the EXCEL program.

After that, it was necessary to correct the spectrum due to the presence of the interstellar medium. In fact, the ratio between the $H\alpha$ and $H\beta$ fluxes usually follows the Balmer decrement with value 2.86. In our analysis, we noticed an alteration of the above mentioned ratio, with a 4.9 value: this is due to the partial absorption of the emitted radiation, especially at short wavelengths, given by dust and gas in between the nebula and us.

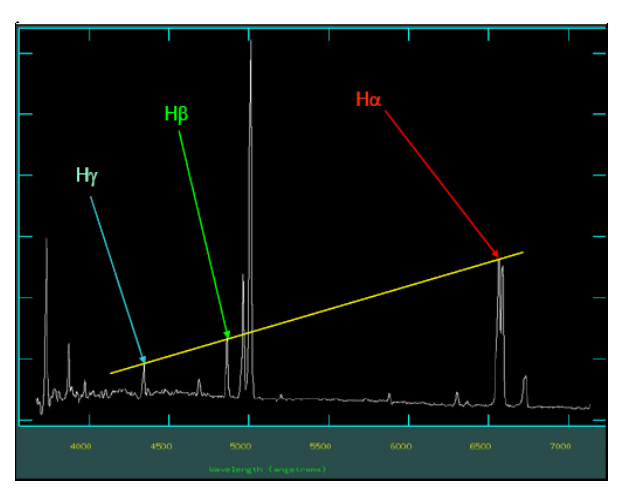


Fig.3: Balmer decrement.

Therefore, we calculated a conversion factor which allowed us to get to the true ratios between the fluxes. In our analysis, this factor is calculated in the following way ($I = intrinsic\ flux\ and\ F = observed\ flux$):

$$\begin{split} I(H\alpha)/I(H\beta) &= 2.86 \\ F(H\alpha)/F(H\beta) &= 4.9 \\ I(H\alpha)/I(H\beta) &= F(H\alpha)/F(H\beta) \ 10^{-0.4297*E(B-V)} \\ E(B-V) &= 0.544 \\ c &= log(I(H\beta)/F(H\beta)) = 1.4436*E(B-V) \\ c &= log(I(H\beta)/F(H\beta)) = 0.78 \end{split}$$

Given this value of c it is possible to find the correction in the visual magnitude of the $H\beta$ through:

$$A(V) = c / 0.4657$$

This variation in magnitude can be extended to all the wavelengths through a dereddening procedure based on the Cardelli, Clayton, and Mathis (1989) reddening curve

$$A(\lambda) = A(V) \cdot D(\lambda)$$

This type of correction is one of IRAF functions, so we could get the true fluxes of all the lines and the corrected flux ratios normalized to $H\beta$.

In Tab. 3 the measured fluxes and the corrected flux ratios normalized to $H\beta$ are reported. The fact that $H\alpha/H\beta$ gives 2.88 guarantees the reliability of the obtained result. The estimated error on the fluxes is around 10^{-14} erg/cm²/s.

Line	Waveleng	Measured Flux	Corrected
	th	erg/cm2/s	F/ Hβ
[OII]	3727	1.870E-12	11.4055
[NeIII]	3869	5.053E-13	2.91692
	3968	1.659E-13	0.91949
Нε	3968	5.809E-14	0.32172
Нδ	4102	1.072E-13	0.5587
Нγ	4340	1.831E-13	0.82101
[OIII]	4363	4.783E-14	0.20913
He I	4471	3.854E-14	0.15993
Нβ	4861	2.921E-13	1.00000
[OIII]	4959	9.028E-13	2.95072
[OIII]	5007	2.716E-12	8.69036
NII	5755	4.364E-14	0.10766
He I	5876	7.731E-14	0.18053
[OI]	6300	1.648E-13	0.34939
[OI]	6363	4.823E-14	0.10447
[ArI]	6548	9.607E-13	1.89953
Ηα	6563	1.438E-12	2.88309
[NII]	6584	3.014E-12	6.01149
HeI	6679	2.588E-14	0.05130
[SII]	6717	7.299E-14	0.14123
[SII]	6731	6.011E-14	0.11824
He I	7065	2.471E-14	0.04159
[ArIII]	7136	1.705E-13	0.29639
[OII]	7321	3.751E-14	0.06355
[OII]	7331	3.515E-14	0.05852
[ArIII]	7752	4.91E-14	0.07503
[SIII]	9069	7.542E-14	0.08951
[SIII]	9531	1.897E-13	0.21152

Then, we measured the fluxes of the lines [OIII] and [SII], which are useful indicators respectively of temperature and electron density. After that, thanks to the IRAF TEMDEN program, we assessed these two values. The procedure consists in providing the program with an initial value for the temperature; then, the TEMDEN program calculates the value of the density on the basis of the temperature we provided. Then, we continued with the calculations inserting step by step the found values of T and $N_{\rm e}$ until we got to a convergence of the values; in our case the program provided:

$$T = 18800 K$$

$$N_e = 150 \text{ cm}^{-3}$$

For the calculations of ionic abundances, we applied some formulas that can be found in Pagel et al. (1989). These allowed us to figure out the ratios between the found ions, using the obtained data concerning the temperature and electron density of the nebula.

$$\begin{aligned} 12 + \log(O^{+}/H^{+}) &= \log \frac{3726 + 3729}{H\beta} + 5,890 \\ &+ \frac{1,676}{t_{2}} - 0,40logt_{2} + \log(1 + 1,35x) \\ \log(O^{+}/N^{+}) &= \log \frac{3726 + 3729}{6548 + 6584} - 0.307 \\ &+ \frac{0.726}{t_{2}} + 0,02logt_{2} + log\frac{1 + 1,35x}{1 + 0,116x} \\ \log(O^{++}/Ne^{++}) &= \log \frac{4959 + 5007}{3869} - 0,215 \\ &- \frac{0,355}{t} - 0,13logt \end{aligned}$$

$$12 + \log(S^{+}/H^{+}) &= \log \frac{6717 + 6731}{H\beta} + 5,423 \\ &+ \frac{0,929}{t_{2}} - 0,28logt_{2} + \log(1 + 1,39x)$$

$$12 + \log(S^{++}/H^{+}) &= \log \frac{9069 + 9532}{H\beta} + 5,863 \\ &+ \frac{0,665}{t} - 0,22logt \\ \log(O^{++}/H^{+}) &= \log \frac{4959 - 5007}{H\beta} + 6,174 \\ &+ \frac{1,251}{t} - 0,55logt \end{aligned}$$

where:

 $t = electron temperature of the interstellar medium in units of <math>10^4 K \equiv t[OIII]$

$$t_2^{-1} = 0,5(t^{-1}+0,8)$$

 $x = 10^{-4}n_e t_2^{-1/2}$

where n_e is the electron density in cm⁻³.

From the ionic abundances we got the total chemical abundances multiplying the obtained values and the real ratios.

The abundances are consequently given by the following formulas (Perinotto et al. 2004):

$$\frac{N(S)}{N(H)} = \frac{N(S^+)}{N(H^+)} \times \frac{N(O)}{N(H)} \times \frac{N(H^+)}{N(O^+)}$$

$$\frac{N(N)}{N(H)} = \frac{N(N^+)}{N(H^+)} \times \frac{N(O)}{N(H)} \times \frac{N(H^+)}{N(O^+)}$$

$$\frac{N(O)}{N(H)} = \frac{N(O^{+})}{N(H^{+})} + \frac{N(O^{++})}{N(H^{+})}$$

The planetary nebula NGC 2346 is characterised by an irregular shape similar to a butterfly. In order to build a model we had to imagine it as a sphere. Furthermore,

we took a black body spectrum as emission spectrum of the star situated in the centre of the nebula.



Fig.4: Image of NGC 2346.

The model elaboration, carried out through the Cloudy program, is based on entering five free parameters:

- 1. Black-body temperature (T);
- 2. Luminosity (L);
- 3. Electronic density (Ne);
- 4. Dimensions (r):
- 5. Chemical abundances:

We obtained the values of these parameters through different methods.

We calculated the electron density of NGC2346, equal to 150 cm⁻³, with the IRAF program that elaborated the previously collected data.

As dimensions of the nebular part, we used three data: internal radius, external radius and depth of the nebular shell.

The external radius was calculated using simple trigonometric relation:

$$R = d \cdot \sin \alpha/2 \approx d \cdot \alpha/2$$

where d refers to the distance between Earth and the nebula (613.5 pc), while R is the external radius and α (0.9') the visual angle. Therefore, the external radius is about $2.5\cdot 10^{17} \, \text{cm}$. The value of the internal radius (r), on the contrary, estimated through the observation of images of the nebula seems to be about 1/10 of the external one (i.e. $2.5\cdot 10^{16} \, \text{cm}$).

The chemical abundances were chosen to be equal to the solar ones.

On the contrary, for the other two parameters of temperature and luminosity, we defined a range within which we made them variable.

We got the models allowing the logarithm of the luminosity (in erg/sec) to vary from a minimum value of 32 to a maximum of 39.

Since the continuum of the spectrum was comparable to the one emitted by an A5 V spectral class star we initially made the hypothesis that the central object, source of ionization of the nebular gas, had a temperature of $10000 \sim 15000 \; \text{K}$, but then, the values of the chemical abundances obtained by the CLOUDY

program at those temperatures were completely different from the values obtained analysing the real spectrum. We realised that the star could not be the one we initially expected.

Therefore, we decided to change the temperature of the black-body from $50000~\rm K$ to $150000~\rm K$ with intervals of $10000~\rm K$.

Among the about eighty models we made, it was necessary to find out the one closest to the experimental values.

To carry out this work, first of all we calculated the difference between each experimental abundance and its corresponding item in each model (deviation). While calculating the deviation it was easy to find out the most appropriate model: the one with the minimum deviation. The model we obtained gave us the values of the unknown parameters: temperature and luminosity.

IV. RESULTS

N(O+)/N(H+)	2.6E-04
N(O++)/N(H+)	6.3E-05
N(S+)/N(H+)	1.8E-07
N(S++)/N(H+)	5.6E-07
N(O++)/N(Ne++)	1.57
N(O+)/N(N+)	5.06
N(O+++)/N(H+)	1.6E-04

Tab.4: Ionic abundances.

N(O)/N(H)	4.8E-04
N(S)/N(H)	3.3E-07
N(N)/N(H)	9.5E-05

Tab.5: Chemical abundances.

The values of the chemical abundance of Sulphur and Nitrogen agree with the ones obtained by Walsh (1983).

In Tab. 6, we reported the experimental data and the ones referring to the model with the minimum deviation. We can see how the two series are comparable (Fig. 5). We also noticed the presence of two abnormal data corresponding to the emission of [OII] and [NII].

The reason of this difference can be related to the fact that the chemical abundance of the various elements is not uniformly spread. but it varies in relation to the distance from the central star.

Lines	λ	experimental	model	residual
[OII]	3729.36	5.976	2.960	9.0984
[NeIII]	3870.15	2.641	1.650	0.9811
[NeIII] HeI	3968.47	0.977	0.500	0.228
Ηδ	4102.01	0.266	0.260	4E-05
Нү	4341.36	0.529	0.470	0.0035
[OIII]	4364.14	0.249	0.160	0.0079
Нβ	4959.85	3.850	3.640	0.0441
[OIII]	5007.8	11.559	10.950	0.3706
[NII]	5757.16	0.107	0.010	0.0093
Hel	5876.4	0.089	0.090	1E-06
[OI]	6301.15	0.149	0.120	0.0009
[OI]	6365.14	0.060	0.040	0.0004
Ηα	6563.59	2.838	2.910	0.0052
[NII]	6584.37	2.602	0.530	4.2912
[SII]	6717.62	0.056	0.460	0.163
[SII]	6731.72	0.056	0.360	0.0923
[ArIII]	7136.26	0.202	0.190	0.0009
[OII]	7321.12	0.033	0.090	0.0032

Tab.6: Comparison between experimental data and with CLOUDY model deviations of minimum variance.

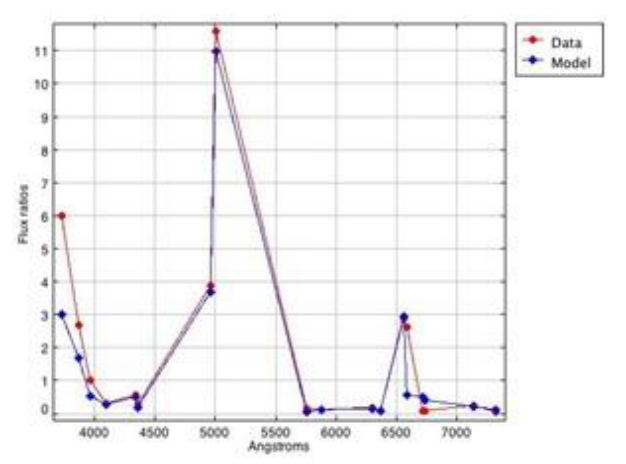


Fig.5: Comparison between the relative intensities of the experimental data and the minor variance model.

The best model gave us for the central source:

$$T = 140000 K$$

$$L \approx 10^{38} \, erg \, / \, s$$

What do these data suggest? First of all we verified that our temperature measurement is in agreement with Walsh (1983).

So what kind of object is the source of the ionization of the nebular gas? A source of about 10000 K (A5 V) cannot justify the nature of the external gas. In literature we found that the central star shows a radial velocity variation typical of a binary system. Therefore, the source of the studied phenomenon is the companion of the central star. This companion might be a star in a pre-white dwarf phase that, probably due to the gravitational field generated by the central star, has lost the external shells as far as it uncovers a very hot core where the He gets burnt.

The peculiar shape like butterfly wings might be explained by the presence of a sort of belt of obscure material influencing the expansion of the nebular gas. In order to check our proposed explanations, a research on the nebula in UV should be carried out. In this band the difference of continuum between an A class star and such a hot source would be so clear as to

V. BIBLIOGRAPHY

Cardelli. J.A., Clayton, G.C., & Mathis, J.S. 1989, ApJ, 345, 245;

Pagel, B.E.J., Simonson, E. A., Terlevich, R. J., Edmunds, M. G. 1992, MNRAS, 255, 325;

Perinotto et al., 2004, MNRAS, 349, 793;

indicate a decisive experimental difference.

Smalley B., 1997, The Observatory, vol.117, 338-343;

Walsh, J.R. 1983, MNRAS, 202, 303;

Walsh & Roy, 1989, MNRAS, 239, 297.

Spectral classification and determination of the star distances using $H\alpha$ emission line

Fabio Lonardi⁽¹⁾, Michele Piccoli⁽¹⁾, Leonardo Manzati⁽²⁾

(1) Liceo scientifico "Primo Levi", San Floriano (2) Liceo scientifico "di Garda", Garda

ABSTRACT

The sky surveys are used to collect in the shortest time possible a great amount of observations in order to make many data available for the users. Obviously, not all the observations have been completely analysed. Most of the objects are catalogued only with some physical characteristics, i.e. the magnitude and the colour. In this study we tried to determine the spectral class and the distance of five objects of the INT/WFC Photometric H α Survey of the Northern Galactic Plane (IPHAS) catalogue.

I.INTRODUCTION

During the days we spent at the Asiago Astrophysical Observatory (Mt. Pennar), we observed and collected data of an appropriately selected group of stars. The stars were selected from the IPHAS catalogue of $H\alpha$ emission-line sources in the northern Galactic plane (Witham et al. 2008). IPHAS contains 4853 point sources that show a photometric evidence of the $H\alpha$ emission line.

The stars in the catalogue represent a variety of stellar types, including early-type emission-line stars, active late type stars, symbiotic binary and compact nebular stars.

We started with a list of 766 sources with very prominent $H\alpha$ emission line and apparent magnitude between 13 and 19.

The aim of our work was to classify the stars by comparing the obtained spectra with the spectra of stars with known spectral class.

We selected 5 stars out of the 766 extracted sources. Since the studied stars are located in the Galactic plane we were forced to tackle the issue of the Galactic extinction.

Once solved the problem and carried out the classification, we were surprised by one of the examined objects. At last, we estimated the distance of the five objects.

II. OBSERVATIONAL DATA

A first selection was carried out choosing sources brighter than mag 16; then we selected 32 sources with apparent magnitude brighter than 14. At the end, we chose among these, 5 stars with r-H α >0.6.

These stars were observed with the 1.2 mt telescope of the Asiago Astrophysical Observatory on February 18th, 2009.

Object name	R.A.	Dec.	Exposure time	U.T.
KW97 27-49	6h 13m 42s	+14° 04'	1200sec	20:50
KW97 20-46	5h 03m 27s	+41° 42' 03"	1200sec	21:37
2MASS J05330904+ 2911030	5h 33m 09s	+29° 11' 03"	1200sec	22:17
2MASS J05390916+ 3544225	5h 39m 9s	+35° 44' 23"	1200sec	22:53
EM VES 880	5h 10m 51s	+43° 21' 30"	1200sec	23:27

Tab.1: The five selected objects with their equatorial coordinates and the exposure time.



Fig.1: 2MASSJ05390916+3544.

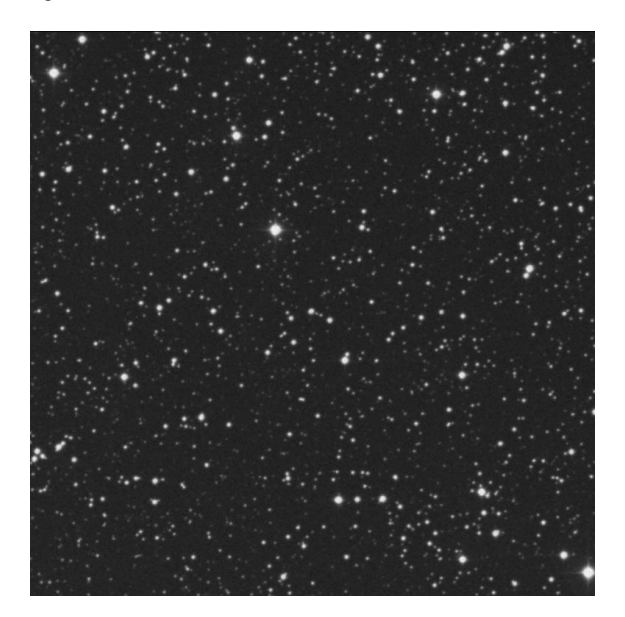


Fig. 2: KW97 20-4.



Fig.3: 2MASS J05330904+2911030.



Fig. 4: EM VES 880.



Fig. 5: KW97 27-46.

III. WORK DESCRIPTION

It was necessary to process the spectra taken during the night, before analyzing them.

First, we corrected the spectra for bias and flat field. Then, for wavelength calibration, we used the emission spectrum of a Hg-Ne-Ar lamp. For the conversion of counts into flux, during the same night, we acquired a spectrum of a spectrophotometric standard star, with known fluxes.

At last, we subtracted from the spectra the sky contribution. After we reduced and calibrated the spectra, we normalized them making the flux=1 at λ =5500Å.

For the analysis and the measurements, we used the IRAF program. To compare the spectra, we used the Topcat program. In the following pictures, we show the calibrated and normalized spectra.

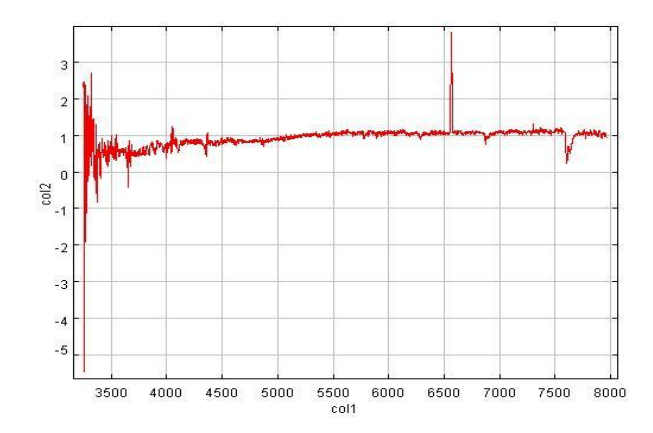


Fig. 6: KW97 27-49.

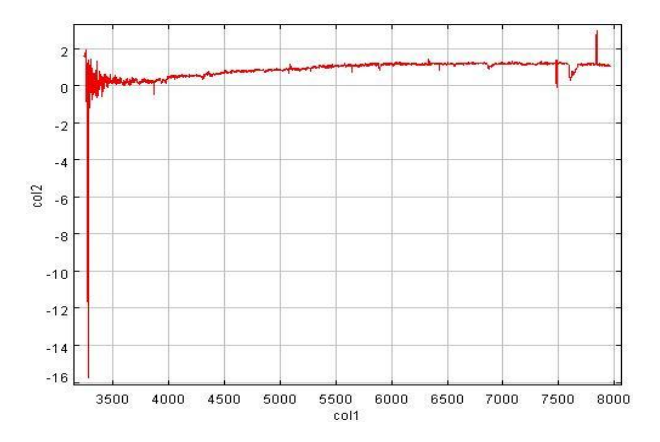


Fig. 7: KW97 20-46.

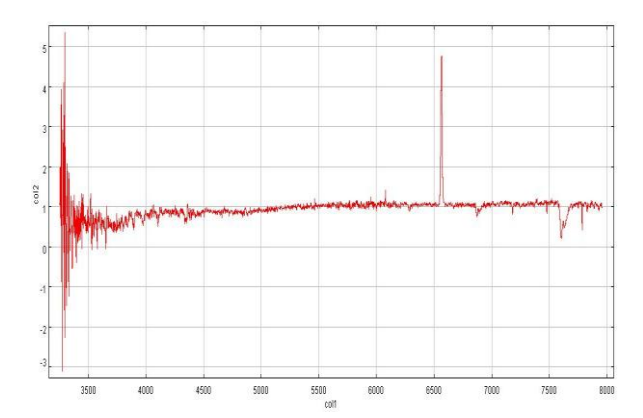


Fig. 8: 2MASS J05330904+2911030.

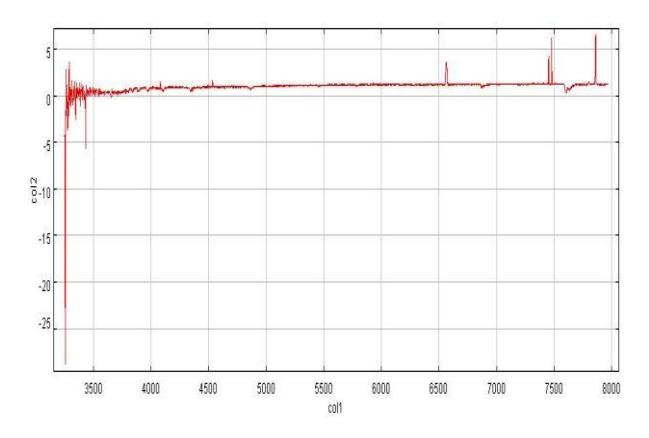


Fig.. 9: 2MASS J05390916+3544225.

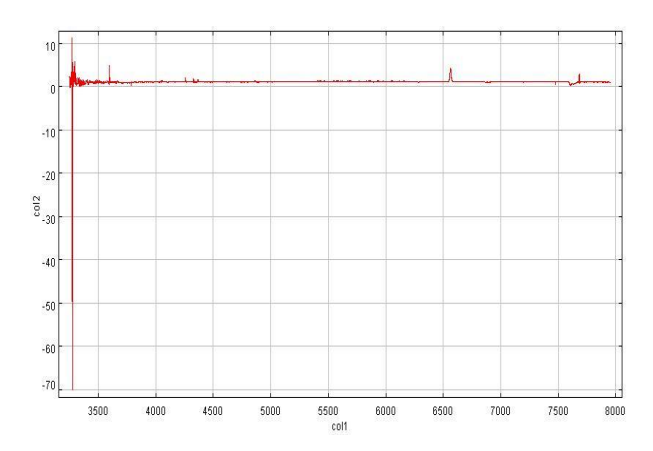


Fig. 10: EM VES 880.

The observed stars were compared with stars of known spectral types in order to look for the similarities between them.

We observed a decrease of the signal in the blue region. This was the effect of the Galactic extinction because the Galactic plane dust absorbs the light of the observed objects mainly in the blue spectral range.

We applied different values for the extinction to the spectra till they became more similar to the reference stars. In order to have a further confirmation of our identification of the spectral classes, we checked the presence of those characteristic lines that identify the spectral classes.

We report the corrected spectra of the stars compared with the spectra of the reference stars which seemed to better correspond.

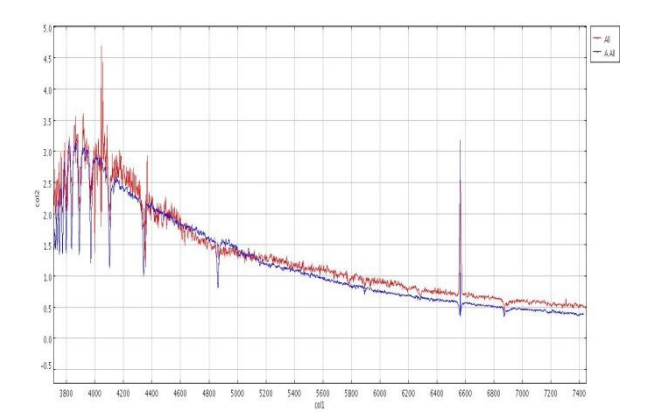


Fig.11: KW 97 27-49(in red) compared with a B6 star (in blue).

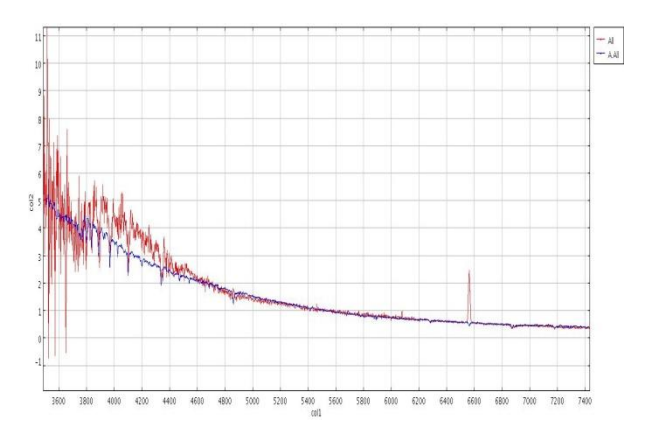


Fig. 12: 2MASS J05330904+2911030(in red) compared with an $\,$ O7 star (in blue).

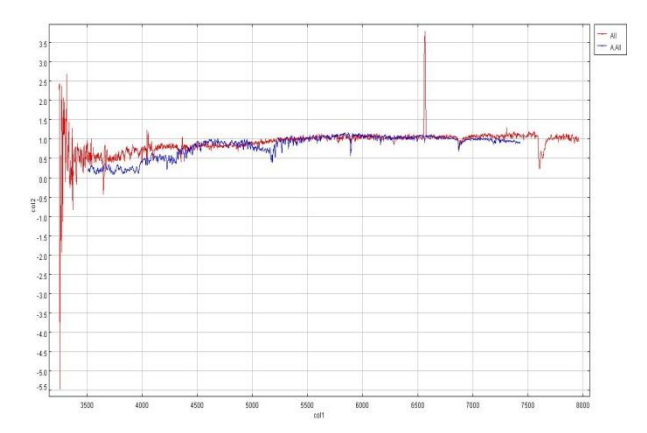


Fig. 13: KW97 20-46 (in red) compared with a K4 star (in blue).

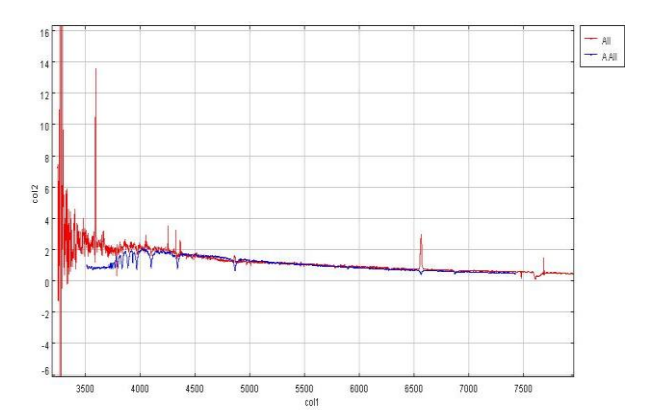


Fig. 14: EM VES880 (in red) compared with an A5 star (in blue).

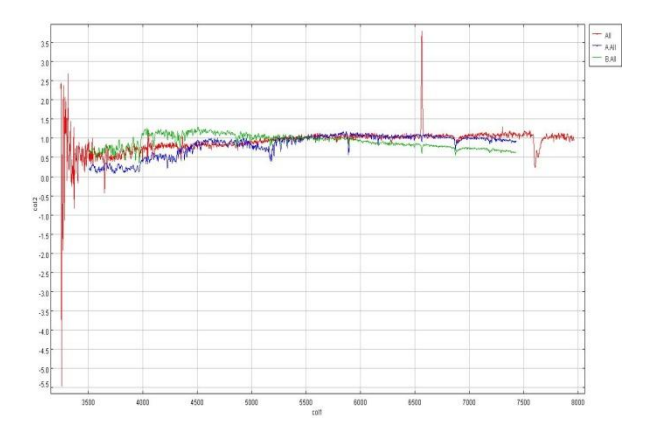


Fig. 15: KW97 20-46 comparison between the observed spectrum and a K4 spectrum (in blue) and a G0 spectrum (in green).

After obtaining the spectral class and the extinction, we could estimate the absolute magnitude of the stars through HR diagram. For apparent magnitudes, we referred to IPHAS, which provided us with the apparent magnitude in r band and r-i colour. We used these data to calculate the apparent magnitude in UBVRI bands.

STAR	r	r-i
KW97 27-49	13.83	0.0010
KW97 20-46	13.59	0.0010
2MASS J0533904+2911030	13.79	0.0020
2MASS J05390916+3544225	13.77	0.0010
EM VES 880	13.57	0.0010

Tab.3: Magnitudes (r) and colors (r-i) of the stars.

STAR	M	A(V)
KW97 27-49	-0.5	+3.0
KW97 20-46	+7.5	0.0
2MASS J0533904+2911030	-4.6	+3.5
2MASS J05390916+3544225	0.0	+3.0
EM VES 880	+2.0	+0.5

Tab. 4: Characteristic absolute magnitude M and extinction A(V) for each star.

We calculated the apparent magnitude with the following relation (Jordi et al. 2006):

$$m = r - 0.153 (r - i) - 0.117$$

Therefore, we estimated the distance of the objects in pc with the distance modulus formula:

$$M - m = 5 - 5 \operatorname{Log}(d) - A$$

From which it follows:

$$d = 10^{\frac{m+5-M-A}{5}}$$

IV. RESULTS

STAR	CLASS	A(V)
KW97 27-49	В6	+3.0
KW97 20-46	K4	0.0
2MASS J0533904+2911030	O8	+3.5
2MASS J05390916+3544225	В8	+3.0
EM VES 880	A5	+0.5

Tab. 5: Spectral classification and Galactic extinction values used to compare the spectra.

As we can see, in four cases our objects are stars of high Main Sequence. This necessarily brought about, especially in three cases, a significant extinction correction. On the contrary, the spectrum of KW9720-46 was better reproduced by the spectrum of a K star. These stars are relatively cold and emit a small fraction of their light in the blue region of the spectrum. In fact, we did not need to correct anything in this case. However, this object was in some way different from the others. We could not find a good correspondence between the reference spectrum and the observed one. We tried to overlap both a K4 and a K5 star without finding a satisfactory result. At the end, we realised that the mentioned object is actually a binary source composed of a K5 type star and a solar type star.

The integration of the two spectra forms a curve that is not a Planck curve. On the contrary, it is the sum of two spectra at different temperatures that give an excess trend both in blue and in red.

STAR	m	d (pc)
KW97 27-49	13.71	174
KW97 20-46	13.47	156
2MASS J0533904+2911030	13.67	9010
2MASS J05390916+3544225	13.65	1348
EM VES 880	13.46	1553

Tab.6: Apparent magnitudes (m) and distances (d) of the five stars.

Considering that the stars had an apparent magnitude 13.4 < m < 13.8, the spectral class was the factor that conditioned the distances in a decisive way. The output confirms it and shows that the star at a lower temperature is definitely the nearest and that the estimated star of type O8 is by far the farthest. The fact that we do not have unreliable distances, i.e. an object out of the Milky Way, allow us to consider correct the obtained analysis.

V. BIBLIOGRAPHY

www.iphas.org

www.simbad.u-strasbg.fr/simbad/

www.sdss.org/dr6/algorithms/sdssUBVRITransform.ht ml

Rosino, 1979, Lezioni di astronomia, Cedam, Padova

Witham, A.R. et al., MNRA. S.384, 1277-1288 (2008)

Star formation rate in spiral galaxies

Mattia Carraro, Daniele Moretto, Filippo Stellin, Gianluca Stellin

Liceo Scientifico "Galileo Galilei", Dolo (VE)

ABSTRACT

We have calculated the star formation rate, the number of solar masses annually formed, in 20 spiral galaxies. Moreover it has been possible to establish the number of ionizing photons and the theoretical number of 05 stars needed to produce these emissions. The twenty galaxies have been selected from the SDSS Data release 6 database.

I. INTRODUCTION

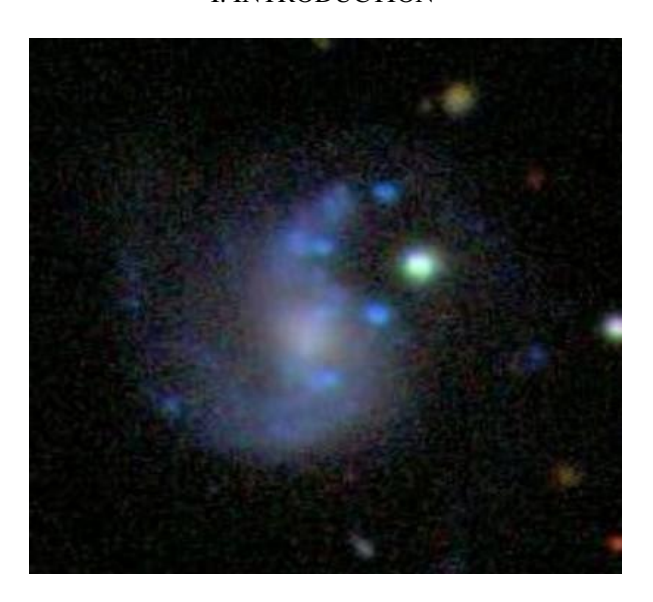
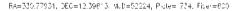


Figure 1: The object SDSS J143245.14+025454.0, it is an example of a barred spiral galaxy.

The computation of the star formation rate (SFR) was accomplished on twenty spiral galaxies, which were accurately selected from a database, according to specific criteria. The objects that were identified have redshifts that range from 0 to 0.035, clearly visible $H\alpha$ and $H\beta$ emission lines, and a high brightness in the g band. In this way, only galaxies rich in young and hot stars were chosen, avoiding elliptical galaxies, which generally have old stars.

II. OBSERVATIONAL DATA

The spiral galaxies chosen for our project were already supplied with data regarding their astronomic coordinates (right ascension and declination), their redshift value z and the fiber magnitudes in filters u, g, r, i, z.



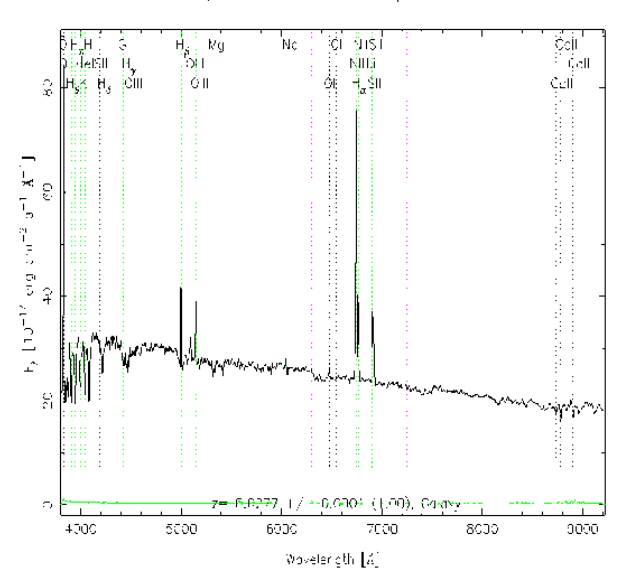


Figure 2: The spectrum of the object SDSS J220307.02+122346.0. An example of a spectrum that shows marked H α and H β emissions.

The fiber magnitudes refer to the flux contained within a circular aperture of 3" in diameter centered on the objects.

The data collected from the studied galaxies are reported in table 1 at the end of this report.

III. WORK DESCRIPTION

To begin, we downloaded from the SDSS Data Release 6 a list of 2000 galaxies with z value that ranges from 0 to 0.03. According to the color-color diagram *u-g* vs. *g-r* we selected 20 galaxies with blue color indices.

Then, we analyzed the spectrum of each galaxy with IRAF, in order to obtain the wavelengths of the emission peaks corresponding to H α , H β and [OIII] lines. We compared these wavelengths with rest frame values (that are respectively 6563Å, 4861Å and 5007Å) to measure again their redshifts.

$$z = \frac{\frac{\lambda_{H\alpha}^{'} - \lambda_{H\alpha}}{\lambda_{H\alpha}} + \frac{\lambda_{H\beta}^{'} - \lambda_{H\beta}}{\lambda_{H\beta}} + \frac{\lambda_{OIII}^{'} - \lambda_{OIII}}{\lambda_{OIII}}}{3}$$

The z values were used to calculate the galaxies' distance (expressed in Mpc), applying Hubble's law:

$$d = \frac{c \cdot z}{H}$$

where c is 299700 km·s⁻¹ and the Hubble's constant H_o is equal to 72 km·Mpc⁻¹·s⁻¹.

With the same software, we measured the fluxes of the emission lines H α and H β (expressed in 10^{-17} erg \cdot s⁻¹ · cm⁻²), that were expected to be significantly different in comparison to the real fluxes emitted by the galaxies. This difference is caused by the *extinction* phenomenon, due to cosmic dust absorbing part of the emitted radiation, in particular at short wavelengths: consequently, the flux appears very reduced in the blue and violet bands.

This effect occurs mainly inside each galaxy, but it is also influenced by the galaxy position relatively to the Milky Way, since the light passes through different dust layers of the Galaxy.

The spectra of our galaxies were corrected for the Milky Way extinction using the task *deredden* and the A(V) values given by NED (NASA Extragalactic Database).

To correct the measured emission line fluxes, we applied the following empirical law, given by Cardelli, Clayton e Mathis [CCM 1989]:

$$\frac{A(\lambda)}{A(V)} = a(y) + \frac{b(y)}{R(V)}$$

At first we determined the value of the *y parameter* related to $\lambda_{H\alpha}$ (6563Å) and $\lambda_{H\beta}$ (4861Å):

$$y = \frac{10^4}{\lambda} - 1.82$$

$$y_{H\alpha} = -0.2963$$
 and $y_{H\beta} = 0.2372$

In this way, we found the values of the parameters a e b characteristic of each wavelength, applying the following polynomial equations:

$$\begin{array}{l} a(y) = 1 \ + \ 0.17699y \ - \ 0.50447y^2 \ - \ 0.02427y^3 \ + \\ 0.72085y^4 + 0.01979y^5 - 0.77530y^6 + 0.32999y^7 \end{array}$$

$$\begin{array}{l} b(y) = 1.41338y + 2.28305y^2 + 1.07233y^3 - 5.38434y^4 \\ -0.62251y^5 + 5.30260y^6 - 2.09002y^7 \end{array}$$

$$a_{H\alpha} = 0.9088$$
; $b_{H\alpha} = -0.2823$

$$a_{H\beta} = 1.0154$$
; $b_{H\beta} = 0.4613$

The selective ratio R(V), on the other hand, depends on the size of the dust grains, which absorb photons, and can have values between 3 and 7: in general, the value 3.1 is adopted.

We calculated the extinctions $A(H\alpha)$ and $A(H\beta)$, replacing the parameters a, b and R(V) in the empirical law mentioned above:

$$A(H\alpha) = 0.8177 \cdot A(V)$$
 [1]
 $A(H\beta) = 1.1642 \cdot A(V)$ [2]

In the following graph the absorption as a function of wavelengths is reported.

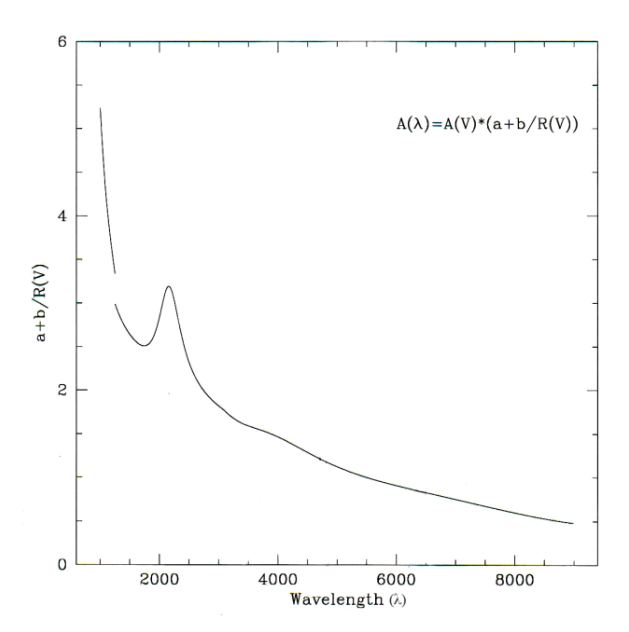


Figure 3: CCM (1989) reddening function.

The wavelength is on the x-axis, while on the y-axis there is the ratio between the absorption in a specific λ and the one corresponding to the photometric V band (centered at 5500Å). We can notice that this ratio increases rapidly at short wavelengths, and reaches values near to zero in the infrared.

Since the value of the absorption at a certain wavelength coincides with the difference between the observed and the real magnitudes at that wavelength, from the Pogson law we derive:

$$A(\lambda) = m_0 - m = -2.5 \log_{10} \left(\frac{F_0}{I} \right)$$

where m_0 is the observed magnitude, while m is the magnitude that the galaxy should have if the radiation were not absorbed.

Consequently, F_0 is the observed flux, and I is the intrinsic flux: in our case F_0 was replaced with the measured fluxes $F_{H\alpha}$ e $F_{H\beta}$:

$$A(H\alpha) = -2.5 \log_{10} \left(\frac{F_{H\alpha}}{I_{H\alpha}} \right)$$

$$A(H\beta) = -2.5 \log_{10} \left(\frac{F_{H\beta}}{I_{H\beta}} \right)$$

Afterwards, we deduced the following equations by exploiting the logarithm properties:

$$\frac{F_{H\alpha}}{I_{H\alpha}} = 10^{-0.4 \cdot A(H\alpha)}$$

$$\frac{F_{H\beta}}{I_{H\beta}} = 10^{-0.4 \cdot A(H\beta)}$$

Then, we obtained the equation of the intrinsic flux ratio:

$$\frac{I_{H\alpha}}{I_{H\beta}} = \frac{F_{H\alpha}}{F_{H\beta}} \cdot 10^{0.4 \cdot A(H\alpha - H\beta)}$$

By replacing $A(H\alpha)$ and $A(H\beta)$ with the equation previously mentioned and given that the intrinsic ratio is 2.86 (Balmer Decrement), we obtained:

$$\frac{I_{H\alpha}}{I_{H\beta}} = 2.86 = \frac{F_{H\alpha}}{F_{H\beta}} \cdot 10^{-0.1386A(V)}$$

from which we have:

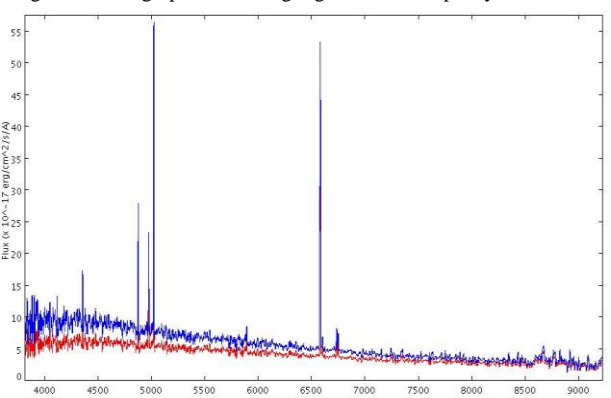
$$A(V) = \frac{\log(2.86) - \log\left(\frac{F_{H\alpha}}{F_{H\beta}}\right)}{-0.1386}$$

At last, we could calculate the intrinsic fluxes $I_{H\alpha}$ and $I_{H\beta}$, starting from the previous equations:

$$I_{H\alpha} = F_{H\alpha} \cdot 10^{0.3271 A(V)}$$

$$I_{H\beta} = F_{H\beta} \cdot 10^{0.4657 A(V)}$$

Figure 4: The graph above highlights the discrepancy between the



real fluxes (in blue) and the observed ones (in red): the high-frequency radiation absorbed by the interstellar medium is emitted at longer wavelengths, in the nearby infrared. The spectrum belongs to the object SDSS J002908.36+155356.8, an Sb galaxy.

Then, we transformed fluxes into luminosities using the distances calculated earlier:

$$L = 4\pi d^2 \cdot I$$

From the fiber magnitudes in u and g filters, we first calculated the apparent magnitude B that corresponds to an aperture of 3 arcseconds on the galaxy centers:

$$B = g - 0.17 \cdot (u - g) + 0.11$$

And, after that, the absolute B magnitude:

$$M_B = m_B + 5 - 5\log(d)$$

where the distance d is expressed in parsec.

Comparing M_B with the solar absolute magnitude $M_{B(\odot)}$ =+5.48 and his luminosity L_{\odot} = 3.9E33 erg/s, we calculated the B luminosity for each galaxy using the formula:

$$L_B = L_{Sun} \cdot 10^{\frac{M_B - M_{B,Sun}}{-2.5}}$$

With the software TopCat, we reported each galaxy in a graph of luminosity of $H\alpha$ emission line (x-axis) versus the B luminosity (y-axis). We used a logarithmic scale and calculated with TopCat the best linear regression function. The data follow a linear function, $log(L_B) = m \cdot log(L_{H\alpha}) + q,$ with slope m=0.997 and intercept q=2.17.

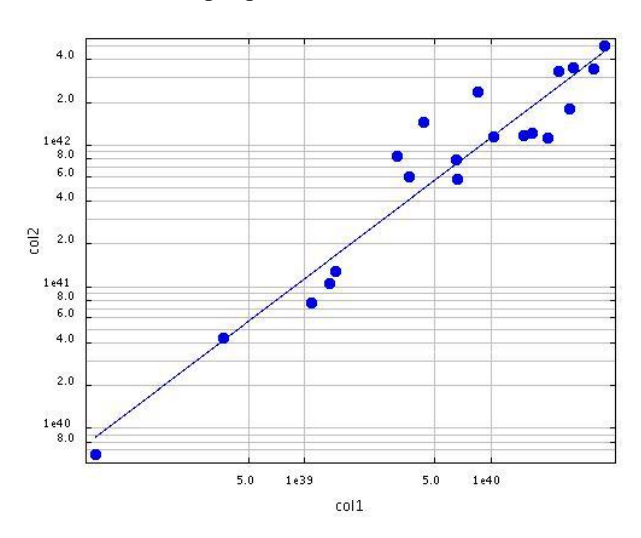


Figure 5: Ha luminosity (x-axis) versus B luminosity (y-axis).

Why a similar relation exists? In order to observe the ionized gas, it is necessary the presence of hot stars (O, B). If there are hot stars, they are so bright that they give substantial contribution to the galaxy radiation. Taking into account the black body function, we know that hot stars contribute more at shorter wavelengths, therefore in the photometric bands U and/or B. In conclusion, even if B and H α luminosities were derived independently, they share the same origin: the presence of hot and bright stars.

As we have previously underlined, the data through which we obtained L_B and $L_{H\alpha}$ are referred only to the central part of the galaxies. In order to give a rough estimate of the $H\alpha$ luminosity of the entire galaxy, we extracted the total magnitudes in the u and g filters from the SDSS Database, and we repeated the same calculations, obtaining the total B luminosity for each galaxy.

Under the hypotheses that the $L_{H\alpha}\text{-}L_B$ relation found earlier can be applied also to the entire galaxies and that ionized gas is homogeneously distributed within each galaxy, we calculated the total $L_{H\alpha}$ with the equation:

$$L_{{\cal H}\alpha-TOT} = 10^{\frac{\log L_{B-TOT}-2.17}{0.997}}$$

Obtained so forth the energy emitted in the H α line by each galaxy, we found the respective number of *ionizing photons* giving origin to that energy emission:

$$Q_{ion} = 7.3 \cdot 10^{11} \cdot L_{H\alpha - TOT}$$

And the star formation rate, expressed in solar masses per year:

$$SFR = 7.9 \cdot 10^{-42} \cdot L_{H\alpha-TOT}$$

IV. RESULTS

The intensity of the $H\alpha$ emission line increases proportionally to the number of hot stars contained in a galaxy, because they are able to produce a significant amount of ionizing photons (having energy higher than 13.6 eV).

If we consider that an O5 star emits about $10^{49.67}$ ionizing photons/sec, we can give an estimate of the expected number of O5 stars in each galaxy:

$$N(O5) = \frac{Q_{ion}}{10^{49.67}}$$

Even if the $H\alpha$ emission is clearly not caused exclusively by O5 stars, which are also very rare, this number can be useful to compare the possible number of young and hot stars in each galaxy.

Therefore, among our galaxies, there are some of them that reach only 2400 O5 stars (like object 5 in the table below), while some other galaxies contain more than 500000 stars, like object 12. This happens because object 5 presents the lowest SFR of the twenty galaxies (only 0.29 $\rm M_{\odot}/\rm yr)$, while object 12 possesses the highest one: it forms about 70 new solar mass stars each year.

High SFR values are tightly referred to galaxies with young star populations, in which the gas reemits the star radiation below Lyman's limit (912Å), in the UV region.

Therefore, only in galaxies containing stars with mass $20M_{\odot}$ and a lifetime less than 20 million years it is possible to measure relevant H α and H β fluxes, and also fluxes in P α , P β , Br α and Br γ lines.

Furthermore, the SFR depends also on the gas density and on the galaxy morphology (see Hubble's classification), and shows a remarkable range from zero in the gas-poor elliptical and S0, to $20~M_{\odot}/\rm{yr}$ in gas-rich spirals. Much larger global SFRs, up to $100~M_{\odot}/\rm{yr}$, can be found in optically selected starburst galaxies, and SFRs as high as $1000~M_{\odot}/\rm{yr}$ may be reached in the most luminous IR starburst ones, as the following table shows.

Type	SFR (M∘·year ⁻¹)
S0, elliptical, dwarf	→0
spiral	20<>100
starbursts	100<>1000
IR starbursts	>>1000

Considering all these factors, we may assert that galaxies similar to object 5, with SFR equal to 0.29 M_{\odot}/yr are dwarf spirals, while others like object 12, with values as high as 70 M_{\odot}/yr can be classified as large spirals (normal or barred).

V. BIBLIOGRAPHY

R. C. Kennicutt jr., *Star Formation in Galaxies along the Hubble Sequence*, Annu. Rev. Astron. Astrophys. 1998. 36:189–231, (1998);

Report on a stage of Asiago, M. Lazzari, M. Rocchetto, I. Vidal, *Misura della Star Formation Rate nelle galassie NGC 1569*, *NGC 2798 e NGC 3227*, 2006/2007 Edition;

Report on a stage of Asiago, F. Barato, E. Battistich, G. Martignon, *Determinazione del tipo spettrale e stima dell'estinzione in stelle con righe di emissione*, 2002/2003 Edition;

Cardelli J.A., Clayton G.C., Mathis J.S., *The Relationship between infrared, optical and ultraviolet extinction*, Ap.J. 345:245-256 (1989);

VI. DATA TABLES

	fiber	Mag	To	tMag	Distance (Mpc)
ObjectID	u	g	u	g	
SDSS J141318.93+013951.8	20.5821	19.2101	18.00	16.75	108.960
SDSS J124745.92+030851.5	20.1333	19.1071	18.94	18.01	87.949
SDSS J093437.00+000245.8	19.6967	18.6693	17.66	16.73	69.165
SDSS J092223.10+504628.9	20.1346	19.0591	17.98	16.99	112.996
SDSS J002908.36+155356.8	20.8136	20.0397	17.67	16.52	11.681
SDSS J024120.21-071705.9	20.4400	19.5706	17.97	17.11	24.348
SDSS J130049.13-012136.4	20.5879	19.6888	18.51	17.58	95.760
SDSS J115314.09-032432.2	18.4131	17.8685	17.00	16.27	18.507
SDSS J121214.73+000420.2	18.3725	17.4426	16.74	15.86	33.421
SDSS J151047.23-002053.9	20.4019	19.4784	17.24	16.17	31.173
SDSS J220307.02+122346.0	19.3559	18.1886	17.71	16.66	116.303
SDSS J141523.71+042430.6	19.1761	18.0893	15.72	14.83	81.057
SDSS J130158.45-034046.8	20.0605	18.8825	17.62	16.59	114.431
SDSS J143245.14+025454.0	19.3130	18.3930	15.79	14.91	22.303
SDSS J173206.08+583713.9	19.0540	18.1154	17.89	16.78	111.734
SDSS J215953.35+112045.1	20.4541	19.3163	18.99	17.87	115.041
SDSS J004118.34-094620.6	19.1990	18.0987	18.20	17.12	116.264
SDSS J135541.65+025215.9	18.2376	17.5065	16.91	15.97	100.053
SDSS J225520.60+130507.3	19.7685	18.8381	18.97	18.09	91.964
SDSS J153413.35+571707.0	18.0433	17.5226	16.55	15.86	47.636

ObjectID	$SFR (M_{\Theta}/yr)$	Ionizing photons	No O5 contained	B total Luminosity	Hα total Luminosity
SDSS J141318.93+013951.8	20.375	7.828E+54	167365	1.068E+43	1.072E+43
SDSS J124745.92+030851.5	4.373	1.680E+54	35921	2.292E+42	2.302E+42
SDSS J093437.00+000245.8	8.792	3.378E+54	72220	4.609E+43	4.627E+42
SDSS J092223.10+504628.9	18.296	7.030E+54	150292	9.591E+42	9.630E+42
SDSS J002908.36+155356.8	0.294	1.130E+53	2415	1.541E+41	1.547E+41
SDSS J024120.21-071705.9	0.776	2.982E+53	6376	4.069E+41	4.085E+41
SDSS J130049.13-012136.4	7.703	2.960E+54	63278	4.038E+42	4.054E+42
SDSS J115314.09-032432.2	0.992	3.812E+53	8150	5.201E+41	5.222E+41
SDSS J121214.73+000420.2	4.611	1.771E+54	37873	2.417E+42	2.427E+42
SDSS J151047.23-002053.9	2.927	1.124E+54	24040	1.534E+42	1.540E+42
SDSS J220307.02+122346.0	26.022	9.998E+54	213753	1.364E+43	1.370E+43
SDSS J141523.71+042430.6	69.923	2.687E+55	574367	3.665E+43	3.680E+43
SDSS J130158.45-034046.8	26.953	1.036E+55	221398	1.413E+43	1.419E+43
SDSS J143245.14+025454.0	4.925	1.892E+54	40458	2.582E+42	2.592E+42
SDSS J173206.08+583713.9	25.152	9.664E+54	206606	1.318E+43	1.323E+43
SDSS J215953.35+112045.1	8.262	3.174E+54	67869	4.331E+42	4.349E+42
SDSS J004118.34-094620.6	16.944	6.510E+54	139181	8.882E+42	8.918E+42
SDSS J135541.65+025215.9	36.991	1.421E+55	303853	1.939E+43	1.947E+43
SDSS J225520.60+130507.3	4.477	1.720E+54	36773	2.347E+42	2.356E+42
SDSS J153413.35+571707.0	9.649	3.707E+54	79263	5.058E+42	5.079E+42

Stellar population synthesis

Francesco Piccolo, Nicolò Lorenzetto, Nicolò Pasini.

Liceo Scientifico "U. Morin", Mestre (VE)

ABSTRACT

We present a stellar population synthesis analysis of ten galaxies selected from the SDSS (Sloan Digital Sky Survey). We combined in different ways ten stellar spectra taken from the same archive in order to get integrated spectra similar to those of the galaxies. Finally, we tried to give an approximate morphological classification of our galaxies.

I. INTRODUCTION

Galaxy morphology is linked to many of the global characteristics of galaxies (e.g. stellar population, angular momentum, star formation rate, gas content). Referring to the Hubble sequence, we could notice, for instance, that ellipticals and spirals show considerable differences in their stellar population: the first ones are made up only of old stars, while the second ones present both a young and an old stellar population.

The spectroscopic characteristics of a galaxy are obviously due to the spectroscopic characteristics of the stars it is made up of, therefore the spectrum of a galaxy can be seen as the integrated spectrum of all the spectra of its stars. In this sense the stellar population synthesis consists in reproducing the integrated spectrum of a galaxy with a linear combination of individual stellar spectra of various types, in order to get an approximate idea of the composition of the galaxy.

Since the 1970's several stellar population synthesis models have been employed (see the "evolutionary population synthesis technique") and, even though modern models still suffer from serious limitations and intrinsic uncertainties, important progresses have been made.

II. OBSERVATIONAL DATA

We selected ten main sequence stars belonging to different spectral classes and ten galaxies at low redshift. The images we analyzed were taken from the Sloan Digital Sky Survey (SDSS) archives. We selected hot, intermediate and cold stars in order to make a comparison between the spectrum of each galaxy and the spectrum resulting from a proportioned combination of the various spectra of the stars. Coordinates, λ_{max} of the fitted black-body spectrum

(Wien's law) and spectral type of the stars are reported in Tab.1, while coordinates and redshifts of the galaxies are reported in Tab.2.

Object	RA (deg)	Dec (deg)	λ_{max}	type
SDSS J002556.90- 093231.1	6.48711	-9.54199	3857	A
SDSS J125417.89+ 003735.0	193.5746	0.62641	4047	A
SDSS J161138.47+ 523820.2	242.9103	52.63895	5581	F
SDSS J032731.34- 063158.6	51.88061	6.53295	5579	F
SDSS J133116.70+ 020833.4	202.8196	2.14265	5580	F
SDSS J171710.76+ 585729.1	259.2949	58.95809	7605	K
SDSS J012647.06+ 141635.8	21.69614	14.27665	4038	A
SDSS J155335.88+ 001534.9	238.3995	0.25971	4796	F
SDSS J205029.53- 052602.0	312.6231	-5.43391	5579	K
SDSS J205326.86- 055301.2	313.3818	-5.88354	4897	F

Tab.1: Coordinates, λ_{max} and spectral type of the selected stars.

Object	RA	Dec	Z
Object	NA	Dec	L
SDSS J105143.92+ 035951.9	162.93301	3.99777	0.0171
SDSS J151713.03+ 552640.4	229.30423	55.44444	0.0269
SDSS J113515.94+ 013819.3	173.8164	1.6387	0.0254
SDSS J214554.67+ 114041.8	326.4778	11.6783	0.0234
SDSS J140733.50+ 071040.3	211.88961	7.17786	0.0238
SDSS J111243.98+ 353356.8	168.18327	35.5658	0.0791
SDSS J150758.49+ 102053.6	226.99373	10.34822	0.0789
SDSS J112642.28- 12732.3	173.74778	0.41924	0.0002
SDSS J141026.83- 04956.5	212.6118	-0.83238	0.0255
SDSS J083737.87+ 441501.4	129.40784	44.25039	0.0269

Tab.2: Coordinates and redshifts of the galaxies.

In Fig.1 it is shown the spectrum of a star while in Fig.2 there is the picture of the spectrum of a galaxy.

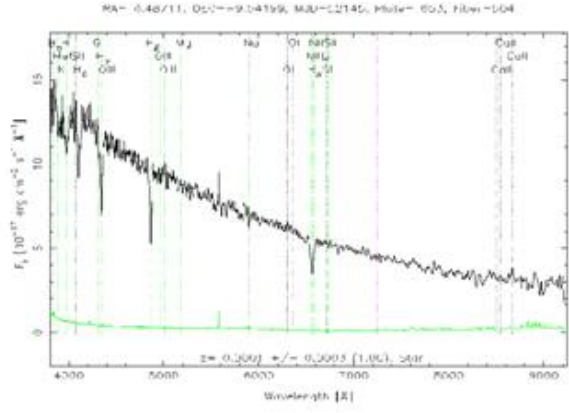


Fig.1: stellar spectrum.

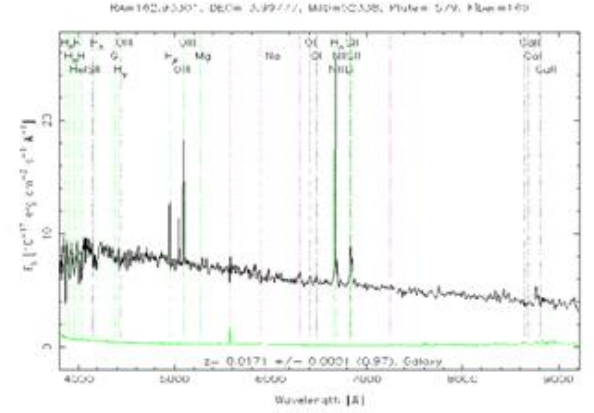


Fig.2: galactic spectrum.

III. WORK DESCRIPTION

We selected the galaxies having a colour index g-r between -1 and 2 and a redshift less than 0.1. Each spectrum extracted from SDSS is composed by four spectra. The first one is the spectrum of the object. Using IRAF we extracted only this spectrum and we made the extinction correction using the visual absorption $A_{\rm V}$.

The next step was to calculate the redshift $(z = \Delta \lambda \lambda_0)$ of every galaxy spectrum and then to deredshift it. We selected the H α line for the emission line galaxies and the Na line for the absorption line galaxies. Computing the difference between the observed and the laboratory wavelengths, we derived the redshifts. In tab. 3 are reported the measured H α or Na line wavelengths, the redshift and the Galactic extinction coefficient used for the correction of the spectrum for each galaxy.

Tab.3

Object	Wavelength	Redshift [z]	Extinction coefficient [A _V]
SDSS J105143.92+ 035951.9	$H\alpha = 6676.5$	0.017	0.141
SDSS J151713.03+ 552640.4	$H\alpha = 6740.1$	0.027	0.049
SDSS J113515.94+ 013819.3	$H\alpha = 6729.9$	0.025	0.091
SDSS J214554.67+ 114041.8	$H\alpha = 6719.3$	0.024	0.359
SDSS J140733.50+ 071040.3	Na = 6033.0	0.024	0.092
SDSS J111243.98+ 353356.8	Na = 6360.0	0.079	0.087
SDSS J150758.49+ 102053.6	Na = 6356.0	0.079	0.120
SDSS J112642.28- 012732.3	Na = 6329.0	0.074	0.112
SDSS J141026.83- 004956.5	$H\alpha = 6730.4$	0.025	0.161
SDSS J083737.87+ 441501.4	$H\alpha = 6741.4$	0.027	0.089

Then, we normalized the spectra of the stars and the galaxies dividing each of them for their flux at 6000Å. All these operations were performed with IRAF, while for the linear combinations of the stellar spectra we used Topcat. We first transformed the spectra in text files where every value of the wavelength was associated with the correspondent value of the flux. Then, we started to combine the stars' spectra to obtain the integrated spectra of the galaxies except for the emission lines. We combined different spectra in different proportions and the coefficients that appeared in front of each spectrum showed the presence in percentage of that kind of star in the galaxy.

Recognizing the spectral class of the stars, we were able to find approximately the percentage of old and young stars composing the galaxies. For example the spectrum of an a elliptical galaxy (Fig.3) was obtained adding the three spectra of F (Fig.4), K (Fig.5) and A (Fig.6) stars.

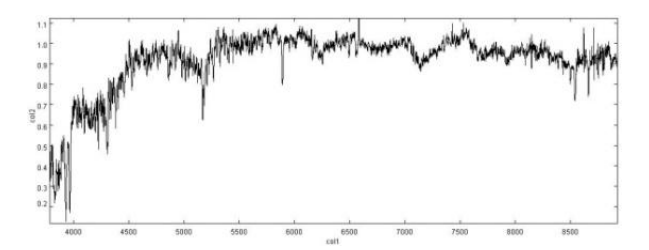


Fig.3: Example of spectrum of an elliptical galaxy.

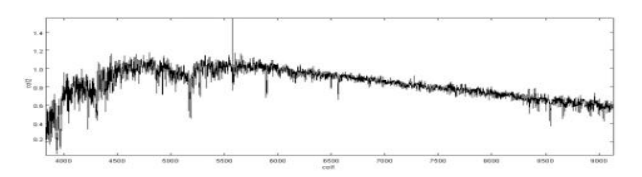


Fig.4: Spectrum of an F star.

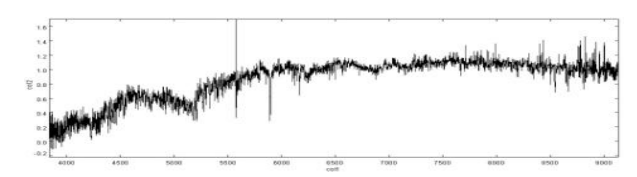


Fig.5: Spectrum of a K star.

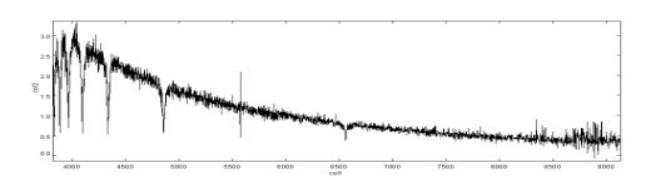


Fig.6: Spectrum of an A star.

The result is shown in Fig.7, in which are visible two different spectra; the galaxy's spectrum is the red one while the integrated spectrum is the blue one:

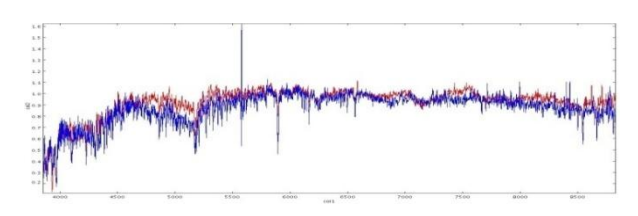


Fig.7: Comparison between the galactic spectrum and the spectrum obtained summing the different types of stars.

IV. RESULTS

We obtained ten different combinations made of 2 or 3 types of stars. However, in some cases, it was difficult to combine the stellar spectra to obtain a good

integration, in particular the spectrum of elliptical galaxies was difficult to reproduce. Moreover, many spectra were similar because many galaxies belonged to the same type. For this reason we report only some graphs. From Fig.8 to Fig.10 there are the most representative galaxies' spectra (red) compared with the integrated spectra (blue).

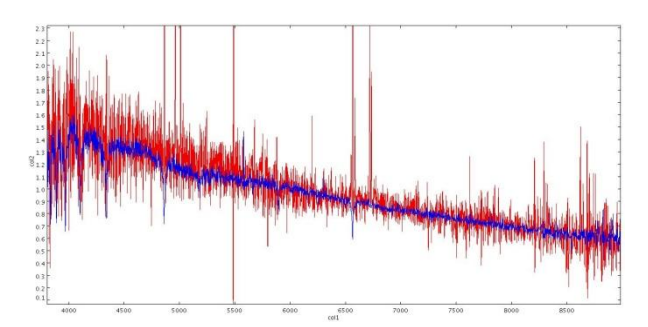


Fig.8: Example of a well reproduced spectrum.

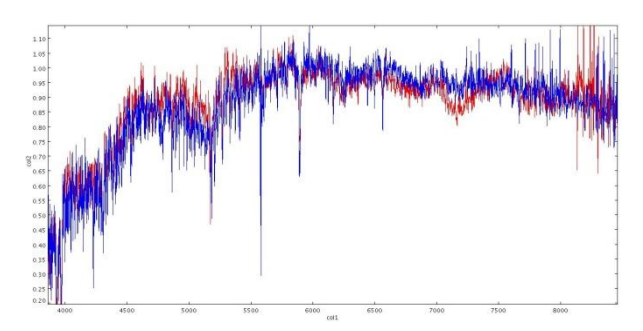


Fig.9: Example of a well reproduced spectrum.

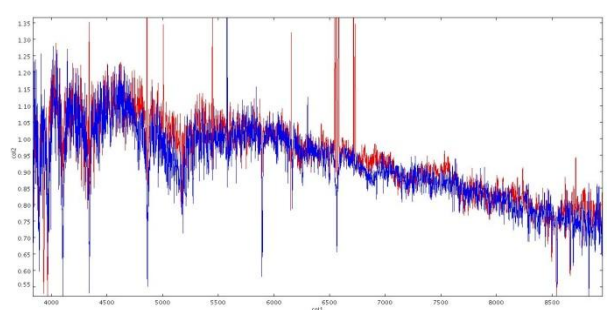


Fig.10: Example of a well reproduced spectrum.

In Tab. 4 we sum up our results: near each galaxy there are the linear combinations of the percentage of stellar types composing the galaxies.

Object	Stellar population synthesis
SDSS J105143.92+035951.9	40% A + 10% F + 20% K
SDSS J151713.03+552640.4	80% F + 20% A
SDSS J113515.94+013819.3	20% A + 30% F + 50% K
SDSS J214554.67+114041.8	50% A + 50% K
SDSS J140733.50+071040.3	30% F + 60% K + 10% A
SDSS J111243.98+353356.8	70% K + 20% F + 10% A
SDSS J150758.49+102053.6	50% F + 50% K
SDSS J112642.28-012732.3	70% K + 20% F + 10% A
SDSS J141026.83-004956.5	40% A + 60% K
SDSS J083737.87+441501.4	60% A + 40% K

Tab.4: table with results.

In conclusion, comparing our graphs with some typical spectra of elliptical, spiral and irregular galaxies and analyzing our stellar population synthesis, we made a catalogue of the objects (Tab.5). Sometimes it was not easy to catalogue the objects, like the last galaxy, which may be an Irregular or a Spiral galaxy.

Object	Type
SDSS J105143.92+035951.9	Spiral
SDSS J151713.03+552640.4	Spiral
SDSS J113515.94+013819.3	Spiral
SDSS J214554.67+114041.8	Spiral
SDSS J140733.50+071040.3	Elliptical
SDSS J111243.98+353356.8	Elliptical
SDSS J150758.49+102053.6	Elliptical
SDSS J112642.28-012732.3	Elliptical
SDSS J141026.83-004956.5	Spiral
SDSS J083737.87+441501.4	Irregular or Spiral

Tab.5: catalogue of the studied galaxies.

Study of the star formation history with STARLIGHT

Enrico Cescon, Luca Fardin, Eleonora Maset, Enrico Pandin, Carlo Maria Scandolo

Liceo Scientifico "Guglielmo Marconi", Conegliano (TV)

ABSTRACT

The aim of this work is to estimate the SFH (Star Formation History) of 50 galaxies through the analysis of their spectra. Comparing data of spiral and elliptical galaxies, it was possible to verify some aspects of the galactic evolution theory regarding star formation periods.

I. INTRODUCTION

Galaxies are large-scale aggregates of stars, gas, and dust kept together by gravitational forces. According to current theories, they started to form between 600 million and 1 billion years after the Big Bang. Hubble's morphological classification divides galaxies into elliptical, spiral and irregular ones. Elliptical galaxies show a quite uniform star distribution and their luminosity gradually decreases from the centre to the edge; they also present only little evidence of gas and dust.



Fig. 1: Elliptical Galaxy M87. You can clearly see the uniform distribution of luminosity.

Spiral galaxies, instead, are characterized by the presence of an evident central bulge and of arms

originating from the bulge. In this case there are large quantities of gas and interstellar dust in the arms.



Fig. 2: Spiral galaxy M81. You can clearly see the presence of the arms.

Irregular galaxies are called in this way because their unusual shape does not allow us to trace them to any category.

According to the classic theories, the shape of galaxies is influenced by two physical parameters, density and angular momentum, that play a fundamental role during formation. If the protogalaxy is very dense, gas condenses very quickly and it is completely transformed into stars, originating an elliptical galaxy. On the contrary, if the protogalaxy is not dense enough, cooling takes place more slowly; gas first condenses in the centre forming the stars of the bulge, then on a plane giving birth to the arms. Moreover, a high angular momentum favours the flattening of the cloud on a plane and the formation of the disc of a spiral. On the basis of galactic evolution theories, in elliptical

galaxies the star formation is concentrated in the first moments of their life. Spiral galaxies present instead many star formation events distributed along their whole existence.

II. OBSERVATIONAL DATA

The data were obtained from the DR6 (*Data Release 6*) archive of *Sloan Digital Sky Survey* (SDSS).

We analyzed the spectra of 50 galaxies with redshift lower than 0.1 and g-r colour index ranging between -0.6 and 1.3.

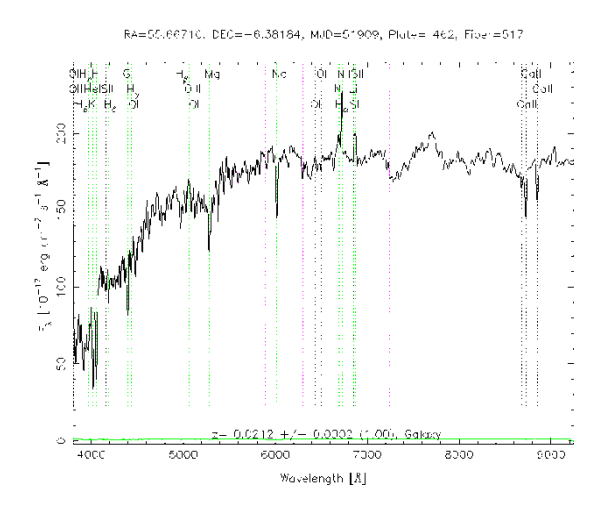


Fig. 3: Spectrum obtained from the observation of a spiral galaxy.

The spectra were taken from regions close to the galactic nucleus. In the spectrum of Fig. 3, the H_{α} emission line, which is found in spiral galaxies, is clearly visible. It is originated by the photoionization of interstellar gas due to young stars belonging to O and B spectral classes. In elliptical galaxies spectra this emission line is absent because stars are older and colder.

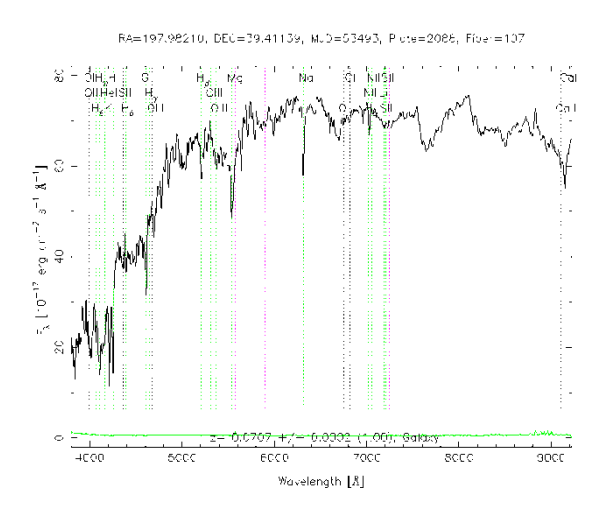


Fig. 4: Spectrum obtained from the observation of an elliptical galaxy.

III. WORK DESCRIPTION

On the basis of redshift and colour index parameters described in the previous paragraph, we downloaded data related to 5000 galaxies from www.sdss.org/dr6. We created a colour-colour diagram using a computer program called TOPCAT, which allowed us to distinguish between bluer and redder galaxies. Blue galaxies have a lower g-r colour index and spiral galaxies are more frequently found among them; red ones are instead generally elliptical. From this graph we selected 50 galaxies: 35 of them were spiral and 15 elliptical. We processed their spectra using program IRAF (Image Reduction and Analysis Facility) in order to put them in the software STARLIGHT. First of all, we removed the effect due to the Galactic extinction, which is the partial light absorption by the dust/ISM of the Milky Way. To do this operation, we used data taken from nasa/ipac extragalactic database (NED). After that, we shifted spectra to redshift z=0. Measuring the wavelength of the H α line, it is possible to calculate the redshift by means of the following formula:

$$z = \frac{\lambda - \lambda_0}{\lambda_0}$$

where λ_0 is the rest frame wavelength, 6563Å, whereas λ is the observed wavelength. Elliptical galaxies do not present the H\alpha emission line, so we considered the Na absorption line, whose rest frame wavelength is 5892Å. The so modified spectra were then put in STARLIGHT. This program, starting from the spectrum of a galaxy, is able to trace back its stellar composition. It combines the spectra of 45 different stellar types of the main sequence: 3 different metallicity classes (0.004 or 0.02 or 0.05) for each of the 15 age classes (from 1 million to 13 billion years). Metallicity indicates metal abundance in a star. A high metallicity might suggest that a star is old or that it is a second generation star, which contains metals produced by previous stars. The program makes a linear combination of sample-spectra at disposal approximate the original spectrum as better as possible. It adopts the following procedure:

$$Sp = \sum_{i=1}^{45} a_i \cdot s_i = a_1 \cdot s_1 + a_2 \cdot s_2 + \dots + a_{45} \cdot s_{45}$$

where Sp is the output spectrum, s is the spectrum of every stellar type and a is the number of stars of that particular type.

Since STARLIGHT uses only stellar spectra, which are exclusively absorption spectra, it cannot reproduce the emission lines we find in spiral galaxies spectra.

Since we were interested only in the different ages of stars, we added the results related to stars with the same age and different metallicity. STARLIGHT gave us tables with the fraction of light emitted by stars of the same age class.

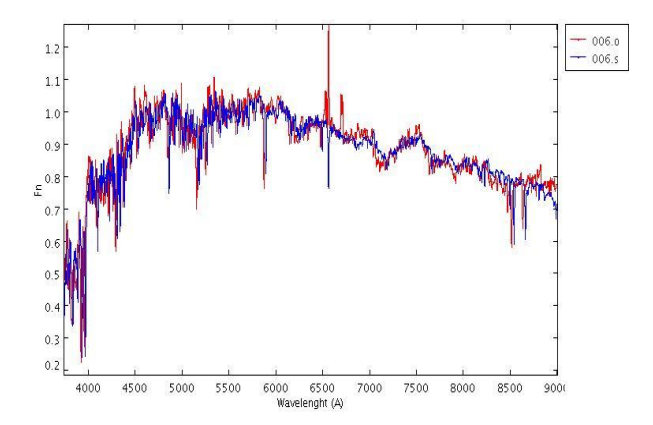


Fig. 5: The red spectrum is the one of fig.3 modified with IRAF. The blue one is the spectrum created by STARLIGHT. You can notice the good approximation, except for the absent rendering of the H_a emission line.

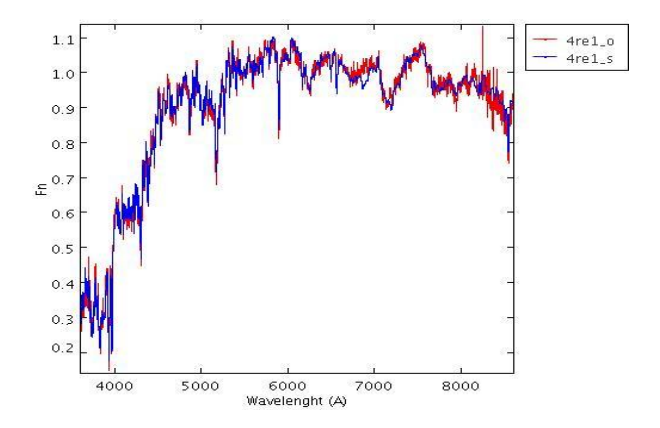


Fig. 6: The red spectrum is the one of fig.4 modified with IRAF. The blue one is the spectrum created by STARLIGHT. You can notice the good approximation.

Age class	Age (yr)	Light %
1	$1.0 \cdot 10^6$	2.78
2	$3.2 \cdot 10^6$	4.77
3	$5.0 \cdot 10^6$	0.00
4	$1.0 \cdot 10^7$	16.43
5	$2.5 \cdot 10^7$	9.82
6	$4.0 \cdot 10^7$	0.36
7	$1.0 \cdot 10^{8}$	1.35
8	2.9·10 ⁸	4.40
9	$6.4 \cdot 10^8$	0.00
10	$9.0 \cdot 10^{8}$	0.00
11	1.4·10 ⁹	6.02
12	$2.5 \cdot 10^9$	28.46
13	5.0·10 ⁹	3.12
14	$1.1 \cdot 10^{10}$	8.77
15	$1.3 \cdot 10^{10}$	15.24

Using TOPCAT again, from these charts we obtained graphs showing stellar formation events during the life of the galaxy. We put the age of the stars in a

logarithmic scale on the X axis, and the percentage of emitted light on the Y axis.

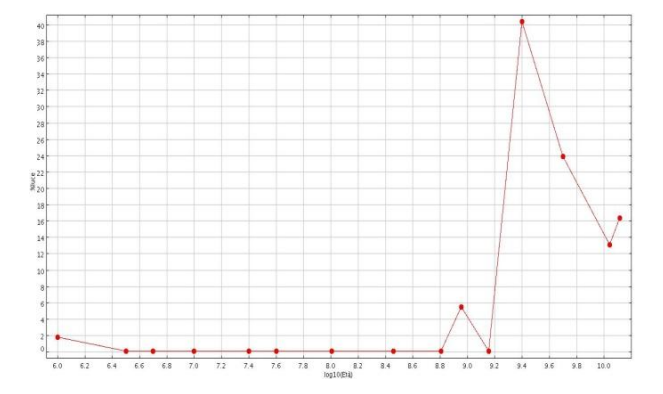


Fig. 7: Graph which represents the star formation history of the spiral galaxy in fig.3; each peak corresponds to a star formation event.

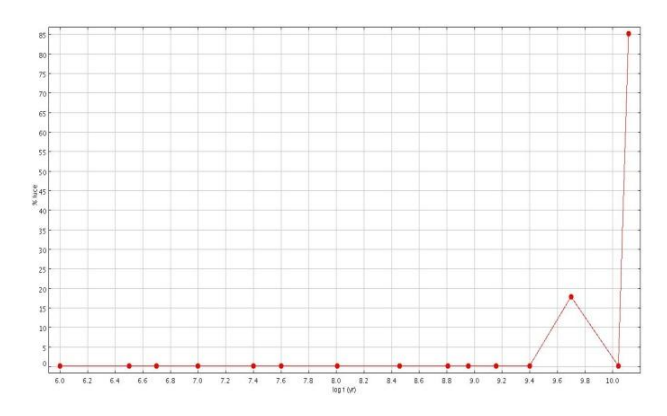


Fig. 8: Graph which represents the star formation history of the elliptical galaxy in fig.4.

IV. RESULTS

From the graphs we obtained, we made some statistical considerations:

- all spiral galaxies have at least 3 star formation events;
- 56% of blue spiral galaxies have at least 8 star formation events, while 90% of red spiral galaxies have less than 8 star formation events;

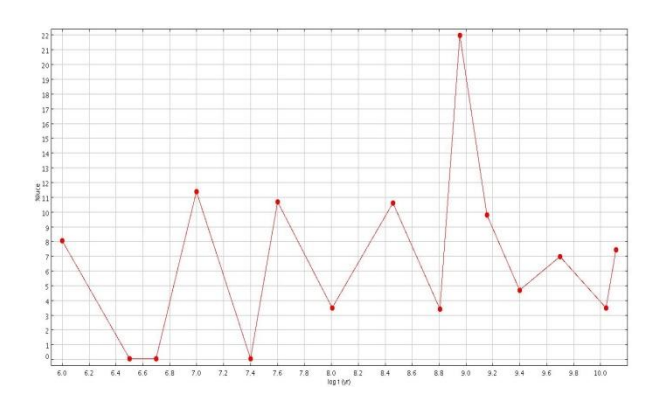


Fig. 9: Typical example of blue spiral galaxy with numerous star formation events.

 elliptical galaxies, which are all red, have at most 5 star formation events;

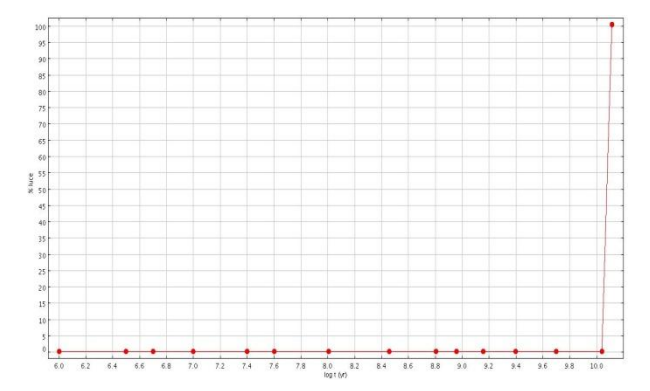


Fig. 10: Typical example of elliptical galaxy with only one star formation event dating to more than 10 billion years ago.

 all blue spiral galaxies have a star formation event more recent than 100 million years ago;

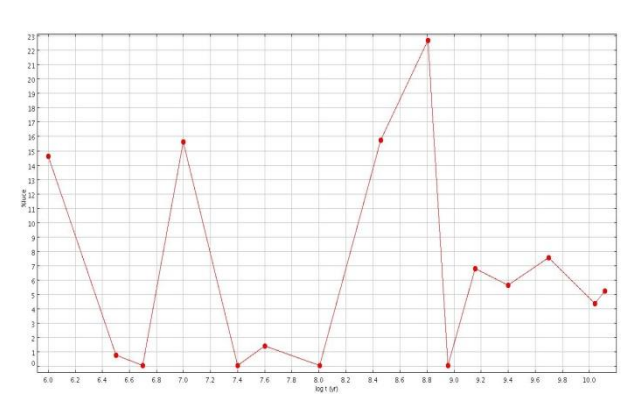


Fig. 11: Graph of a spiral galaxy with star formation events dating to 1 and 10 million years ago.

• 6 red galaxies out of 25 have a star formation event more recent than 100 million years ago; among them only one is elliptical;

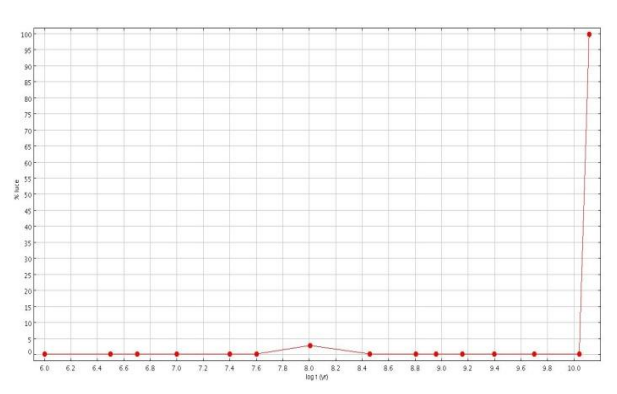


Fig. 12: Graph of the only analyzed elliptical galaxy which has a star formation event happened 100 million years ago.

As predicted by galactic evolution theories, obtained data show that in elliptical galaxies the initial collapse quickly converts all the gas into stars; in this way the star formation process does not last for the whole galaxy lifetime. Elliptical galaxies are, in this way, composed by red old stars.

In spiral galaxies the presence of gas and dust in the disk allows a more homogeneous star formation process. Therefore, they contain younger and hotter stars than elliptical galaxies, as already verified by Bano et al. [1].

From the fact that elliptical galaxies are only red and that the blue ones are spiral, and considering what we previously said, we can infer that the ellipticals are the oldest galaxies if the universe, as reported by Ralf Bender ^[2].

V. BIBLIOGRAPHY

[1] Studio della Popolazione Stellare nelle Galassie by M. Bano, A. Campa, M. Gusella, F. Righetti - "The sky as a laboratory 2006-2007", 2007.

[2] Galaxies Cosmology and Dark Matter by Bender R. – Lecture, 2000.

Star formation history in the Small Magellanic Cloud: the case of NGC 602 by M. Cignoni, E. Sabbi et al. – The Astrophysical Journal, 2009

Introduzione all'astronomia by H. L. Shipman – Zanichelli, 2000

http://www.sdss.org/dr6

http://nedwww.ipac.caltech.edu/

Index

ugriz photometry of candidate galaxy groups: 2MASXJ14391186+1415215 and 2MASXJ14530794+2554327	p.	1
Analysis of the luminosity of elliptical galaxies	p.	5
Morphological analysis of the galaxy NGC4686	p.	9
Morphological study of elliptical galaxies	p.	13
Morphology of the galaxies around the X-ray source 2MASXJ14391186+1415215 through GIM2D	p.	17
Velocity dispersion in elliptical galaxies	p.	21
Photometric redshifts of the galaxies near the X-ray source 2MASX J14391186+1415215	p.	25
Optical counterparts of Swift X-ray sources	p.	29
Optical spectroscopy of comet C/2007 N3 Lulin	p.	33
Spectral classification of the supernova SN2009af	p.	37
Photometric analysis of the open cluster NGC2420 and the globular cluster NGC6229	p.	41
Properties of stars: temperature, colour index and equivalent width of spectral lines	p.	45
Spectroscopic analysis of NGC2346 following hypothesis concerning its central object	p.	49
Spectral classification and determination of the star distances using $H\alpha$ emission line	p.	55
Star formation rate in spiral galaxies	p.	61
Stellar population synthesis	p.	67
Study of the star formation history with STARLIGHT	p.	71